PART TWO

PERSONAL INFORMATION

29th August 1955

Gdańsk

4C Borówkowa St,
Otomin,
Kolbudy Municipality,
80-174 Gdańsk

2B Zator-Przytockiego St,
Apt 12, Wrzeszcz,
80-245 Gdańsk

Gdańsk University of Technology,
11/12 Narutowicza St,
80-233 Gdańsk

Academic teacher,
chemical engineer

Cathodic protection inspector

+ 48 601 529 730

kazdarow@pg.edu.pl

Kazimierz Darowicki – Wikipedia, the free encyclopedia

Kazimierz Darowicki

ORCID ID: 0000-0002-5457-5008

MAJOR BASIC RESEARCH ACHIEVEMENTS

TABLE OF CONTENTS

The corrosion potential is the resultant of the kinetic equilibrium between the metal/alloy dissolution reaction rate and the depolarization reaction rate. Depending on changes in the rate of both processes, the corrosion potential drifts. If we study corrosion processes under conditions of a steady potential (potentiostatically), we must take into account that due to the drift of the corrosion potential, a variable, uncontrolled in time polarization is created. The corrosion potential, despite initial equality with the steady potential, changes relative to the steady potential as corrosion processes progress. This is understandable behaviour, corrosion processes are non-equilibrium ones dependent on the kinetics of coupled metal dissolution and depolarization reactions.

Electrochemical Impedance Spectroscopy (EIS) technique is currently one of the most widely used measurement techniques. This method comes down to determining the transmission parameters of the investigated process in the form of an impedance/admittance spectrum or complex electrical capacitance. The measurement is performed sequentially, one at a time for each measurement frequency and for a fixed range. Measurement for each frequency continues for, approximately: $\Delta t_i = \frac{p}{f_i}$ where: p – number of periods required for correct measurement, f_i – measurement frequency. The total measurement time of the entire spectrum depends on the selected frequencies and their number, and is equal $\Delta T = p\sum_{i=1}^{n}\frac{1}{f_i}$. In practice, the measurement time of the entire spectrum takes up to 20 minutes. During this time, the investigated corrosion/electrochemical process should be time-independent and the determined impedance values for individual frequencies should be coherent. Unfortunately, this is just an assumption. Studying dynamic processes such as corrosion processes using static techniques is often unjustified and leads to incorrect results and, consequently, to incorrect interpretations. Measurement for the first frequency consumes time p/f_1. The time after which the second measurement is performer equals $p\left(\frac{1}{f_1}+\frac{1}{f_2}\right)$. If the process is non-stationary, after this time the state of the system is different than at the beginning. For the i-th frequency, time is equal to $p\left(\frac{1}{f_1}+\frac{1}{f_2}+\cdots+\frac{1}{f_i}\right)$. In this case, the measurements for each frequency correspond to a different state of the investigated process, the impedance spectrum is incoherent. Valuable coherent impedance spectra for non-stationary electrochemical processes can be obtained by dynamic methods.

Electrochemical processes, including corrosion processes, are non-linear in nature. Therefore, the determined electrochemical impedance depends on the magnitude of the signal amplitude. To avoid this undesirable effect, measurements are carried out under linearization conditions. A low amplitude value is selected so that the response signal for each frequency satisfies the condition of linearity with respect to the perturbation signal. On the other hand, the amplitude of the perturbation signal must be large enough to provide the required measurement accuracy. These two, cardinal issues related to oscillatory processes, harmonic measurements, impedance measurements, electrochemical noise measurements determine my main research area.

Due to their non-linearity and non-stationarity, corrosion processes require more sophisticated, dynamic measurement techniques. The presented theoretical analyses and the corresponding results of experimental research are my original achievements obtained in cooperation with my employees. In research on non-stationary processes, I rely on digital signal processing methods. In digital signal processing, time-frequency transformations are used to determine variable frequency characteristics as a function of time or another independent variable. In addition to the commonly used short-time Fourier transformation, there are other methods in the literature, such as wavelet transformation or Wigner-Ville distribution. To present my achievements in the field of analyses of non-stationary electrochemical and corrosion processes, I decided to briefly present various transformations. These vary in terms of possible resolution in time and frequency and possible artifacts. Finally, the discussion includes a gallery of time-frequency representations of numerous signals from different application areas to enable visual comparison.

1. NON-LINEAR ELECTROCHEMICAL IMPEDANCE SPECTROSCOPY

The use of transmittance analysers resulted in a rapid development of Electrochemical Impedance Spectroscopy applications. Frequency response analysis (FRA) method, as the method based on the use of a transmittance analyser is called, belongs to the group of frequency-by-frequency methods. The idea of measurement is presented in Fig. 1.1.

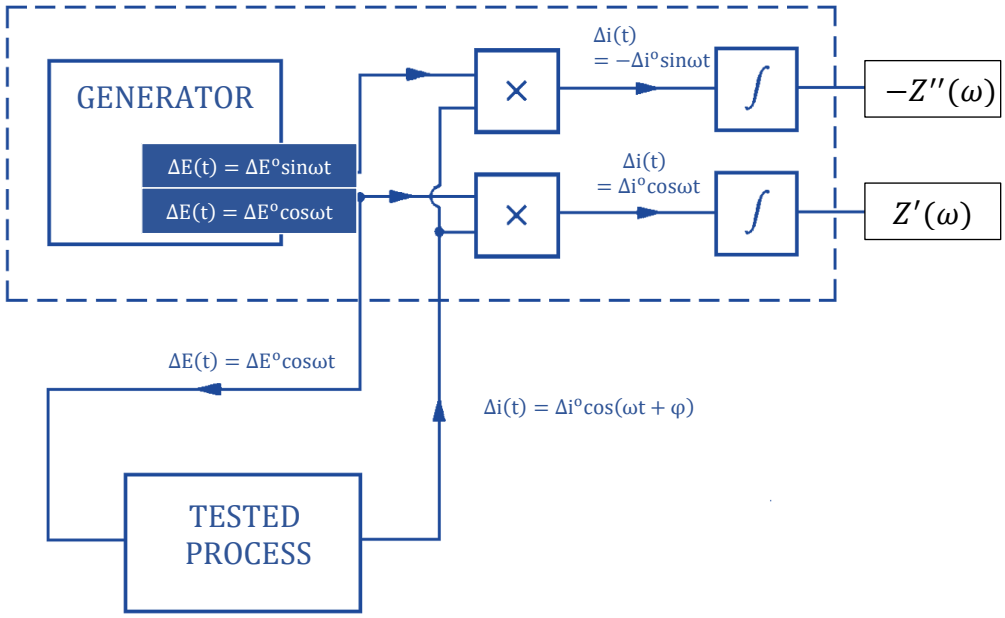

Fig. 1-1. Scheme of transmittance analyser operation

Sinusoidal potential signal of frequency $\Delta E(t) = \Delta E^o cos\omega t$ affects the investigated system. At the same time, a potential signal shifted in phase by an angle $\pi/2$, namely $\Delta E(t) = \Delta E^o sin\omega t$ is generated. The current response signal $\Delta i(t) = \Delta i^o cos(\omega t + \varphi)$ is phase-shifted with respect to the perturbation signal $\Delta E(t) = \Delta E^o cos\omega t$. Multiplying the response signal $\Delta i(t)$ by the perturbation signal in the phase $\Delta E(t) = \Delta E^o cos\omega t$ in one channel and multiplying the response signal $\Delta i(t)$ by the perturbation signal shifted by an angle $\pi/2$ namely $\Delta E^o sin\omega t$ signal, we obtain the real and imaginary components of the response current. Integrating these current components eliminates random interference. In a further stage, it allows determination of the real and imaginary parts of the measured impedance $Z(j\omega) = Z'(\omega) + jZ''(\omega)$. By changing the perturbation frequencies, we obtain an impedance spectrum that is a set of determined impedances for subsequent frequencies. Note that regardless of the magnitude of amplitude, the frequency of the current response is identical to the frequency of potential perturbation. Harmonic components with frequencies that are multiples of the fundamental frequency are filtered out and do not affect the magnitude of the measured impedance.

Classic impedance investigations are carried out under conditions of stationarity, causality and linearization of the tested electrochemical system. Electrochemical systems are non-linear systems. Therefore, for any amplitude of potential oscillatory perturbation:

$$\Delta E(t) = \Delta E^o cos\omega t \tag{1-1}$$

where: $\Delta E(t)$ – voltage cosine perturbation signal, ΔE^o – amplitude of the cosine perturbation signal, ω – angular frequency, t – time.

The alternating current can be represented as a Taylor series:

$$\Delta i(t) \approx \left(\frac{di}{dE}\right)_{E_S} \Delta E^o cos\omega t + \frac{1}{2!}\left(\frac{d^2 i}{dE^2}\right)_{E_S} (\Delta E^o cos\omega t)^2 + \frac{1}{3!}\left(\frac{d^3 i}{dE^3}\right)_{E_S} (\Delta E^o cos\omega t)^3 + \frac{1}{4!}\left(\frac{d^4 i}{dE^4}\right)_{E_S} (\Delta E^o cos\omega t)^4 + \frac{1}{5!}\left(\frac{d^5 i}{dE^5}\right)_{E_S} (\Delta E^o cos\omega t)^5 + \cdots \frac{1}{n!}\left(\frac{d^n i}{dE^n}\right)_{E_S} (\Delta E^o cos\omega t)^n \quad (1\text{-}2)$$

where: $\Delta i(t)$ – variable current response signal.

E_S potential, in which impedance measurements are carried out, is described by linear equations

The linearization condition is implemented by using a sinusoidal perturbation signal with a small amplitude and sequentially changing frequency. Due to this, the electrochemical process in the vicinity of the E_S potential at which impedance measurements are carried out, is described by linear equations:

$$\Delta i(t) \approx \left(\frac{di}{dE}\right)_{E_S} \Delta E^o cos\omega t \quad (1\text{-}3)$$

The further terms of the series are negligibly small in relation to the first term. In this case, performing impedance measurements significantly simplifies measurement methodology and frequency analysis of impedance spectra. The use of a high amplitude sinusoidal perturbation signal makes it necessary to include further harmonic components in the response signal, not just the fundamental component. *(K. Darowicki, The amplitude analysis of impedance spectra, Electrochimica Acta, Volume 40, Issue 4, March 1995, Pages 439-445).* Under non-linearity conditions, the polarization resistance is a function of the amplitude of the potential perturbation signal:

$$\frac{1}{R_P(\Delta E)} \approx \left(\frac{di}{dE}\right)_E + \frac{1}{8}\left(\frac{d^3 i}{dE^3}\right)_{E_S} \Delta E^{o\,2} + \cdots \quad (1\text{-}4)$$

where: $R_P(\Delta E)$ – polarization resistance.

The derived dependence was verified by examining changes in the impedance of the model electrical circuit as a function of the perturbation amplitude.

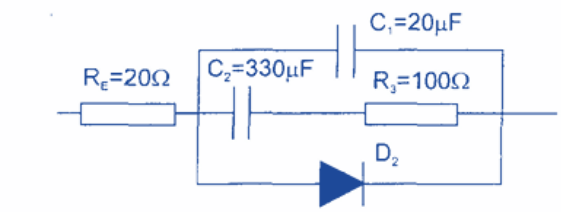

Fig. 1-2. Investigated non-linear electrical circuit, C_1 and C_2 - capacitors, R_E and R_3 – resistors, D - diode

Fig. 1-3. shows non-linear impedance spectra determined for different amplitudes of the perturbation signal.

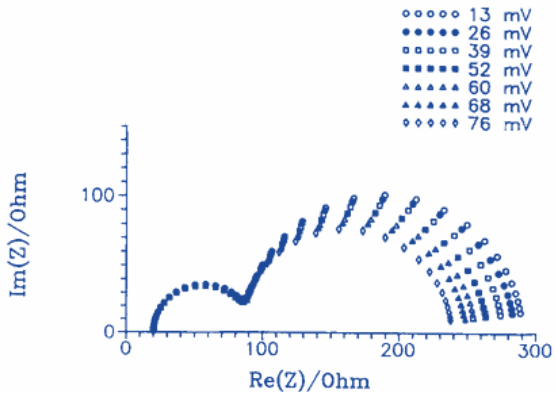

Fig. 1-3. Impedance spectra of the non-linear electrical system determined for the potential E = 0.500 V and individual amplitudes of the sinusoidal perturbation signal

Analysis of spectra as a function of perturbation amplitude confirmed the correctness of the derived relationship. The determined value of the diode voltage coefficient using the polarization method perfectly coincides with the value determined on the basis of amplitude analysis of impedance spectra. Additionally, the amplitude analysis performed allows to determine the impedance for a hypothetical perturbation signal amplitude of zero. It also allows to establish the amplitude dependence or lack thereof for the individual electrical elements of the equivalent circuit.

The amplitude analysis performed was an interpretation of linearization. (*K. Darowicki, Linearization in impedance measurements, Electrochimica Acta,Volume 42, Issue 12, Pages 1781 – 17881997, K. Darowicki, Deviation from linearity in electrochemical impedance spectroscopy, Polish Journal of Chemistry, Volume 71, Issue 8, Pages 1133 – 1139 August 1997).*

If the Faradaic rectification current is negligibly small and the third harmonic of the response signal is negligibly small compared to the main harmonic component, the investigated process occurs under linearization conditions. For these conditions, a linear relationship is met:

$$\Delta E(\omega) \cong Z(j\omega)\Delta i(\omega) \tag{1-5}$$

where: $Z(j\omega)$ - impedance, $j^2 = -1$

The first-order electrode reaction is described by the general equation:

$$Ox + ne \underset{V_A}{\overset{V_C}{\rightleftharpoons}} Red \tag{1-6}$$

where: Ox- oxidized form, Red – reduced form, V_C – reduction reaction rate, V_A – oxidation reaction rate.

The reaction is represented by Randles electrical equivalent circuit.

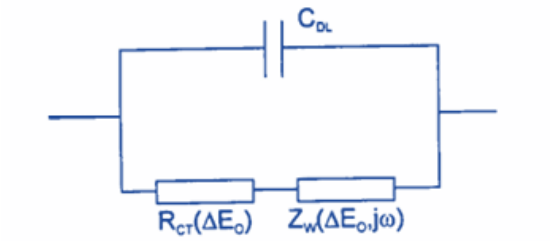

Fig. 1-4. Electrical equivalent circuit for the first-order electrode reaction. C_{DL} – capacitance of electrical double layer, $R_{CT}(\Delta Eo)$ – charge transfer resistance, $Z_W(j\omega, \Delta Eo)$ – Warburg impedance

Based on the Taylor series expansion method, the dependence between the charge transfer resistance and the Warburg coefficient as a function of the amplitude of the sinusoidal potential perturbation was determined:

$$\frac{1}{R_{CT}(\Delta E_o)} \approx nF\left[\left(\frac{\partial V_C}{\partial E}\right)_{c_{Ox}} - \left(\frac{\partial V_A}{\partial E}\right)_{c_{Red}}\right] + \frac{nF}{8}\left[\left(\frac{\partial^3 V_C}{\partial E^3}\right)_{c_{Ox}} - \left(\frac{\partial^3 V_A}{\partial E^3}\right)_{c_{Red}}\right]\Delta E_o^2 \quad (1\text{-}7A)$$

$$W(\Delta E_o) \approx R_{CT}(\Delta E_o)\left\{\frac{\left(\frac{\partial V_C}{\partial c_{Ox}}\right)_E}{\sqrt{2D_{Ox}}} + \frac{\left(\frac{\partial V_A}{\partial c_{Red}}\right)_E}{\sqrt{2D_{Red}}} + \frac{1}{8}\left[\frac{\left(\frac{\partial^3 V_C}{\partial^2 E \partial c_{Ox}}\right)_E}{\sqrt{2D_{Ox}}} + \frac{\left(\frac{\partial^3 V_A}{\partial^2 E c_{Red}}\right)_E}{\sqrt{2D_{Red}}}\right]\Delta E_o^2\right\} \quad (1\text{-}7B)$$

where: $R_{CT}(\Delta E_o)$ – charge transfer resistance, $W(\Delta E_o)$ – Warburg coefficient.

It was assumed that the capacitance of the electrical double layer is a linear parameter with a constant value. For the assumed approximation, the inverse of the resistance is a linear function of the square of the perturbation amplitude. The Warburg coefficient shows an identical relationship. The slopes of these linear relationships, together with the determined intercepts, allow for a comprehensive physicochemical analysis of the first-order electrode reaction. In addition to the kinetic parameters, the values of diffusion coefficients can be determined. (*K. Darowicki, Fundamental-harmonic impedance of first-order electrode reactions, Electrochimica Acta, Volume 39, Issue, 18, December 1994, Pages 2757-2762).*

Amplitude analysis can be performed for more complex electrochemical reactions. For example, a two-step reaction was analyzed:

$$A \xrightarrow{V_1} (B)_{AD} + e \quad (1\text{-}8A)$$

$$(B)_{AD} \xrightarrow{V_2} C + e \quad (1\text{-}8B)$$

where: A – reduced form, (B) – adsorber intermediate product, C – reduced form, V_1 – rate of the first stage, V_2 – rate of the second stage.

The reaction analyzed is a two-step one accompanied by adsorption of the intermediate product. The rate of the first stage depends on the potential, the surface excess of the intermediate product and the concentration of the A-form on the electrode surface. The rate of the second stage depends on the potential and surface excess of the intermediate product.

$$V_1(E,\Gamma) = k_1 c_A(\Gamma_\infty - \Gamma);$$

$$V_2 = k_2\Gamma \quad (1\text{-}9B)$$

where: Γ- surface excess of adsorbed active complex, Γ_∞- maximum surface excess, k_1- rate constant of the first stage, k_2 – rate constant of the second stage, c_A – concentration of the A-form

For the assumed parameter values: $k_1 = 10^6 exp(60E) cms^{-1}, k_2\, exp(10E) s^{-1}$, $\Gamma_\infty = 2 \cdot 10^{-9}\, mol/cm^2, c_A = 10^{-6} mol/$ the theoretical polarization relationship shown in Fig. 1-5 was determined.

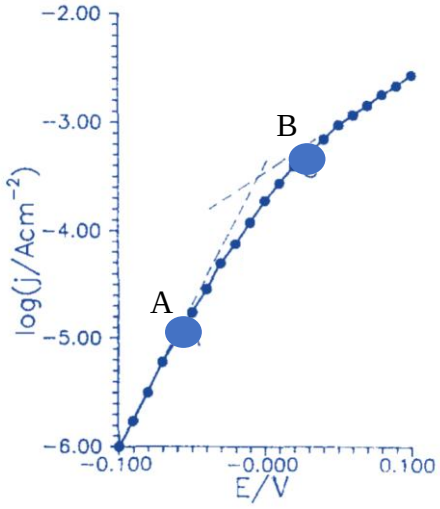

Fig. 1-5. Simulated polarization curve of a two-step electrode reaction determined for the assumed parameter values: $k_1 = 10^6 exp(60E) cms^{-1}, k_2 = exp(10E)s^{-1}, \Gamma_\infty = 2 \cdot 10^{-9}\, mol/cm^2, c_A = 10^{-6} mol/cm^2$

The influence of amplitude on the shape of the impedance spectra determined for points (A) and (B) is documented by following diagrams:

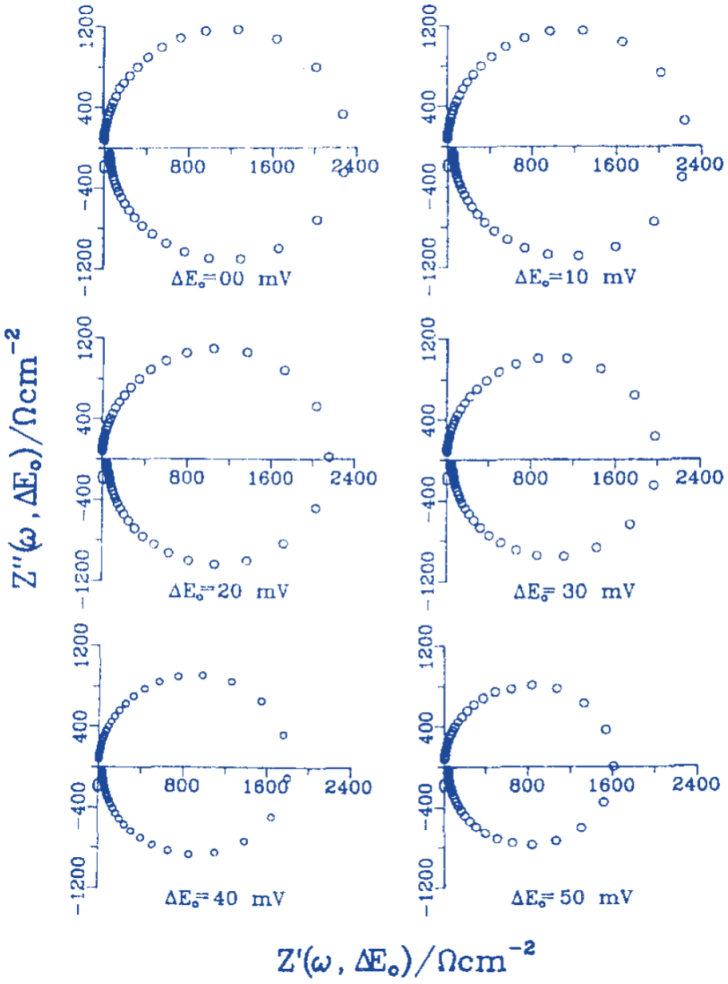

Fig. 1-6. Simulated impedance spectra determined at point (A) of the polarization curve. $E = -0.060\, V, k_1 = 10^6 exp(60E)\ cms^{-1}, k_2 = exp(10E)s^{-1}, \Gamma_\infty = 2.10^{-9}\, mol/cm^2, c_A = 10^{-6} mol/cm^2$

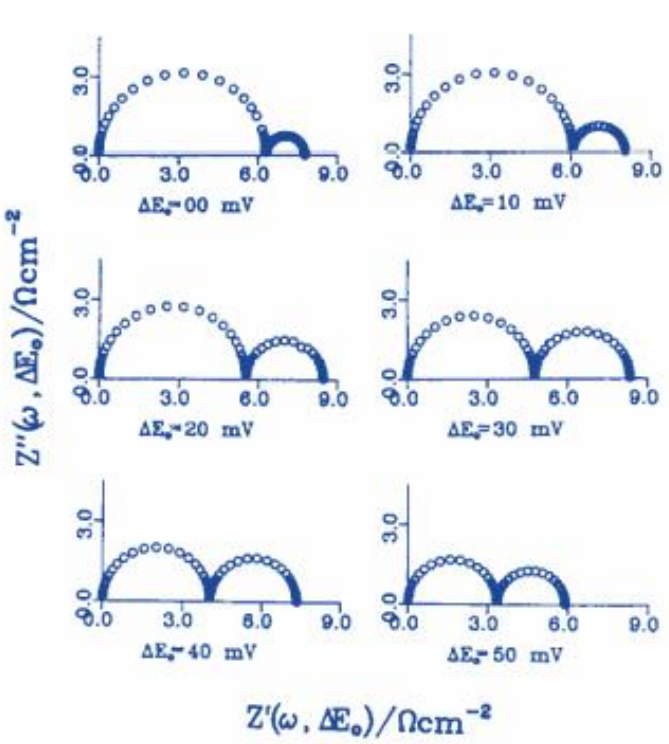

Fig. 1-7. Simulated impedance spectra determined at point (B) of the polarization curve. $E = 0.060\,V$, $k_1 = 10^6 exp(60E)\ cms^{-1}, k_2 = exp(10E)s^{-1}$, $\Gamma_\infty = 2.10^{-9}\,mol/cm^2, c_A = 10^{-6} mol/cm^3$

For non-linear conditions, the charge transfer resistance and the remaining quantities are equal (*K. Darowicki, Theoretical description of fundamental-harmonic impedance of a two-step electrode reaction, Electrochimica Acta, Volume 40, Issue 6, Pages 767 – 774 April 1995.):*

$$\frac{1}{R_\infty(\Delta E_o)} \approx \frac{F(b_1+b_2)k_1k_2c_A\Gamma_\infty}{k_2+k_1c_A} + \frac{F(b_1^3+b_2^3)k_1k_2c_A\Gamma_\infty}{8(k_2+k_1c_A)}\Delta E_o^2 \qquad (1\text{-}10)$$

The adsorption resistance depends parabolically on the amplitude of the potential perturbation:

$$\frac{1}{R_0(\Delta E_o)\tau(\Delta E_o)} \approx \frac{Fk_1k_2c_A\Gamma_\infty}{k_2+k_1c_A}\left\{(k_2-k_1c_A)(b_1+b_2) + \frac{[(k_2-k_1c_A)(b_1^3-b_2^3)-2(b_1+b_2)(b_1^2k_1c_A+b_2^2k_2)]}{8}\Delta E_o^2\right\} \qquad (1\text{-}11)$$

where: $R_\infty(\Delta E_o)$ – charge transfer resistance, $R_0(\Delta E_o)$ – adsorption resistance, $\tau(\Delta E_o)$ – relaxation time of adsorption of intermediate product.

The relaxation time of adsorption is also a parabolic function of the amplitude of the potential perturbation:

$$\frac{1}{\tau(\Delta E_o)} \approx b_1k_1c_A + b_2k_2 + \frac{(b_1k_1c_A+b_2k_2)}{4}\Delta E_o^2 \qquad (1\text{-}12)$$

The dependence of the fundamental harmonic impedance on the amplitude of the perturbation signal is particularly evident in the case of measurements for a large amplitude. Conducting impedance measurements under non-linear conditions has two basic aspects. Amplitude analysis of impedance spectra enables the determination of the kinetic parameters of a two-step electrode reaction. The second aspect of non-linear measurements is the ability via extrapolation to determine impedance

spectra corresponding to the zero amplitude of the perturbation signal. The kinetic parameters determined in this way correspond to the free run of the electrode reaction. However, the application of big perturbation amplitude signals can cause changes in the physicochemical state on the electrode surface.

Determining the dependence of the charge transfer resistance on the amplitude of the sinusoidal perturbation signal makes it possible to find the charge transfer coefficient. *(K. Darowicki, J. Orlikowski, Fast method for the determination of the charge transfer coefficient of an electrode reaction, Electrochimica Acta, Volume 44, Issue 2-3, Pages 433 - 43615 September 1998).* Another issue is determining the steady state under high-amplitude impedance measurements. In this case, for the fixed potential E_S apart from the i_S current, the Faradaic rectification current flows.
(K. Darowicki. The fixed state in impedance measurements of a two-step electrode reaction proceeding with accompanying adsorption of an intermediate product, Electrochimica Acta, Volume 42, Issue 7, Pages 1073 – 1079, 1997)

The utilization of relatively high-amplitude signals in corrosion makes it possible to determine the corrosion rate without unnecessary additional assumptions.

Under activation control conditions, the current related to corrosion process is given by the equation:

$$i(E) = i_{corr}\left\{exp\left[\frac{2.3}{b_{AT}}(E - E_{CORR})\right] - exp\left[-\frac{2.3}{b_{CT}}(E - E_{CORR})\right]\right\} \quad (1\text{-}13)$$

where: $i(E)$ – current, i_{corr}– corrosion current, b_{AT} – anodic Tafel coefficient, b_{CT} – cathodic Tafel coefficient, E_{CORR}- corrosion potential.

Introduction of the following dependences:

$$b_A = \frac{2.3}{b_{AT}};\ \ b_C = \frac{2.3}{b_{CT}};\ E - E_{CORR} = \Delta E_o cos\omega t$$

makes it possible to determine fundamental harmonic component:

$$\Delta i(\omega, \Delta E) = i_{corr}\left[(b_A + b_C)\Delta E_o + \frac{(b_A^3 + b_C^3)}{8}\Delta E_o^3 + \frac{(b_A^5 + b_C^5)}{192}\Delta E_o^5 + \cdots\right] cos\omega t \quad (1\text{-}14)$$

where: $\Delta i(\omega, \Delta E)$ – first harmonic of current.

For these conditions, the inverse of the polarization resistance is given by the relationship (*K. Darowicki, Corrosion rate measurements by non-linear electrochemical impedance spectroscopy, Corrosion Science, Volume 37, Issue 6, June 1995, Pages 913-925)*:

$$\frac{1}{R_P(\Delta E_o)} = i_{corr}\left[(b_A + b_C) + \frac{(b_A^3 + b_C^3)}{8}\Delta E_o^2 + \frac{(b_A^5 + b_C^5)}{192}\Delta E_o^4 + \cdots\right] \quad (1\text{-}15)$$

In the case of linear measurements, the corrosion rate is determined by the Stern-Geary equation:

$$i_{corr} = \frac{1}{(b_A + b_C)R_P(\Delta E_o)} \quad (1\text{-}16)$$

In linear measurements, the value $\frac{1}{(b_A + b_C)}$ cannot be determined from a single spectrum. In practice, this value is assumed to be constant at $\frac{1}{(b_A + b_C)} = 0.020V$. This assumption is a very general approximation. Additionally, this results in independence of $(b_A + b_C)$ of time. Under non-linear conditions, the values of the $b_A;\ b_C$ coefficients are determined from the relationship (1-15).

We have shown that the analysis of the impedance of the first harmonic as a function of the amplitude of voltage perturbation provides in-depth knowledge of the electrochemical or corrosion process.

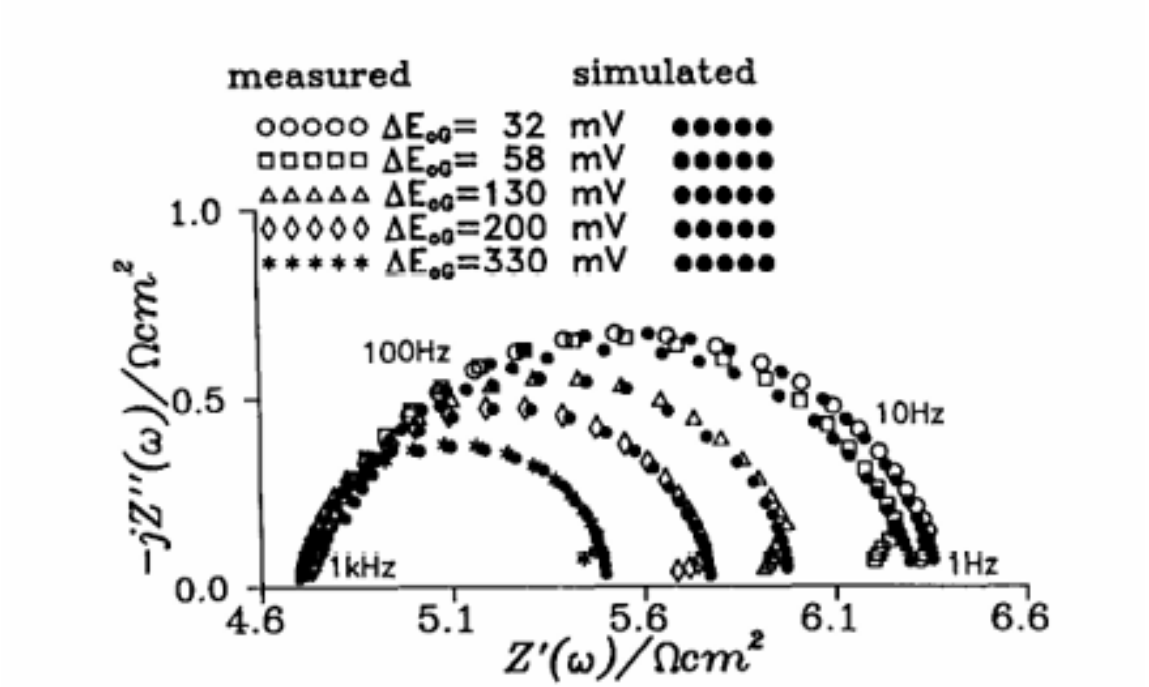

Fig. 1-8. Experimental and simulated impedance spectra of carbon steel dissolution in $0.5\ M\ (H,Na)_2SO_4,\ \ pH = 0.78$ determined for various amplitudes of sinusoidal potential perturbation. Corrosion potential $E_{CORR} = -0.531\ V\ (SCE)$

Amplitude analysis of the measured and simulated spectra confirmed the correctness of the mathematical analyses performed. A modification of the expired measurement solution is the use of a multi-frequency signal with modulated amplitudes. This allows the measurement time to be reduced, making it possible to monitor the corrosion rate of systems subject to rapid changes. In this way, the limitation resulting from the lack of a stationarity condition during impedance measurements is overcome. (*P. Slepski, M. Szocinski, G. Lentka, K. Darowicki, Novel fast non-linear electrochemical impedance method for corrosion investigations, Measurement, Volume 173, March 2021, 108667; P. Slepski, M. Szocinski, K. Darowicki, New method of non-linear electrochemical impedance spectroscopy with an amplitude-modulated perturbation signal, Journal of the Electrochemical Society, Volume 166, Issue 15, Pages C559 - C5632019).*

Despite the development of numerous electrochemical techniques, monitoring the corrosion rate is not an easy task. Methods that allow direct measurement of corrosion current typically result in irreversible changes to the sample structure. Non-destructive methods usually provide only indirect results in terms of charge transfer resistance. The proposed methods represent a compromise, on the one hand the amplitudes of the perturbation signals are large enough that the measurement is non-linear. On the other hand, they are small enough to limit irreversible changes.

2. TIME-FREQUENCY ANALYSIS OF PHYSICOCHEMICAL PROCESSES

The autocorrelation function of the $s(t)$ signal allows determination of the correlation of the $s(t)$ signal with a delayed copy of itself $s(t-\tau)$. This creates a mathematical tool for identifying repeating patterns or hidden periodicities in a signal obscured by noise. In order to analyse non-stationary processes, Wagner proposed the form of the autocorrelation function in the form:

$$ACF(t,\tau) = s\left(t+\frac{\tau}{2}\right)s^*\left(t-\frac{\tau}{2}\right) \tag{2-1}$$

where: $ACF(t,\tau)$ – autocorrelation function, τ – shift time, $s(t)$ – analysed signal, $s^*(t)$ – coupled signal.

The autocorrelation function defined in this way is a basis of time-frequency analysis, the diagram of which is shown in Fig. 2-1.

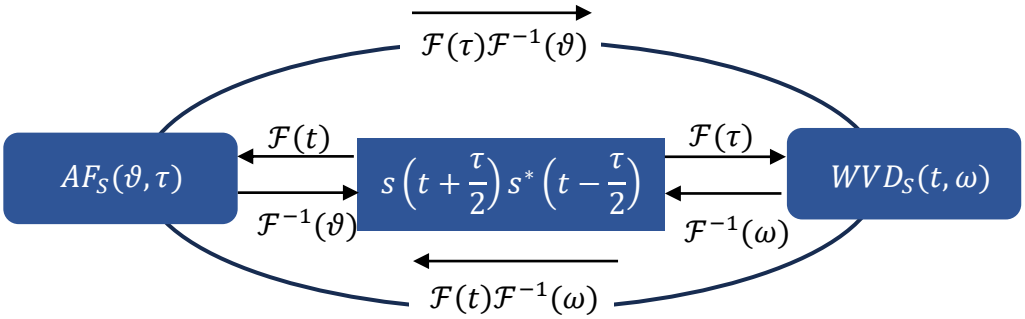

Fig. 2-1 Relationships between different distributions based on the autocorrelation function, $F(\tau)$ – Fourier transformation relative to shift time, $F(t)$ – Fourier transformation relative to current time, F^{-1}- inverse Fourier transformation, $WVD_s(t,\omega)$ – Wigner-Ville distribution, $AF_s(\vartheta,\tau)$ – ambiguity function

The Fourier transformation of the autocorrelation function with respect to the current time t leads to the ambiguity function $AF_s(\vartheta,\tau)$, which is a complex quantity:

$$AF_s(\vartheta,\tau) = \int s\left(t+\frac{\tau}{2}\right)s^*\left(t-\frac{\tau}{2}\right)exp(-j\vartheta t)dt \tag{2-2}$$

Due to the accurate detection of frequency shifts (Doppler effect), it is widely used in radar and sonar technologies.

A non-stationary power spectrum called the Wigner-Ville distribution is obtained by the Fourier transformation with respect to the shift time τ:

$$WVD_s(t,\omega) = \int s\left(t+\frac{\tau}{2}\right)s^*\left(t-\frac{\tau}{2}\right)exp(-j\omega\tau)d\tau \tag{2-3}$$

Unlike the ambiguity function, the Wigner-Ville distribution is a real quantity that describes the energy distribution of a non-stationary signal as a function of frequency. Distribution is a parabolic transformation, which has consequences. If the analyzed signal is a composition of a series of signals, the Wigner-Ville distribution of this complex signal is not a simple composition of the distribution of these signals. For example, the combination of two sine signals $s(t) = expj\omega_1 t + expj\omega_2 t$ as a result of the Wigner-Ville distribution gives the following equation:

$$WVD_s(t,\omega) = 2\pi\delta(\omega-\omega_1) + 2\pi\delta(\omega-\omega_2) + 4\pi\delta\left[\omega-\left(\frac{\omega_1+\omega_2}{2}\right)\right]\cos(\omega_1-\omega_2) \tag{2-4}$$

The distribution diagram of $WVD_s(t,\omega)$ is shown in Fig. 2-2.

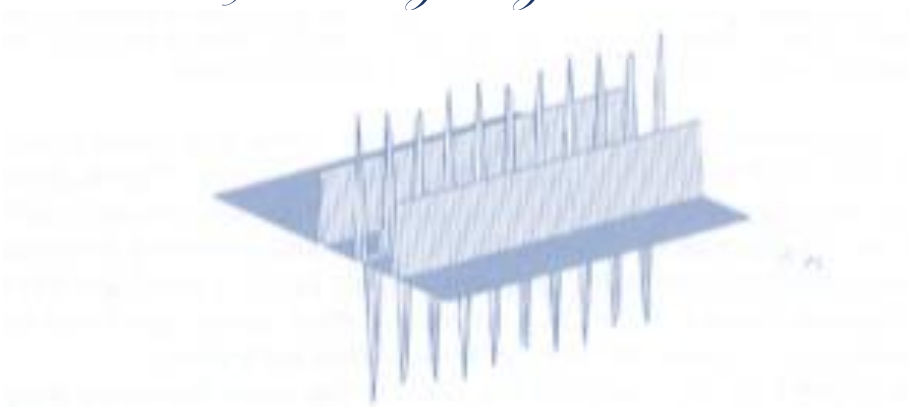

Fig. 2-2. Wigner-Ville distribution spectrogram of two sinusoidal signals $expj\omega_1 t + expj\omega_2 t$

The spectrogram shows two auto-bands with uniform energy distribution. These are the main bands $2\pi\delta(\omega - \omega_1)$ and $2\pi\delta(\omega - \omega_2)$. There is also an additional band called the interference (cross) band or inter-band. Unlike the main bands, it is an oscillating band, the amplitude of which depends on frequency changes, and the frequency of oscillation is a frequency difference $(\omega_1 - \omega_2)$.

The Belousov-Zhabotinsky reaction is a model example of a non-stationary oscillatory process. The reaction consists in the reversible oxidation of malonic acid to carbon dioxide by bromates.

$$2CH_2(COOH)_2 + 4BrO^{-3} = 4Br^- + 9CO_2 + 6H_2O \quad (2\text{-}5)$$

The catalyst for this reaction is cerium ions, the concentration of which varies according to the reaction:

$$2BrO^{-3} + 12H^+ + 10Ce^{3+} = Br_2 + 6H_2O + 10Ce^{4+} \quad (2\text{-}6)$$

Measuring the redox potential of Ce^{4+}/Ce^{3+} allows tracking the oscillatory nature of the Belousov-Zhabotinsky reaction. Processes of this type are studied classically in the time domain based on bifurcation theory.

As a result of the conducted research, I proposed a different analysis method, which involves transferring the analysis from the time domain to the frequency domain. Due to its non-stationary nature, I used the Wigner-Ville distribution. *(K. Darowicki, A. Krakowiak, A. Zieliński, The Wigner-Ville distribution in the analysis of deterministic components of spontaneous oscillations,* Polish Journal of Chemistry, *Volume 75, Issue 3, Pages 443 – 4522001).*
Fig. 2-3. Presents exemplary time changes in the potential of Ce^{4+}/Ce^{3+} reaction.

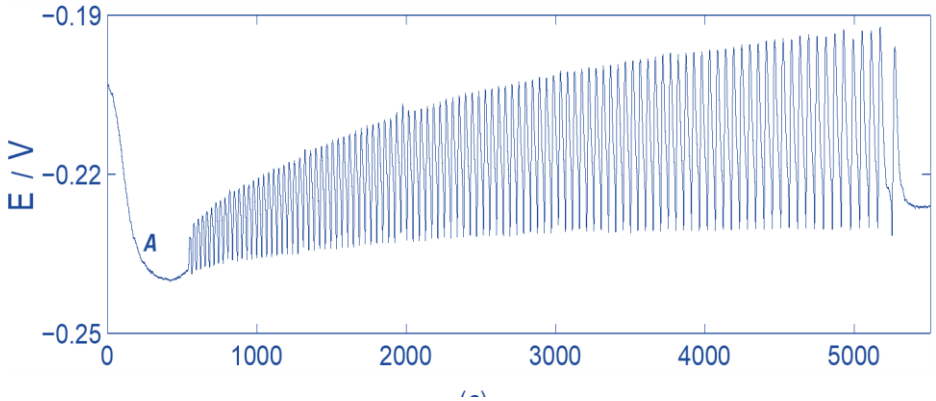

Fig. 2-3. Oscillations of the redox potential of the Belousov-Zhabotinsky reaction for initial concentrations of reactants: $[KBrO_3 = 0.07M]$, $[CH_2(COOH)_2] = 0.2\ M$, $[H_2SO_4] = 0.6M$, $[Ce(SO_4)_2 4H_2O] = 0.001\ M$. Sampling frequency $10\ Hz$

The transformation of the register of potential change in time, according to the Wigner-Ville distribution, leads to the following diagram.

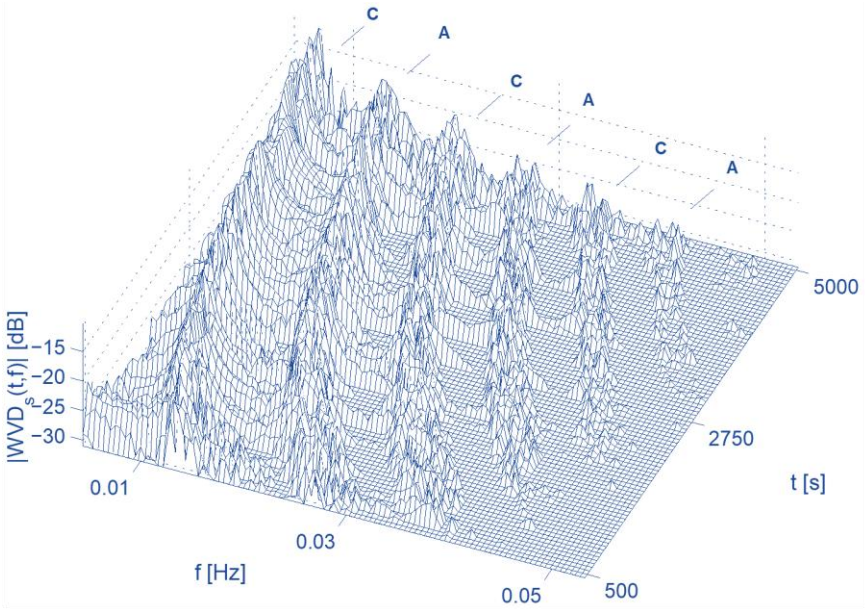

Fig. 2-4. The Wigner-Ville distribution spectrogram of the oscillations in time illustrated in Fig. 2-3. Auto-bands are marked with the symbol A, inter-bands are marked with the symbol C.

The diagram reveals a number of time-dependent frequency bands. Having extensive experience, one can determine their character. The bands marked with the symbol A are auto-bands, the bands marked with the symbol C are inter-bands. When analysing complex processes, the appearance of inter-bands is a major inconvenience, creating serious interpretation problems. It is worth noting that in the case of simple processes, detailed inter-band analysis provides valuable information or gives credibility to the adopted oscillation model. In this way, we obtain additional information about the variability of the investigated process. As it has already been stated, in many complex cases, a significant problem in the analysis of distribution spectrograms is the presence of interference bands. The attenuation effect of these bands is obtained by introducing appropriately defined kernel functions into the Wigner-Ville distribution. (*K. Darowicki, W. Felisiak. Application of Cohen's class time-frequency distributions in the Belousov-Zhabotinsky reaction analysis, International Journal of Bifurcation and Chaos in Applied Sciences and Engineering, Volume 14, Issue 10, Pages 3679 – 3688 October 2004*; *K. Darowicki, A. Krakowiak, A. Zielinski, A New Methods of Spectral Analysis of Current Oscillations of Electrochemical Processes, Journal of the Electrochemical Society, Open Access, Volume 148, Issue 5, Pages E233-E236May 2001*; *K. Darowicki, A. Krakowiak, A. Zielinski, Analysis of spontaneous electrochemical oscillations by energy distribution technique, Electrochimica Acta, Volume 48, Issue 11, Pages 1559 - 156615 May 2003).*
By defining the kernel function according to the equation

$$\phi(t,\tau) = \frac{1}{\sqrt{4\pi\alpha\tau^2}} exp\left(-\frac{t^2}{4\alpha\tau^2}\right) \tag{2-7}$$

where: $\phi(t,\tau)$ – exponential kernel function, α – kernel bandwidth parameter

and by introducing it into the Wigner-Ville distribution formula, we get the Choi-Williams distribution:

$$CWD(t,\omega) = \int\int \frac{1}{\sqrt{4\pi\alpha\tau^2}} exp\left[-\frac{(t-u)^2}{4\alpha\tau^2}\right] s\left(u+\frac{\tau}{2}\right) s^*\left(u-\frac{\tau}{2}\right) \exp(-j\omega\tau)\, dud\tau \tag{2-8}$$

A Choi-Williams distribution diagram corresponding to the recorded time variations of the BZ oscillation (Fig. 2-3) is shown in Fig. 2-5.

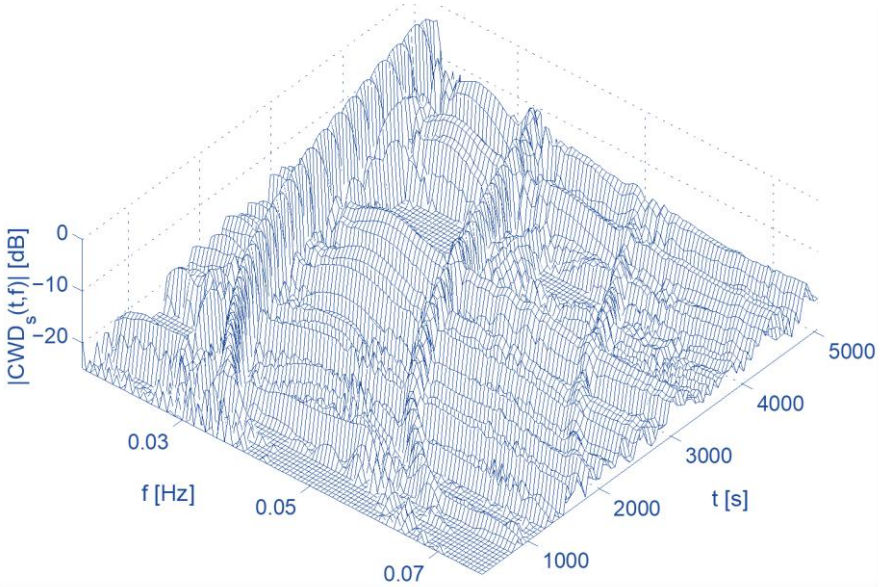

Fig. 2-5A. Choi–Williams distribution of oscillatory changes in potential of the BZ reaction (Fig. 2-3) determined for the kernel function parameter $\alpha = 1$

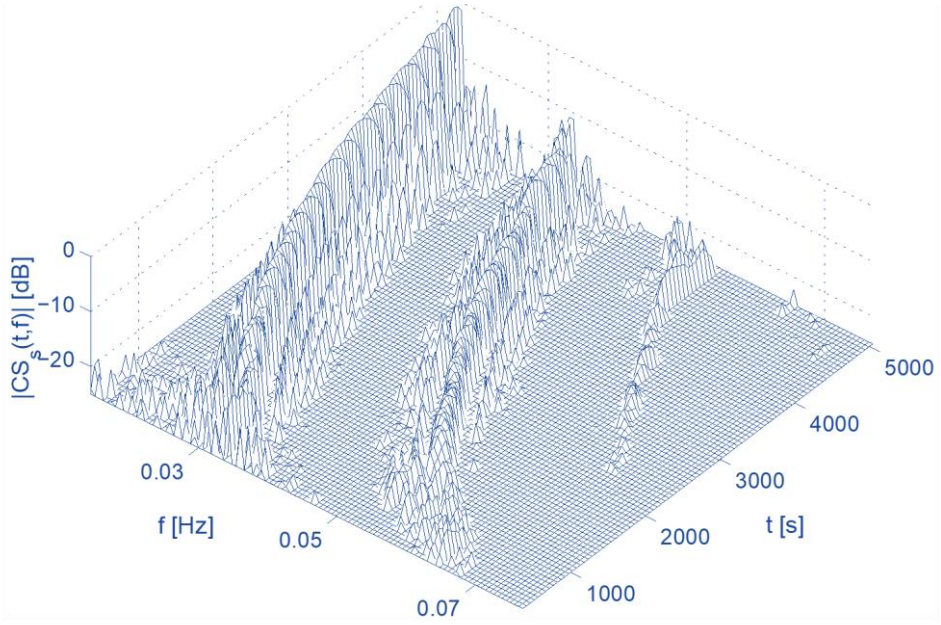

Fig. 2-5B. Choi–Williams distribution of oscillatory changes in potential of the BZ reaction (Fig. 2-3) determined for the kernel function parameter $\alpha = 0.05$.

As the value of the alpha parameter decreases, the attenuation of interference bands becomes gradually visible, and main bands become more and more exposed. The results of the analysis are even more unequivocal when we use the following equation as a kernel function:

$$\phi(t,\tau) = \begin{cases} \frac{1}{\tau} exp(-\alpha\tau^2) \; dla \; |\tau| \geq 2|t| \\ 0 \qquad\quad dla \;\; |\tau| < 2|t| \end{cases} \tag{2-9}$$

In this case, we obtain a cone-shaped distribution.

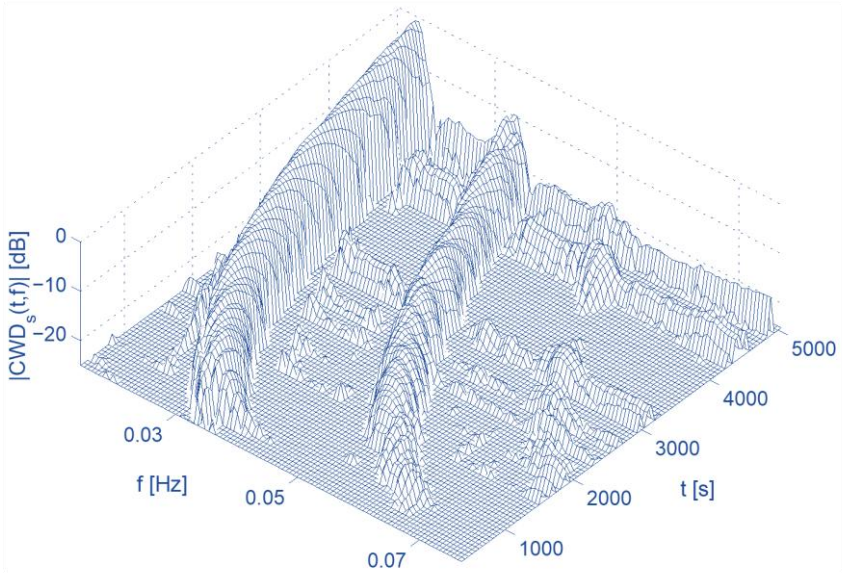

Fig. 2-6A. Cone-shaped distribution of oscillatory changes in potential of the BZ reaction (Fig. 2-3) determined for the kernel function parameter $\alpha = 0.05$.

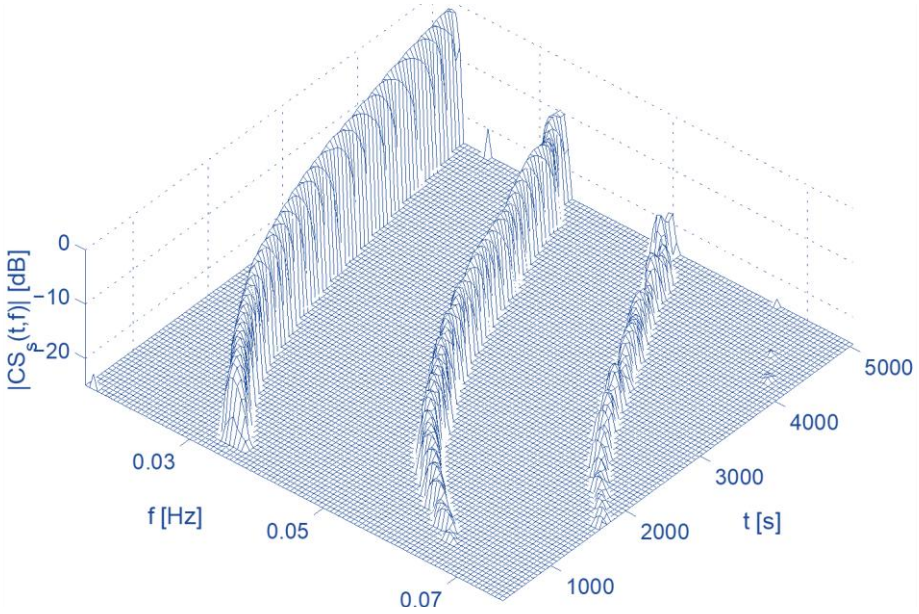

Fig. 2-6B. Cone-shaped distribution of oscillatory changes in potential of the BZ reaction (Fig. 2-3) determined for the kernel function parameter $\alpha = 1$.

In the case of cone-shaped distribution, attenuation of interference bands is the most effective. For the alpha parameter equal to one, the interference bands have been completely removed.

The wavelet transformation is extremely useful in the analysis of spontaneous oscillations. (*K. Darowicki, W. Felisiak, A. Zieliński. Application of discrete wavelet transform in the analysis of nonlinear chemical system, Journal of Mathematical Chemistry, Volume 38, Issue 4, Pages 701 - 711July 2005).*

The applications of discrete wavelet transformation in the analysis of the Belousov-Zhabotinsky oscillatory reaction made it possible to recognize individual reaction stages. The characteristic moments, corresponding to chemical transformations, were clearly visible as details of the distribution on the calculated scalograms. It has been shown that this method can provide information about the dynamics of chemical oscillations. Based on the analysis of local maxima on a wavelet scalogram, the nature of the oscillation frequency attenuation can be determined.

Distributions based on autocorrelation functions are not the only forms of studying non-stationary processes. A much simpler method of analyzing non-stationary processes is the short-time Fourier transformation (STFT). The operation of this transform is described by the equation:

$$STFT(t,\omega) = \int s(\tau)\gamma^*(\tau - t)\exp(-j\omega\tau)\,d\tau \tag{2-10}$$

where: $\gamma^*(\tau - t)$ - analysing window function.

This window moves over a given time register. Each time, the window cuts out a fragment of the tested signal that corresponds to the time instant t. This fragment is then subjected to the Fourier transformation. In this way, we obtain a frequency spectrum determined for time t. In the next step, the analysing window moves to the next time and the operation is repeated identically. The operation of the STFT transformation is illustrated by the scheme shown in Fig. 2-7.

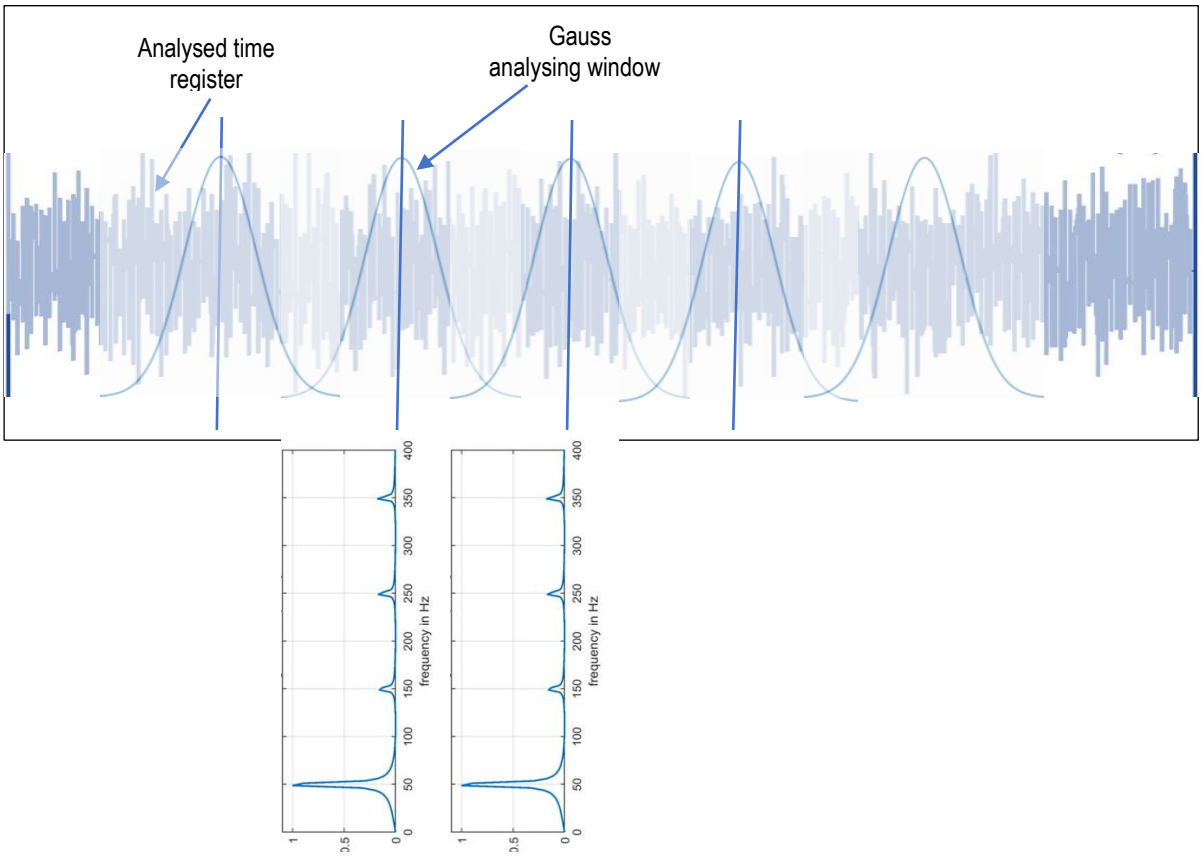

Fig. 2-7. A scheme illustrating the operation of short-time Fourier transformation (STFT)

The collection of local spectral power density spectra as a function of time gives the STFT spectrogram. The size and type of analysis window play a fundamental role in this type of time-frequency analysis. From a mathematical point of view, the optimal window is the Gaussian peak. he Gaussian peak located at time t_o is given by the relationship:

$$s(t) = \sqrt{\frac{\alpha}{2\pi}}exp\left\{-\frac{\alpha}{2}(t - t_o)^2\right\} \tag{2-11}$$

Its Fourier transform is equal to:

$$S(\omega) = \int \sqrt{\frac{\alpha}{2\pi}}exp\left\{-\frac{\alpha}{2}(t - t_o)^2\right\}\exp(-j\omega t)\,dt \Leftrightarrow exp\left\{-\frac{\omega^2}{2\alpha} + j\omega t_o\right\} \tag{2-12}$$

Thus, the Gaussian peak after transformation from the time domain to the frequency domain is also a Gaussian peak. An increase in the width of the Gaussian peak in the time domain Δ_t (deterioration of time selection) results in a decrease in the

width of this peak in the frequency domain Δ_ω (improvement in frequency resolution). Frequency resolution and time selection are closely related:

$$\Delta_t \Delta_\omega = \frac{1}{2}$$

For windows of a different type:

$$\Delta_t \Delta_\omega > \frac{1}{2} \qquad (2\text{-}14)$$

Knowledge of these basic relationships allowed for the determination of STFT spectrograms of chemical oscillations. Fig. 2.8 shows oscillations of potential of the Belousov-Zhabotinsky reaction. The first visual assessment reveals a number of characteristic time fragments (segments).

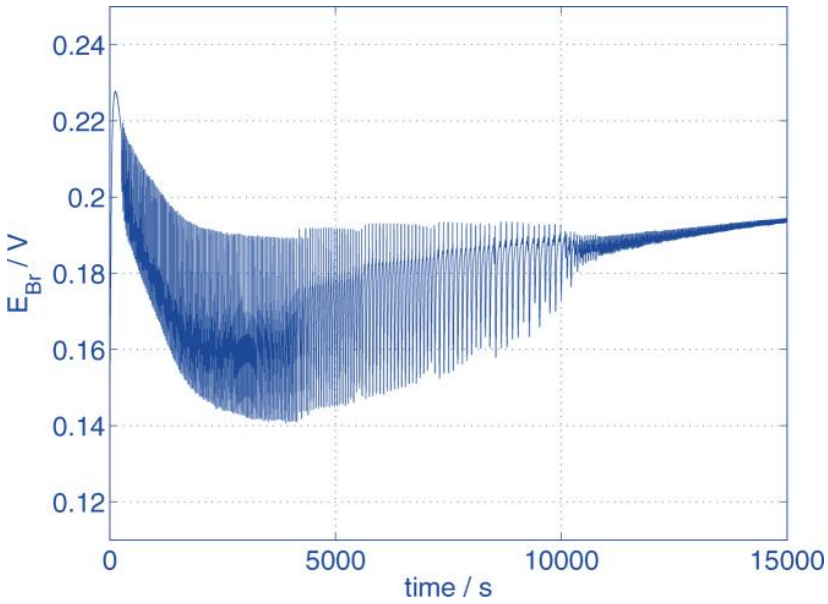

Fig. 2-8. Register of changes in the redox potential of the Belousov-Zhabotinsky reaction

Determining the *STFT* spectrogram of the Belousov-Zhabotinsky oscillations shown in Fig. 2-8 allows observation of the phenomenon of frequency multiplication and their changes over time.

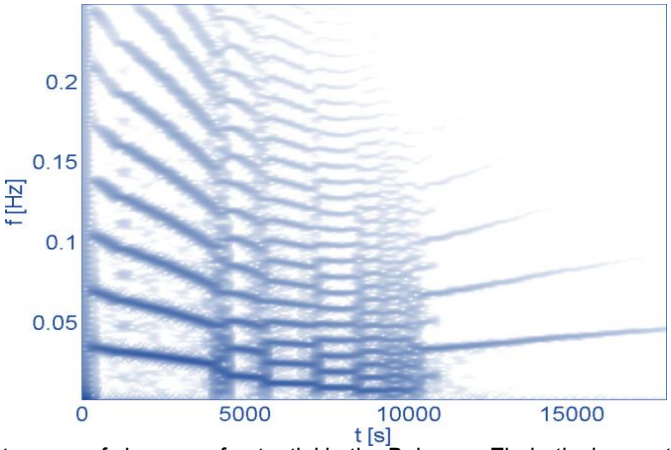

Fig. 2-9. STFT spectrogram of changes of potential in the Belousov-Zhabotinsky reaction shown in Fig. 2-8

In each segment, changes in the oscillation frequency are deterministic, and the formation of successive segments is directly related to multiplications of previous frequencies. These transitions are stepwise. (*K. Darowicki, W. Felisiak, A. Zielinski, A novel method of spectral analysis of oscillatory Belousov-Zhabotinsky reaction, Journal of Mathematical Chemistry, Volume 33, Issue 3-4, Pages 245 – 254 May 2003; K. Darowicki, W. Felisiak, On the joint time-frequency characteristics of chemical oscillations, Journal of Computational Chemitry, Volume 27, Issue 8, Pages 961 – 965 June 2006}.*

Oscillatory reactions are a large research area. As we have shown, the use of time-frequency analysis methods is fully justified. However, there are other phenomena that can be successfully studied in the joint time-frequency domain. Such a phenomenon is the Portevin-LeChatelier (PLC) effect revealed in stress-strain investigations, Fig. 2-10. The observed serration refers to a set of plastic instabilities, manifesting as a non-monotonic stress-strain behaviour. We performed a time-frequency analysis of this effect. (*K. Darowicki, J. Orlikowski, A. Zielinski, Frequency bands selection of the Portevin-LeChatelier effect, Computational Materials Science, Volume 43, Issue 2, Pages 366 - 373August 2008).*

.

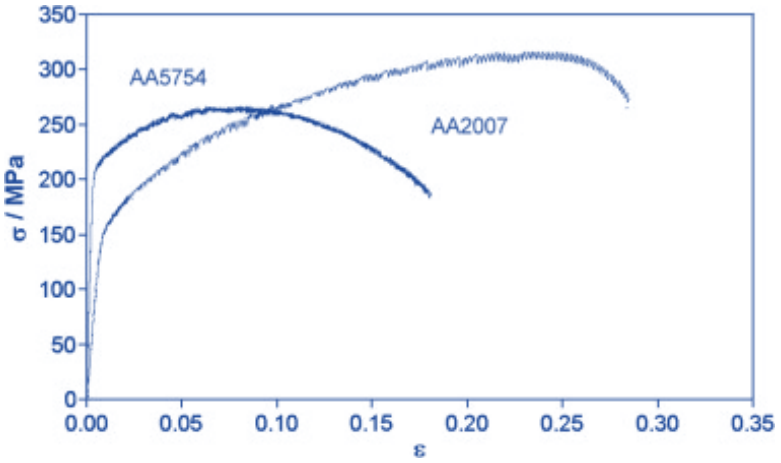

Fig. 2-10. Mechanical stress-strain dependences determined for AA5754 and AA2007 alloys (strain rate 0.002 s^{-1})

Conducting a deeper time-frequency analysis revealed the formation of frequency bands related to the structure of the tested alloys.

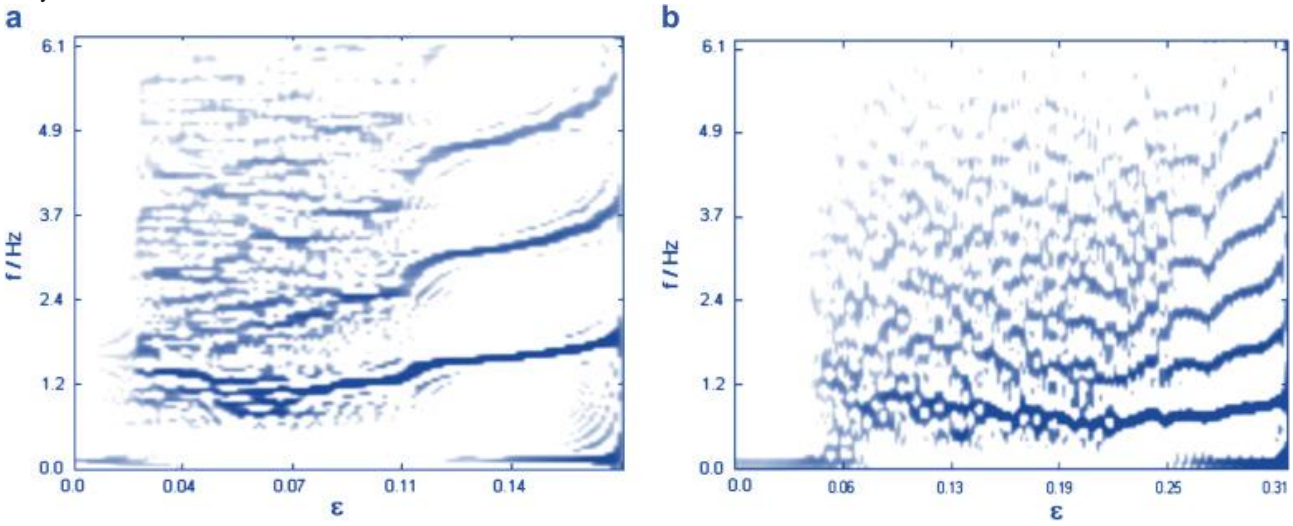

Fig. 2-11. Cone-shaped distributions of stress-strain registers determined for alloys AA5754 and AA2007 (strain rate 0.0002 s^{-1})

The time-frequency characteristics of the Portevin-LeChatelier process are our original achievement

The proposed filtering method allowed for selective separation of different types of serration, making it possible to obtain mechanical characteristics. The analysis allowed for the precise determination of the strain ranges in which individual types of serration occur. Moreover, it was possible to estimate changes in the frequency of the serration process in the strain domain. Serration frequency characteristics revealed the discrete structure of individual bands, which undergo monotonic

changes during the stretching process. The presented methodology allows for a much more accurate analysis of mechanical registers compared to previously used solutions.

3. ELECTROCHEMICAL NOISE

The corrosion process is manifested by current and/or potential fluctuations of low frequency and infinitesimally low amplitude. These fluctuations are called Electrochemical Noise (EN). Electrochemical noise can be measured separately (then only potential or current noise at a given moment is measured) or simultaneously (then both noise signals are measured at the same time). During separate measurements, potential noise can be measured as potential fluctuations between two nominally similar working electrodes or between a working electrode and a zero-noise reference electrode. Current electrochemical noise can be measured as the current fluctuation between the working electrode and the counter electrode under potentiostatic control conditions or between two nominally identical working electrodes. Simultaneous measurement is more effective, in this mode, potential noise and current noise are measured simultaneously. This mode is implemented either by coupling two nominally identical working electrodes connected by a zero-ammeter. At the same time, the potential noise of these coupled electrodes versus the reference electrode is measured. Electrochemical noise can be measured conventionally in a three-electrode system in which current noise is measured between the working electrode and the counter electrode, while potential noise is measured between the working electrode and the zero-noise reference electrode. (*J. Smulko, K. Darowicki, P. Wysocki, Digital measurement system for electrochemical noise, Polish Journal of Chemistry, Volume 72, Issue 7, Pages 1237 – 1241 July 1998).* The essence of measuring electrochemical noise is the lack of external perturbation, natural fluctuations are recorded. From the point of view of interpretation, stationarity is a convenient simplification. (*K. Darowicki, A. Zielinski, The analysis of stationary electrochemical noise, Polish Journal of Chemistry, Volume 78, Issue 9, Pages 1261 – 1268 September 2004)*

In practice, the EN technique is mainly used to identify local corrosion.

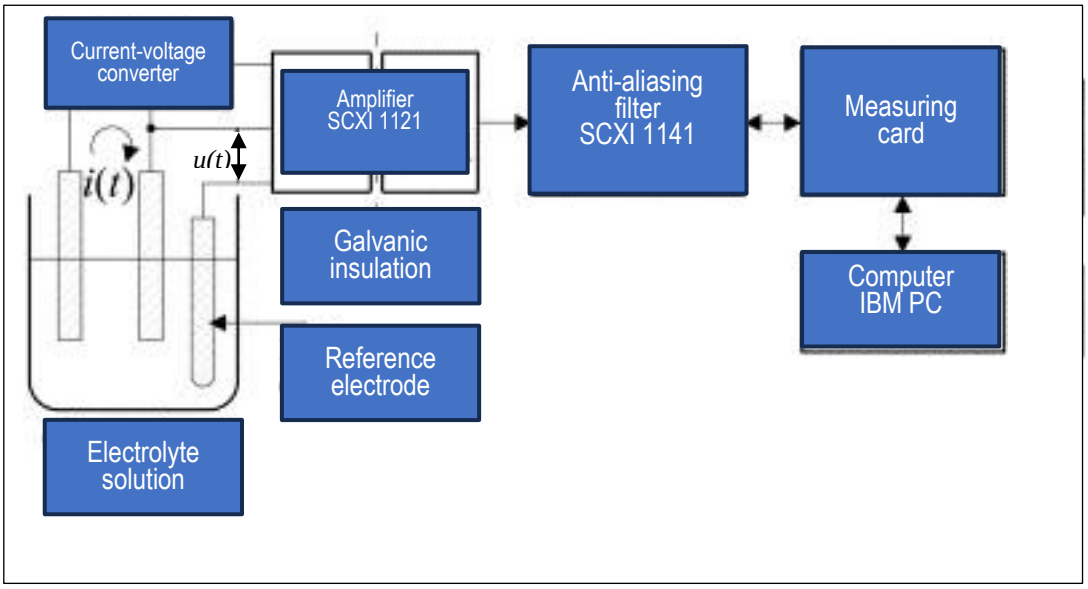

Fig. 3-1. Digital three-electrode electrochemical noise measurement system, *i(t)* – recorded current electrochemical noise , *u(t)* – recorded voltage electrochemical noise

The current noise and voltage noise of three identical electrodes made of carbon steel are shown in Fig. 3-2.

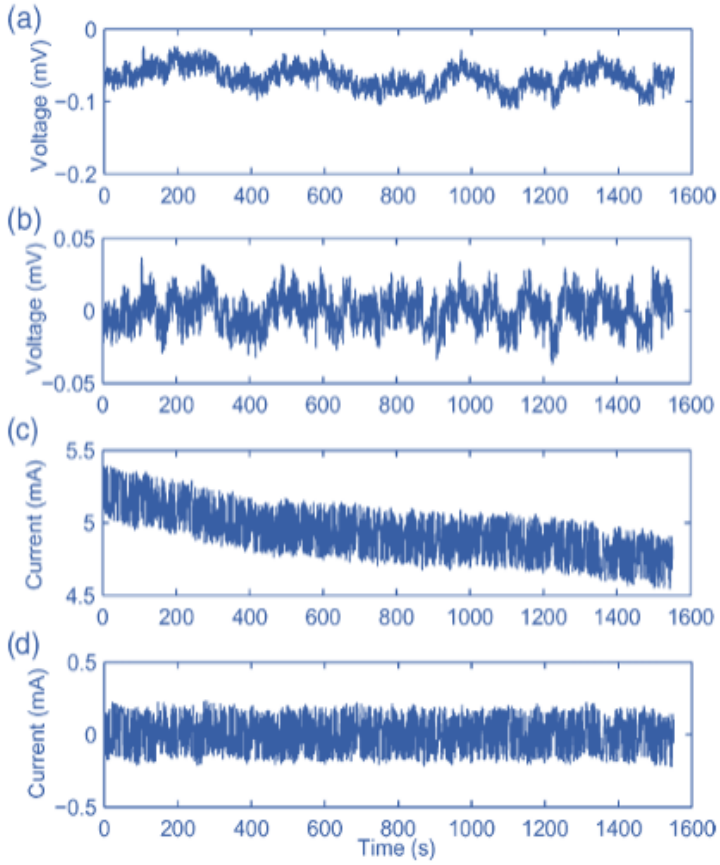

Fig. 3-2. Exemplary electrochemical noise registers. (a) observed voltage noise, (b) voltage noise after trend removal, (c) observed current noise, (d) current noise after trend removal

Sources of electrochemical noise are represented in an electrical equivalent circuit of the corrosion process of steel in an acidic environment.

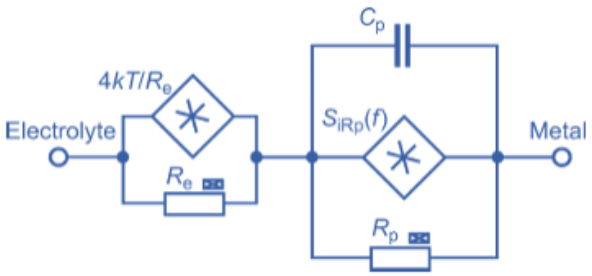

Fig. 3-3. Noise electrical equivalent circuit.

Voltage noise was processed and analysed according to the diagram shown in Fig. 3-4.

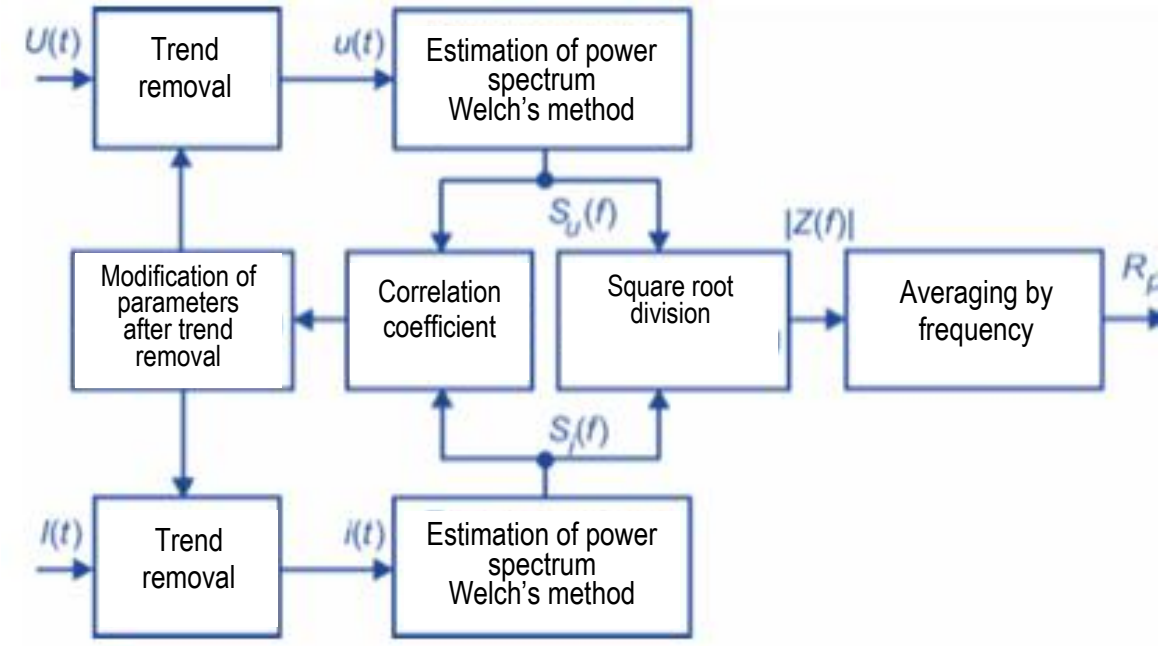

Fig. 3-4. Author's method for calculating polarization resistance, $S_i(f)$ - spectral power density of current noise, $S_u(f)$ - spectral power density of voltage noise, $|Z(f)|$ – impedance modulus, R_P – polarization resistance, f – frequency.

Adoption of the noise circuit (Figure 3-3) allows determination of the spectral power density of the recorded current noise. When a trend is removed, the spectral power density is equal to:

$$S_i(f) = 2S_{iR_P}(f)|Z(f)|^2 + 4kTR_E|2Z(f) + R_E| + S_{in}(f) \tag{3-1}$$

where $S_i(f)$ - spectral power density of the input current noise source of the internal measurement system, $Z(f) = Rp/(1 + j2\pi fRpCp)$ - impedance of parallel connection of Rp and Cp. This equation was derived by summing two independent current noise sources having the same power spectra $S_{iR_P}(f)$.

After removing the trend, the spectral power density of the voltage noise is equal:

$$S_u(f) = 1.5S_{iR_P}(f)|Z(f)|^2 + 4kTR_E + S_{un}(f) \tag{3-2}$$

where $S_{un}(f)$ is the spectral power density of the input voltage noise source of the internal measurement system.

Equation (3-2) refers to the noise circuit formed between two shorted working electrodes and a reference electrode. Neglecting thermal noise leads to the equations:

$$S_i(f) = 0.5S_{iR_P}(f) \tag{3-3a}$$

$$S_u(f) = 1.5S_{iR_P}(f)|Z(f)|^2 \tag{3-3b}$$

these, in turn, allow determination of polarization resistances based on simultaneous spectral analysis of voltage noise and current noise:

$$Rp \approx \lim_{f\to 0} Z(f) = \lim_{f\to 0}\left|\frac{Rp}{1 + j2\pi fRpCp}\right| = \sqrt{\frac{1}{3}}\sqrt{\frac{S_u(f)}{S_i(f)}} \tag{3-4}$$

The described method was successfully used in a real corrosion system — water-main pipe. It takes into account all problems that arise when analysing real data: the need to effectively remove trends from noise registers and the recording of a limited time frame in which the stochastic signal is observed.

Estimating a linear correlation coefficient between spectral power densities of trendless current and voltage noise gives information on whether recorded noise records are caused by the same noise sources that represent uniform corrosion

processes. The obtained results confirm that some noise records may be more questionable than others and should not be used to estimate Rp values. Correctly recorded electrochemical noise registers have a correlation coefficient between $S_i(f)$ and $S_u(f)$, that is higher than the assumed limit value. This limit was lowered compared to the value predicted by the statistical test conducted.(*J. Smulko, K. Darowicki, A. Zieliński, Detection of random transients caused by pitting Corrosion, Electrochimica Acta, Volume 47, Issue 8, 1 February 2002, Pages 1297-1303).* The proposed method and the possibility of excluding questionable registers make the described and discussed method of analysing electrochemical noise more reliable than a simple method based solely on the estimation of noise resistance.

The presented method of analysing electrochemical noise is our original achievement and provides prospects for its use in online corrosion monitoring. Proposed method for determining polarization resistance, Rp is distinguished by the fact that the resistance is determined without external perturbation.

The electrochemical noise of local corrosion processes, such as pitting corrosion, is non-stationary. In this case, electrochemical noise can be interpreted as a superposition of numerous elementary transient signals located at randomly distributed time instants. Due to the inherent non-stationarity of this type of record, it is necessary to introduce a methodology enabling the analysis of the time evolution of the spectral power density. Two types of transformations are presented to obtain time-dependent spectra: $STFT(f,t)$ and wavelet transformation.(*K. Darowicki, A. Zielinski, Joint time–frequency analysis of electrochemical noise, Journal of Electroanalytical Chemistry, Volume 504, Issue 2, 18 May 2001, Pages 201-207).*

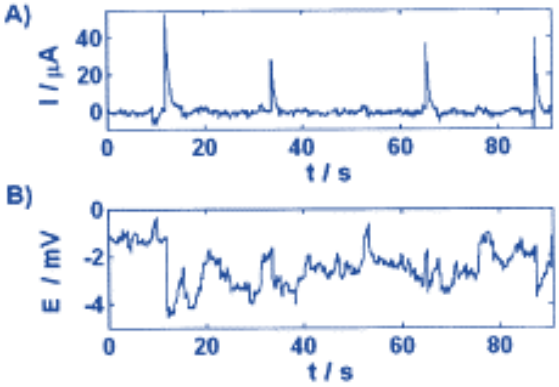

Fig. 3-5. Electrochemical noise time registers of a 304 steel electrode in a 0.6 M $FeCl_3$ solution. Sampling frequency 45 Hz, (A) current electrochemical noise, (B) voltage electrochemical noise

Corresponding spectrograms $STFT\ (f,t)$ are presented in Fig. 3-6.

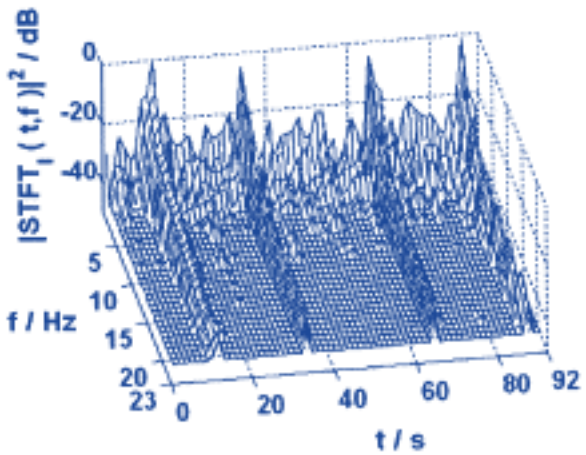

Fig. 3-6A. The STFT spectra of the current noise shown in Fig. 3.5A. A Hanning window of length 128 pt. was used. 304 steel immersed in a 0.6 M $FeCl_3$ solution. Sampling frequency 45 Hz.

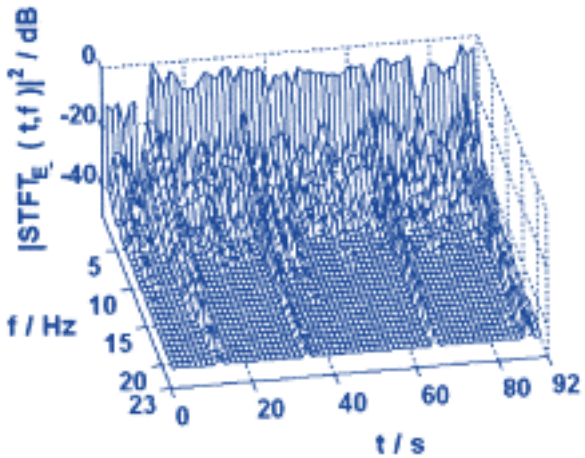

Fig. 3-6B. The STFT spectra of the voltage noise shown in Fig. 3.5B. A Hanning window of length 128 pt. was used. 304 steel immersed in a 0.6 M FeCl3 solution. Sampling frequency 45 Hz.

Another form of time-frequency analysis is the wavelet transformation. In this case, the analysis is performed based on selected base functions. Sine functions are not used.

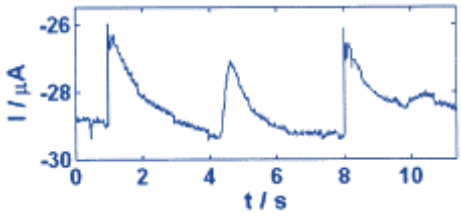

Fig. 3-7. Current noise time register of a 304 steel electrode in a 0.6 M $FeCl_3$ solution. Sampling rate $45\ Hz$.

The current noise register is a composition of instantaneous, sharp increases and exponential decreases in current values. Such behaviour cannot be represented as a composition of elementary sinusoidal signals. Instead of a sine wave, one should choose a different nature of the base function, the so-called mother wavelet. In this way, each transient signal can be represented as a composition of a mother wavelet and a set of wavelets that are rescales of the mother wavelet. A 'simlet8' wavelet was used to analyse the recorded electrochemical current noise of the steel electrode 304 in the $FeCl_3$ solution.

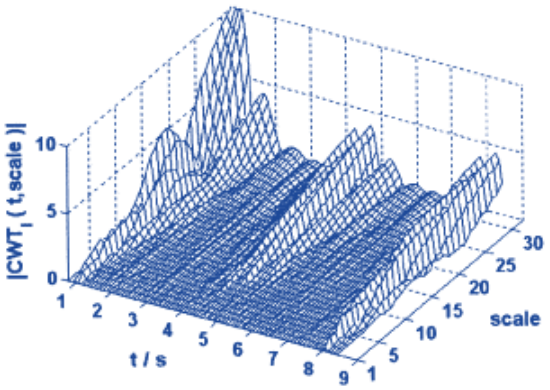

Fig. 3-8. Continuous wavelet transformation module of current noise (Figures 3-7) as a function of time and scale. The analysis was performed using a „symlet 8" wavelet. 304 steel electrode in 0.6 M FeCl3 solution. Sampling frequency 45 Hz.

The obtained scalogram allows for a more detailed analysis of individual events, such as a sudden increase and exponential decrease in current.

The presented methodology is innovative in the study of electrochemical and corrosion processes.

The non-stationary signals encountered in electrochemical practice come from the non-linear and temporal variability of the parameters characterizing the investigated systems. We have shown that the classical analysis technique, based on the Fourier transformation, is insufficient for systems subject to changes over time.

The JTFA technique, which ensures simultaneous examination of the time and frequency properties of a given system, is currently the only tool allowing the application of spectral analysis to the class of non-stationary signals (*K. Darowicki, A. Zielinski, Application of non-stationary techniques in the analysis of electrochemical noise, Fluctuation and Noise Letters, Volume 4, Issue 2, Pages L267-L272 June 2004).*
Despite its undoubted usefulness, there are some limitations to the applicability of the techniques mentioned above. Some of them are fundamental principles, such as the uncertainty principle, equation (2-14), and cannot be eliminated. This introduces the need to use compromises, which, however, cannot lead to incorrect interpretation of measurement results. The proper selection of analysis parameters in discrete domains, determining the redundancy/resolution of the transformation, is another aspect. For the wavelet transformation, there are a number of available base functions. Choosing the right one for a given application is an important practical question. All these issues remain open in the analysis of electrochemical noise.

One of the basic tools in the analysis of stochastic processes is the autocorrelation function related to the power spectrum through the Wiener–Khinchin theorem. Consequently, it is possible to construct frequency spectra, the order of which is higher than 2. This is realized by the transformation of correlation series known as cumulants. The third-order cumulant of the zero mean stochastic stationary signal is given by the formula:

$$c_{3x}(t_1, t_2) = E[x^*(t)x(t + t_1) + x(t + t_2)] \quad 3\text{-}5$$

where: $c_{3x}(t_1, t_2)$ – the third-order cumulant.

The Fourier transformation of the third-order cumulant leads to the third-order spectrum of the known bispectrum:

$$C_{3x}(f_1, f_2) = \sum_{t_1 \to -\infty}^{\infty} \sum_{t_2 \to -\infty}^{\infty} c_{3x}(t_1, t_2)\exp(-2j\pi f_1 t_1)\exp(-2j\pi f_2 t_2) \quad 3\text{-}6$$

Normalized function $C_{3x}(f_1, f_2)$ is called the autobicoherence function:

$$B_{3x}(f_1, f_2) = \frac{C_{3x}(f_1, f_2)}{\sqrt{S_{xx}(f_1 + f_2)S_{xx}(f_1)S_{xx}(f_2)}} \quad 3\text{-}7$$

where: $B_{3x}(f_1, f_2)$ – autobicoherence function, $S_{xx}(f)$ – spectral power density of x signal.
Bispectrum is a tool to assess the stationarity of electrochemical noise. It is worth noting that stationarity is crucial for the correctness of further analysis of electrochemical noise. For a properly sampled stationary stochastic process, the bispectrum should be zero. Fig. 3-9 shows two exemplary time registers. The first time register is Gaussian white noise (0.1). The second time register is a white noise and ramp signal.

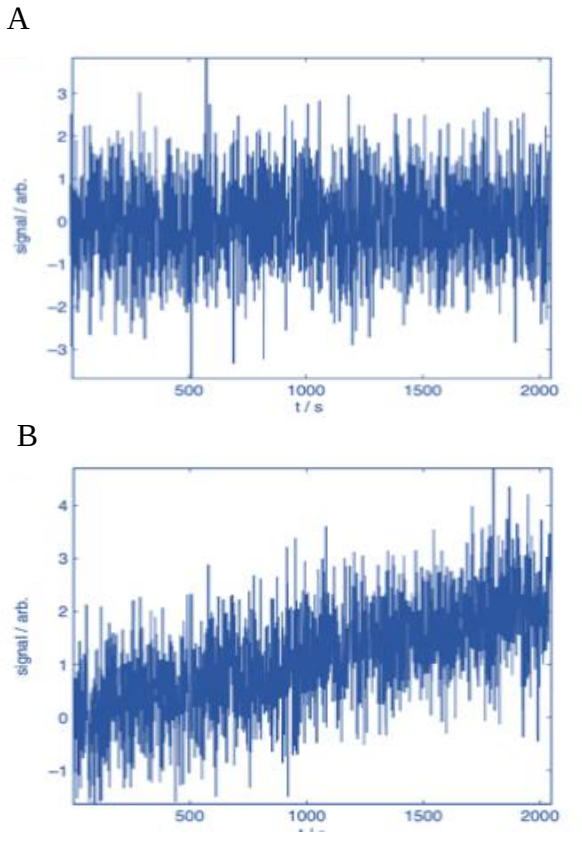

Fig. 3-9A. Exemplary stochastic time registers. (a) Gaussian white noise (0,1) and normalized bispectrum, (B) Sum of white noise and ramp signal

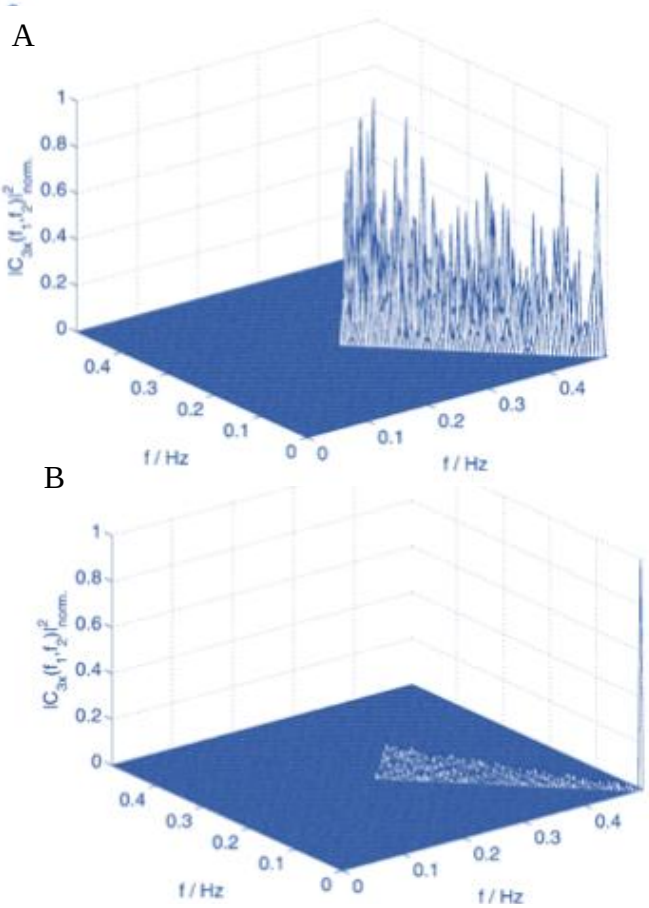

Fig. 3-9B. Normalized bispectra (A) Gaussian white noise (0,1) and normalized bispectrum, (B) Sum of white noise and ramp signal

The pre es the shap ive tool bet chemical n all frequen trum is visible for specific frequencies; an intense peak located near the bifrequency (0; 0.5) Hz can be seen. An additional value of this transformation analysis is the ability to perform a stationarity test from one time register. (*K. Darowicki, A. Zielinski, Analysis of electrochemical noise by means of bispectral technique, Journal of Solid State Electrochemistry, Volume 11, Issue 1, Pages 109 – 116 November 2006).*

Third-order spectral projection was used to analyse the actual current registers of CrNi18-9 steel electrodes in 1 M $FeCl_3$.

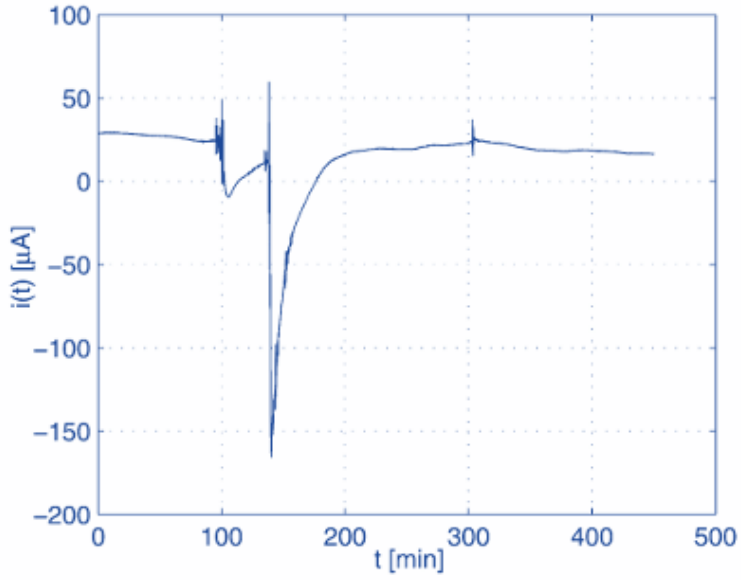

Fig. 3-10. Exemplary register of changes in the current of a single event as a function of time on a CrNi18-9 steel electrode in 1 M $FeCl_3$ solution.

The observed transient phenomenon is typical of pitting corrosion. The number of visible transitions in data records was stable during data recording. The observed electrochemical noise was treated as a random signal, which is a composition of elementary transient signals (rapid increase in current, exponential decrease).
The characteristics of the system can only be recognized by statistical analysis of the recorded noise. (*J. Smulko, K. Darowicki, Pitting corrosion in steel and electrochemical noise intensity, Electrochemistry Communications, Volume 4, Issue 5, May 2002, Pages 388-39).*
Based on time-frequency analysis, we are unable to determine whether non-linear events are significant or not. Our aim was to characterize the non-linear components of observed fluctuations by using a third-order cumulant and its Fourier transform called the bispectrum. (*J. Smulko, K. Darowicki, A. Zielinski, Detection of random transients caused by pitting Corrosion, Electrochimica Acta 47 (2002) 1297–1303).*
The electrode surface showed distinct pitting of varying size and depth. Each working electrode of about 3.5 cm^2 surface area had over a dozen visible and separate pits up to about 1 mm deep and no more than 1–3 mm^2 in size. Fig. 3-11 shows the spectral power density of the recorded current noises. The $S_i(f)$ function obtained for all electrode sets had a visible drop around the frequency $f \sim 10^{-2}\ Hz$, which is important for the presence of transitions in the recorded noise. Spectral power densities were calculated using the Welsh's averaged method from noise records, each approximately 6×10^5 noise samples long. A single spectrum was calculated from 214 samples using Hanning windowing. Such a large number of samples for each spectrum made it possible to estimate the spectral power density at very low frequencies up to single millihertz. The spectral power densities in Fig. 3-11 were averaged over L = 36 spectra. The random error of the calculated spectral power density was inversely proportional to the square root of L, corresponding to 16%. The values of the total weight loss, Δm, for the working electrodes are also given in Fig. 3-11.

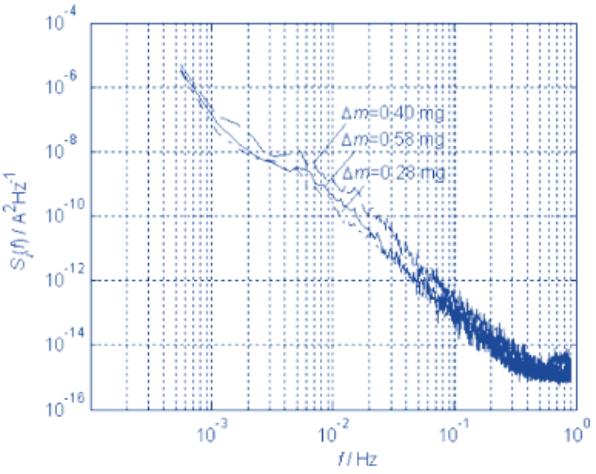

Fig. 3-11. Spectral power density $S_i(t)$ of recorded current noise for three identical electrodes of CrNi18-9 steel in 1 M $FeCl_3$ together with corresponding Δm mass losses Δm

The corresponding bispectrograms of the determined time registers of current noise are shown in Fig. 3-12.

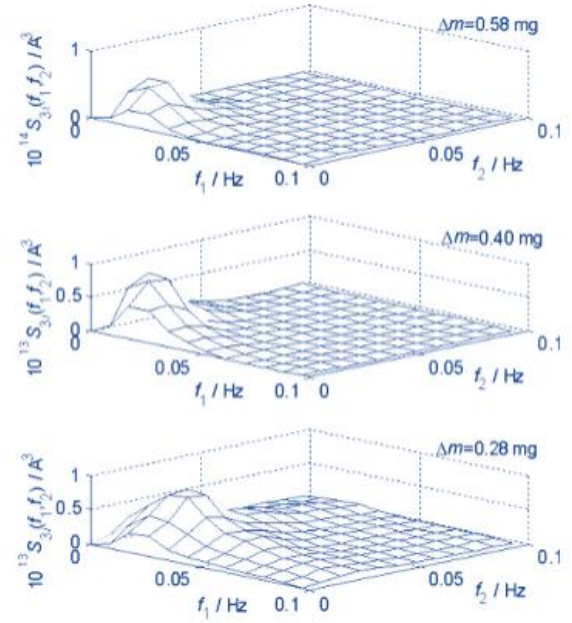

Fig. 3-12. Bispectra $S_{3i}(f_1, f_2)$ of recorded current noise for three identical carbon steel electrodes together with corresponding mass losses Δm

The different bispectrogram shapes observed can be explained by the effectiveness of electrode repassivation processes. The measured, different changes in the mass of the working electrodes reflect different positions of the maximum on the bispectrum. This suggests that the bispectrum can be thought of as a potentially sensitive measure of pitting corrosion processes. We would like to emphasize that there is no independent evidence to support the explanation presented, but the proposed reasoning explains the behaviour of the calculated bispectrum functions and is supported by theoretical pitting corrosion models. Other published results of the use of the bispectrum function confirm that the bispectrum appears to indicate structure in the noise data studied (presence of transient states). The proposed non-linearity measures in the noise records provide additional information about the nature of the observed corrosion process. The suggested explanation for the course of the bispectrum links its behaviour to repassivation processes in metastable pitting events.

Our achievement is the development of a new method for analysing electrochemical noise. Bispectrum can be thought of as a potentially sensitive measure of the stationarity and non-stationarity of pitting corrosion processes.

The intensity and identification of corrosion processes are one of the more serious monitoring issues. In pitting corrosion, a local type of corrosion attack, a very popular method of analysing noise data is to study its pitting index and spectral power density. The value of the pitting index is based on the measured average current, while the observed current noise is mainly caused by one of two partial currents (anodic or cathodic). This fact significantly limits the use of the pitting index for recognizing and assessing local corrosion. When transient states characteristic of pitting corrosion occur in the data record, the spectral power density of the noise has different slopes in some frequency regions. The mentioned fact ensures the detection of pitting corrosion, but does not provide any information about its intensity. Another method is based on a wavelet transformation that decomposes the recorded noise into parameters related to band-filtered noise components. The energy or standard deviation of the successive components can be easily calculated. The distribution of the estimated standard deviation of the noise components may be characteristic of different corrosion processes. It is important to recognize which components are most valuable for assessing pitting corrosion intensity and which are mainly caused by other noise sources. (*J. Smulko, K. Darowicki, A. Zielinski, Pitting corrosion in steel and electrochemical noise intensity, Electrochemistry Communications, Volume 4, Issue 5, Pages 388 – 391, 2002).*

While studying the pitting corrosion of CrNi18-9 steel in 1 M $FeCl_3$, we noted elementary transient signals in the electrochemical current noise registers. The shapes of the recorded transient events can be characterized by a rapid increase in the instantaneous value of the current and an exponential decrease to the previous state. If transient events take an exponential course ($\sim exp(-t/\tau)$, then a decrease around the frequency $f_s = 1/2\pi\tau$ should be observed on the spectral power density spectrum.

The time notation of the discrete signal $x(t_n)\ n = 1, 2 \ldots . n$ can be decomposed using a wavelet transformation into a set of bands called approximations and details, which are low-frequency and high-frequency components of the discrete signal $x(t_n)\ n = 1, 2 \ldots . n$. Mallat proposed a discrete wavelet transformation algorithm that performs such an operation.

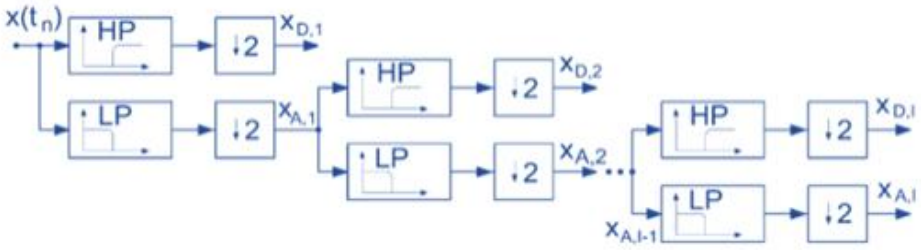

Fig. 3-13. Filter bank implementing discrete signal division $x(t_n)\ n = 1, 2 \ldots . n$ into details by wavelet transformation.

The filter bank shown in Fig. 3-13 at its core is an algorithm for decomposing the discrete signal $x(t_n)\ n = 1, 2 \ldots . n$ via discrete wavelet transformation. At each decomposition level, the analyzed signal is filtered by a pair of high-pass (HP) and low-pass (LP) digital filters, called mirror or quadrature filters. After filtering, the output signals were sampled. Based on the correlation of mass loss with standard deviations of individual details, we proposed a new parameter for assessing the intensity of pitting corrosion. This parameter is the standard deviation σ_{Di}.

The linearization condition is closely related to harmonic analysis. The main effect of non-linearity has been shown to be the generation of higher than fundamental harmonics in the output signal. In the case of linear systems, when a monofrequency sinusoidal perturbation is applied, a monofrequency sinusoidal output signal of the same frequency is obtained. In contrast, when a single frequency sinusoidal perturbation is applied to a non-linear system, the output signal will consist of a fundamental signal (a sinusoidal signal with the same frequency as the perturbation signal) with harmonic, sinusoidal signals superimposed thereon at frequencies corresponding to integer multiples of the fundamental frequency.

To demonstrate the usefulness of time-frequency methods, a model system simulating the first-order electrode reaction occurring under activation control conditions was investigated. (*K. Darowicki, Frequency dispersion of harmonic components of the current of an electrode process, Journal of Electroanalytical Chemistry, Volume 394, Issue 1-2, Pages 81 - 8619 September 1995).*

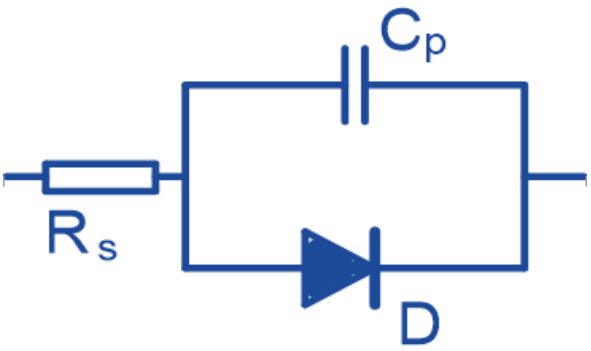

Fig. 4-1. Model non-linear electrical circuit: C_P- parallel capacitance simulating double electrical layer capacitance, D – diode simulating the first-order electrode reaction, R_S – series resistance simulating electrolyte resistance.

The capacitor represents the capacitance of the electrical double layer. The current characteristic of the diode given by the following equation:

$$i(E) = i(E_S)expb_D(E - E_S) \tag{4-1}$$

corresponds to the Volmer-Butler relationship.

The system defined in this way was subjected to the following perturbation:

$$E(t) = E_S + \left(\frac{dE}{dt}\right)t + \Delta E_o cos\omega_o t \tag{4-2}$$

The theoretically determined current for the electrical model is equal:

$$i(t) \approx i(E_S)expb_D\left[\left(\frac{dE}{dt}\right)t + \Delta E_o cos\omega_o t\right] + C_p\left\{\frac{d\left[\left(\frac{dE}{dt}\right)t + \Delta E_o cos\omega_o t\right]}{dt}\right\}$$
$$= i(\omega = 0, t) + \Delta i(\omega_o, t) + \Delta i(2\omega_o, t) + \Delta i(3\omega_o, t) + \cdots$$
$$= i(\omega = 0, t) + vC_p + i(E_S)\left[1 + \frac{b_D^2 \Delta E_o^2}{4}\right]exp(b_D vt)$$
$$+ i(E_S)\left[b_D \Delta E_o + \frac{b_D^3 \Delta E_o^3}{8} + \cdots\right]exp(b_D vt)cos\omega_o t - C\Delta E_o sin\omega_o t$$
$$+ i(E_S)\left[\frac{b_D^2 \Delta E_o^2}{24} + \cdots\right]exp(b_D vt)cos2\omega_o t + i(E_S)\left[\frac{b_D^3 \Delta E_o^3}{8} + \cdots\right]exp(b_D vt)cos3\omega_o t \quad (4\text{-}3)$$

Regardless of the theoretically derived relationships, the current was measured experimentally.

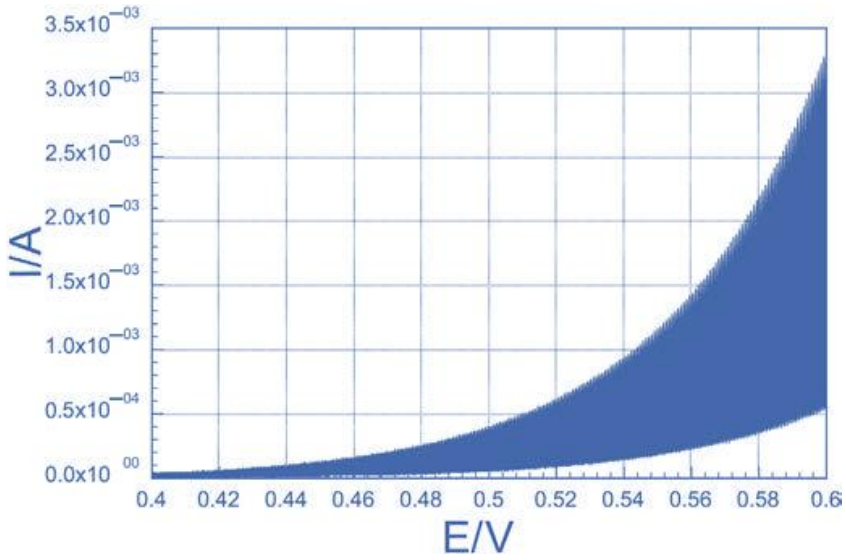

Fig. 4.2. Recorded current changes caused by the voltage perturbation signal. Amplitude of voltage perturbation signal $\Delta E_o = 30\ mV$, frequency of voltage perturbation $f_o = 80Hz$, potential scan rate $v = \frac{dE}{dt} = 2mV/s$, initial potential $E_S = 0.400V$, sampling frequency $f_S = 1.2\ kHz$

To assess the usefulness of the Gabor transformation in harmonic analysis, the recorded current changes were transformed. The obtained spectrogram is shown in Fig. 4-3.

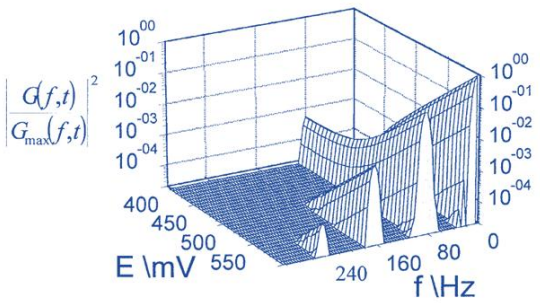

Fig. 4-3. Gabor spectrogram of the current flowing through the model electrical circuit

Zero harmonic is a direct current. In a logarithmic system, the dependence of this current on the potential is described by the voltage constant of a diode. The first harmonic at the beginning of polarization is constant and defined by the value vC_p. As the

value of the potential increases, we obtain a linear dependence between the logarithm of the first harmonic of the current and the potential. This slope is equal to the voltage constant of the diode. The slopes of the logarithm of the second harmonic and the third harmonic of the current versus the potential also determine the value of voltage constant of the diode. (*K. Darowicki, A. Krakowiak, Harmonic analysis of the current of an electric system simulating the electrode process in conditions of linearly changing potential.* Instrumentation Science and Technology, *Volume 30, Issue 3, Pages 341 – 352 August 2002; K. Darowicki, A. Krakowiak, Harmonic analysis of the current of an electric system simulating the electrode process in conditions of linearly changing potential, Instrumentation Science and Technology, Volume 30, Issue 3, Pages 341 - 352August 2002)*

Harmonic component	Voltage coefficient of a diode b_D/V^{-1}
$\Delta i(0,E)$	0.0201
$\Delta i(f_o,E)$	0.0202
$\Delta i(2f_o,E)$	0.0201
$\Delta i(3f_o,E)$	0.0202

Nominal value of voltage constant of the diode $b_D = 0.020\ V^{-1}$

In the case of non-stationary signals, correct spectral analysis requires the use of a different type of transformation than the Fourier transformation. The Gabor transformation is one of time-frequency analysis methods. Mathematical analysis of the current of the electrode process using the Gabor transformation confirmed the effectiveness of this analysis method. (*K. Darowicki, A. Krakowiak , The application of Gabor transformation in the harmonic analysis of corrosion processes, Anti-Corrosion Methods and Materials, Volume 50, Issue 3, Pages 193 – 200, 2003; L. Burczyk, K. Darowicki, Determination of local corrosion current from individual harmonic components, Journal of the Electrochemical Society, Volume 164, Issue 13, Pages C796 - C8002017).*

We are pioneers in the harmonic time-frequency analysis of electrode processes

The usefulness of this method of analysis in electrochemical studies of non-stationary processes was unequivocally demonstrated by conducting a digital Gabor spectral analysis of changes in the current of a model electrical circuit. In particular, the usefulness of the Gabor transformation was demonstrated in the harmonic analysis of non-stationary electrode processes. The Gabor spectrogram correctly reflects the distribution of the studied current into individual harmonic components. At the same time, it correctly reflects changes in the harmonic component as a function of potential. However, harmonic studies of the model electrical circuit are not comparable to studies of the actual electrode process. In most theoretical considerations of electrode reactions, higher current harmonics are omitted.
The reduction of Cd^{2+} in sulfate solution was selected for testing. Cd^{2+} ion reduction on a dropping mercury electrode (DME) is a relatively well-known reversible electrode process. That is why we employed this reaction to test our digital measurement system.
The harmonic components of the electrode reaction current at the mercury electrode are determined by the equations:

$$\Delta i(\omega,E) = \left\{ \left[\frac{(nF)^2 A}{\sqrt{2}RT} \left(c_{red}^o \sqrt{\omega D_{red}} + c_{ox}^o \sqrt{\omega D_{ox}} \right) \frac{\sqrt{\frac{D_{ox}}{D_{red}}} \frac{c_{ox}^o}{c_{red}^o} exp\left(\frac{nF(E-E^O)}{RT} \right)^2}{\left[1 + \sqrt{\frac{D_{ox}}{D_{red}}} \frac{c_{ox}^o}{c_{red}^o} exp \frac{nF(E-E^O)}{RT} \right]^2} \right]^2 \right.$$
$$\left. + \left[\frac{(nF)^2 A}{\sqrt{2}RT} \left(c_{red}^o \sqrt{\omega D_{red}} + c_{ox}^o \sqrt{\omega D_{ox}} \right) \frac{\sqrt{\frac{D_{ox}}{D_{red}}} \frac{c_{ox}^o}{c_{red}^o} exp\left(\frac{nF(E-E^O)}{RT} \right)^2}{\left[1 + \sqrt{\frac{D_{ox}}{D_{red}}} \frac{c_{ox}^o}{c_{red}^o} exp \frac{nF(E-E^O)}{RT} \right]^2} + \omega CA \right]^2 \right\}^2 \Delta E_o \quad (4\text{-}4A)$$

$$\Delta i(2\omega,E)=\frac{(nF)^3A}{\sqrt{8}(RT)^2}\left(c_{red}^o\sqrt{\omega D_{red}}+c_{ox}^o\sqrt{\omega D_{ox}}\right)\frac{\left[\sqrt{\frac{D_{ox}}{D_{red}}}\frac{c_{ox}^o}{c_{red}^o}exp\left(\frac{nF(E-E^O)}{RT}\right)\right]\left|1-\sqrt{\frac{D_{ox}}{D_{red}}}\frac{c_{ox}^o}{c_{red}^o}exp\left(\frac{nF(E-E^O)}{RT}\right)\right|}{\left[1-\sqrt{\frac{D_{ox}}{D_{red}}}\frac{c_{ox}^o}{c_{red}^o}exp\left(\frac{nF(E-E^O)}{RT}\right)\right]^3}\Delta E_o^2$$

(4-4B)

$$\Delta i(3\omega,E)=\frac{\sqrt{3}(nF)^4A}{192(RT)^3}\left(c_{red}^o\sqrt{\omega D_{red}}+c_{ox}^o\sqrt{\omega D_{ox}}\right)\frac{\left|3-2cosh^2\left(\frac{nF(E-E_{1/2})}{2RT}\right)\right|}{\left[cosh^4\left(\frac{nF(E-E_{1/2})}{2RT}\right)\right]}\Delta E_o^2$$

(4-4C)

Each harmonic component depends characteristically on the potential. The shape of the simulated three current harmonics is shown in Fig. 4-4.

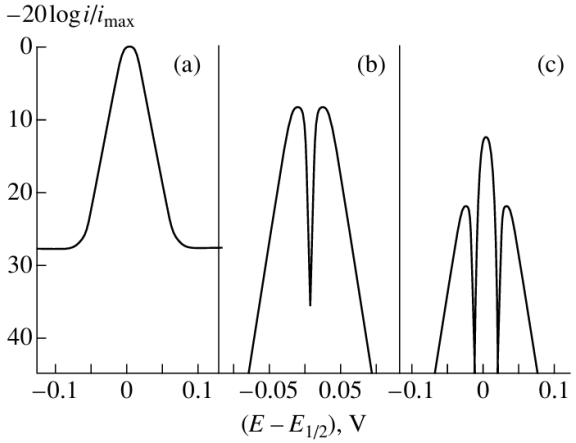

Fig. 4-4. The shape of the harmonic components of the reduction reaction current: (a) the first harmonic, (b) the second harmonic, (c) the third harmonic

A single peak corresponds to the first harmonic. The doublet corresponds to the second harmonic, while the triplet corresponds to the third harmonic. In the case of cadmium reduction at the mercury electrode, the current distribution should result in identical relationships. Fig. 4-5 shows a harmonic chronovoltamperogram of the cadmium reduction reaction on a dropping mercury electrode. (*K. Darowicki, A. Krakowiak, Digital harmonic analysis of cadmium ion reduction on a dropping mercury electrode, Russian Journal of Electrochemistry, Volume 39, 2003, Pages 134–140).*

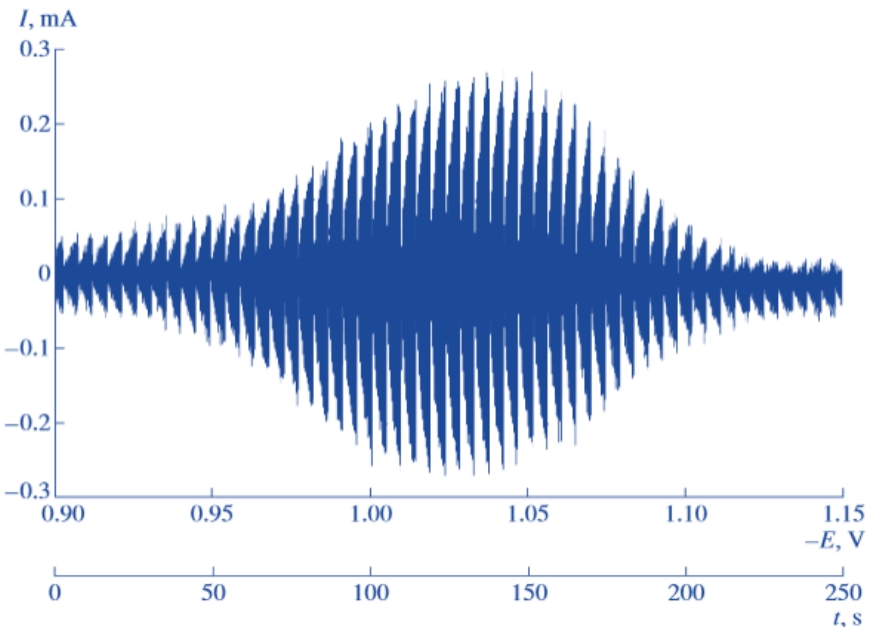

Fig. 4-5. Polyharmonic chronovoltamperogram of reduction reaction of $0.002\ M\ Cd^{2+}$in $0.5M\ Na_2SO_4$ on dropping mercury electrode as a function of potential. Drop duration time $t = 6s$, potential scan rate $v = 1mVs^{-1}$, perturbation frequency $f_o = 80\ Hz$, amplitude of voltage perturbation $\Delta E_o = 30\ mV\ (rms)$, sampling frequency $f_S = 650\ Hz$

Digitally recorded current changes were subjected to the STFT transformation, aimed at revealing of harmonic components and their characteristic shape. An image of the transformation performed is shown in Fig. 4-6.

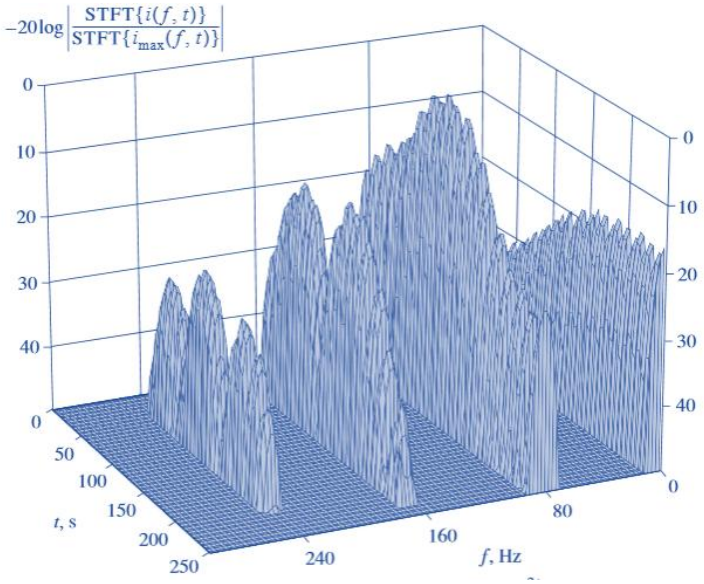

Fig. 4-6. Gabor spectrogram of reduction reaction of $0.002\ M\ Cd^{2+}$in $0.5M\ Na_2SO_4$ on dropping mercury electrode as a function of potential. Dop duration time $t = 6s$, potential scan rate $v = 1mVs^{-1}$, perturbation frequency $f_o = 80\ Hz$, amplitude of voltage perturbation $\Delta E_o = 30\ mV\ (rms)$, sampling frequency $f_S = 650\ Hz$

Three harmonic components were revealed on the spectrogram. According to theoretical analysis, the first harmonic is in the form of one peak, the maximum of which corresponds to the $E_{1/2}$ potential. The second harmonic consists of two peaks, while the third is a composition of three peaks. Pulse cyclic current changes on the harmonic chronovotamperogram are related to the expansion of the mercury drop. Gabor spectrogram reflects these changes.

The form of the harmonic components is modified if the perturbation signal has a polyharmonic structure. We discussed this issue in the paper. (*K. Darowicki, J. Majewska, The effect of a polyharmonic structure of the perturbation signal on the results of harmonic analysis of the current of a first-order electrode reaction, Electrochimica Acta, Volume 44, Issues 2–3, 15 September 1998, Pages 483-490)*

In the case of a monoharmonic perturbation signal, the analysis of the harmonic components of the current is relatively simple and well documented. Measurement and analysis of higher than third harmonic components of current require preliminary spectral analysis of the perturbation signal. Determining the fourth and higher harmonic components calls for taking into account the possible polyharmonic structure of the perturbation signal. Additionally, the charge/discharge current of the electrical double layer capacitance should be taken into account. In harmonic studies, it is important to remember the fundamental issue that harmonic components are generated in the case of activation control. (*K. Darowicki, J. Majewska, Harmonic analysis of electrochemical and corrosion systems - a review, Corrosion Reviews, Volume 17, Issue 5-6, Pages 383 – 400 December 1999).* The main advantage of harmonic analysis is that corrosion current and Tafel coefficients can be obtained via a single measurement. Another advantage of this method, compared to impedance measurements, is the use of a single frequency. In addition, the perturbation signal usually has a low amplitude (below $30\ mV$), which helps to maintain a steady state. However, under certain circumstances, the low amplitude can become a disadvantage. The generated and effective voltage perturbations are not equal. This is due to the ohmic drop caused by the solution resistance. The difference between the two voltages decreases when the solution resistance is low compared to the polarization resistance. Another important aspect of harmonic analysis is the perturbation frequency. Values below $0.1\ Hz$ are used in most cases. This condition is dictated by the effect of the capacitive current associated with charging and discharging of the double layer at higher frequencies. Nevertheless, as previously reported, the upper frequency limit depends on the specific properties of the system under study and the assumed relative error. The presented advantages created the possibility of local corrosion measurements. *(L. Burczyk, K. Darowicki, Determination of local corrosion current from individual harmonic components, Journal of the Electrochemical Society, Volume 164, Issue 13, Pages C796 - C8002017).*

A scheme of the electrochemical microscope for local harmonic measurements and surface corrosion mapping is shown in Fig. 4-7.

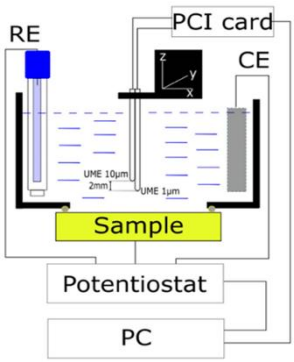

Fig. 4-7. Electrochemical microscope for surface corrosion mapping operating on the principle of harmonic measurements

A microscope consists of two measuring-conditioning systems. The first classic three-electrode system is used to determine and control the potential of the investigated electrode, on which sinusoidal changes are superimposed. The electrode surface is scanned with an ultramicroelectrode. We presented the application of harmonic response on a local scale. Using an appropriate measurement system and mathematical approach, it is possible to calculate the corrosion current and both Tafel coefficients on a microscale. In the case of harmonic response analysis in scanning mode, the selection of the appropriate frequency is crucial for a reasonable experiment time and therefore reliable results. The use of harmonic analysis on a local scale allowed revealing of differences in the corrosion current of individual phases.

The description of harmonic analysis of electrode processes also had another meaning. Theoretical considerations and research on real systems using harmonic analysis and acquired experience were only an introduction to further, main investigations. The development of a new, original measurement technique of Dynamic Electrochemical Impedance Spectroscopy and its implementation into measurement practice was my main research direction and fundamental scientific achievement.

5. DYNAMIC ELECTROCHEMICAL IMPEDANCE SPECTROSCOPY

Electrochemical Impedance Spectroscopy (EIS) allows the determination of the kinetic and mechanistic parameters of various electrochemical systems. It is widely used in corrosion research, semiconductor research, energy conversion and storage technologies, chemical sensors and bio-sensors, non-invasive diagnostics, etc. The EIS technique is based on perturbation of the electrochemical system at equilibrium or steady state, by applying a sinusoidal AC voltage or current signal over a wide frequency range and monitoring the sinusoidal response of current or voltage, respectively. The EIS technique cannot be used in non-stationary conditions; this is the basic limitation of this stationary investigation method.

5.1. Description of the method and its validation

Dynamic Electrochemical Impedance Spectroscopy was developed on the basis of research on non-stationary physicochemical processes. This method differs from the EIS method in that it can be used in research on non-stationary processes. Thus, it overcomes the main limitation of the applicability of the EIS. In the DEIS method I developed, the perturbation signal is a combination of elementary sinusoidal measurement signals with selected frequencies and adopted amplitude values. The response signal is also a multi-frequency signal. However, the magnitude of the amplitudes depends on the nature of the process being studied. The elementary response signals are shifted by specific phase angles relative to the elementary signals of the perturbation signal pack.

The specific feature of this method is the use of an analysis window. This window cuts out a portion of the perturbation signal and response signal synchronously at one time instant.

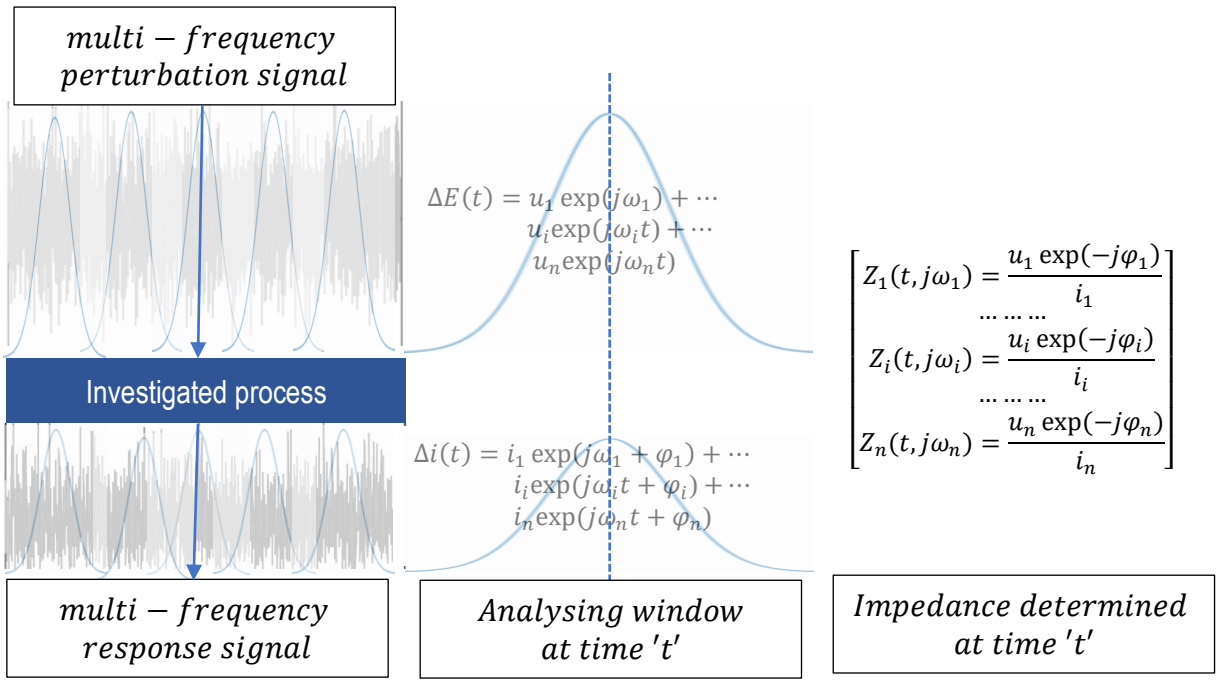

Fig. 5-1. Scheme of impedance measurement in non-stationary conditions. Dynamic Electrochemical Impedance Spectroscopy

Then, the cut pack of response signals that corresponds to the time t_i is decomposed into elementary current signals. In this way, for the time-located t_i analysing window, we obtain an impedance spectrum $\boldsymbol{Z}(t_i, j\omega) = \{Z(t, j\omega_i) + \cdots + Z(t, j\omega_n)\}$.

$$\boldsymbol{Z}(t_i, j\omega) = \begin{vmatrix} \left\{\frac{STFT\{u(t,j\omega)\}}{STFT\{i(t,j\omega)\}}\right\}_{\omega=\omega_1, t=t_i} \\ \cdots \\ \left\{\frac{STFT\{u(t,j\omega)\}}{STFT\{i(t,j\omega)\}}\right\}_{\omega=\omega_i, t=t_i} \\ \cdots \\ \left\{\frac{STFT\{u(t,j\omega)\}}{STFT\{i(t,j\omega)\}}\right\}_{\omega=\omega_n, t=t_i} \end{vmatrix}; \quad \boldsymbol{Z}(t_{i+1}, j\omega) = \begin{vmatrix} \left\{\frac{STFT\{u(t,j\omega)\}}{STFT\{i(t,j\omega)\}}\right\}_{\omega=\omega_1, t=t_{i+1}} \\ \cdots \\ \left\{\frac{STFT\{u(t,j\omega)\}}{STFT\{i(t,j\omega)\}}\right\}_{\omega=\omega_i, t=t_{i+1}} \\ \cdots \\ \left\{\frac{STFT\{u(t,j\omega)\}}{STFT\{i(t,j\omega)\}}\right\}_{\omega=\omega_n, t=t_{i+1}} \end{vmatrix} \quad (5\text{-}1)$$

In the next step, the analysing window is moved to time t_{i+1}. The operation of cutting a portion of the composite response signal is repeated. The decomposition of this pack leads to the next spectrum $\boldsymbol{Z}(t_{i+1}, j\omega) = \{Z(t, j\omega_1) + \cdots + Z(t, j\omega_n)\}$. As a result, we obtain a set of impedance spectra forming an impedance spectrogram. The number of spectra depends on the relationship between the length of the time register and the length of the analysis window. Determination of instantaneous impedance spectra comes down to the operation of the STFT transformation of the perturbation signal pack and the STFT transformation of the response signal pack.

The selection of window length is not arbitrary and depends strictly on the lowest measurement frequency and type of window. For the Gaussian window, time selection and frequency resolution are given by the equation (2-13). Thus, the quality of the mapping of variability over time depends on the length of the window. Consequently, the lowest useful frequency in the pack is defined. If we increase the analysing window length, we improve the frequency resolution and, conversely, reducing the window length, improves the reproduction of changes over time, but deteriorates the frequency resolution.

Theoretical description, the construction of a digital DEIS measurement system is our individual achievement. The DEIS research presented later is our pioneering achievements.

The idea of measuring impedance in non-stationary conditions and the theoretical description are presented in detail in the publications (*K. Darowicki, Theoretical description of the measuring method of instantaneous impedance spectra, Journal of Electroanalytical Chemistry, Volume 486, Issue 2, 29 May 2000, Pages 101-105; K Darowicki, J Orlikowski, G Lentka, Instantaneous impedance spectra of a non-stationary model electrical system, Journal of Electroanalytical Chemistry, Volume 486, Issue 2, 29 May 2000, Pages 106-110)*. The developed measurement methodology was verified based on the model electrical circuit, Fig. 4-1. The obtained spectrogram is shown in Fig. 5.2.

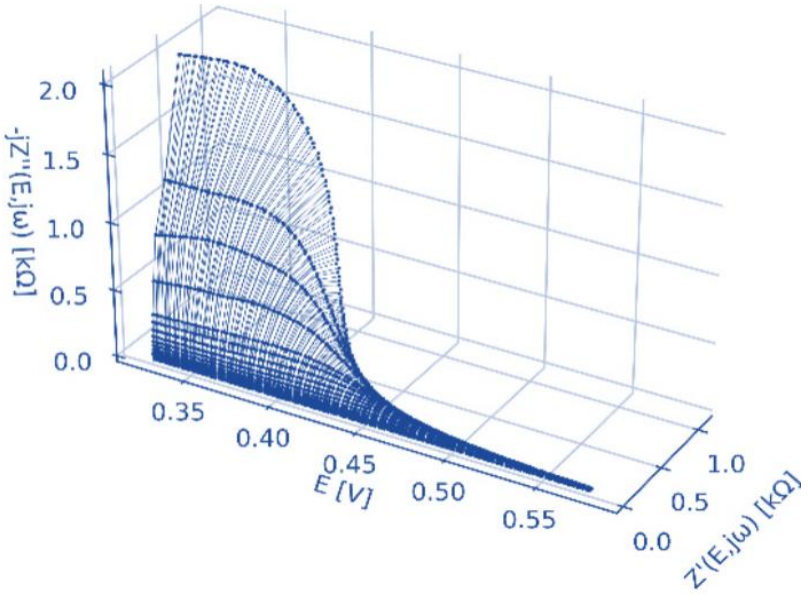

Fig. 5-2. Spectrogram of a model electrical circuit. Electrical capacity of a capacitor $C_p = 20\ \mu F$, voltage coefficient of a diode $b_D = 0.020\ V^{-1}$, resistance in series $R_s = 10\Omega$, potential scan rate in conducting direction of a diode $dE/dt = 2mV/s$

The analysis of individual impedance spectra reproduced the nominal values of the electrical elements used in a way that did not raise any doubts. To check the coherence of individual impedance spectra, their Kronig-Kramers transformation was performed (*K. Darowicki, J. Kawula, Validity of impedance spectra obtained by dynamic electrochemical impedance spectroscopy verified by Kramers-Kronig transformation, Polish Journal of Chemistry, Volume 78, Issue 9, Pages 1255 – 1260,*

September 2004). The verification confirmed that the obtained spectra of the model electrical circuit determined by the STFT transformation are correct in relation to the KK transformation.

5.2. Impedance of the first-order electrode reaction

Reduction of Cd (II) ions on a dropping mercury electrode (DME) has been widely used to test electrode reaction models. Today, some features of the process appear to be well established, such as the CEE mechanism (C: chemical reaction, E: electron transfer). In a $0.5\ M\ Na_2SO_4$ environment, the standard rate constant is equal to $k_s = 0.06\ cm \cdot s^{-1}$. The reaction takes place under activation-diffusion control conditions.

To verify the DEIS methodology and check its usefulness, impedance measurements of this process were carried out (*K. Darowicki, P. Slepski, Dynamic electrochemical impedance spectroscopy of the first order electrode reaction, Journal of Electroanalytical Chemistry, Volume 547, Issue 1, 24 April 2003, Pages 1-8).*

Fig. 5.-3. presents the impedance spectrogram of the reaction $Cd^{2+} + 2e^- = Hg(Cd)$

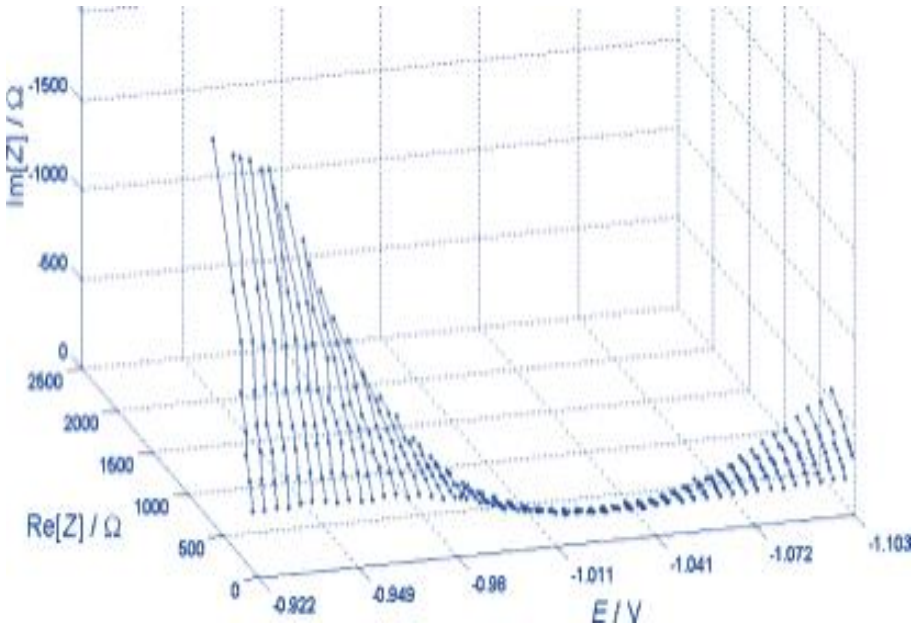

Fig. 5-3. Impedance spectrogram of the $2\ mM\ Cd^{2+}$ reduction reaction on a dropping mercury electrode in $0.5\ M\ Na_2SO_4$, potential scan rate $\frac{dE}{dt} = 2mV/s$, drop duration time $t = 6.2\ s$, drop surface area $S = 0.023\ cm^2$

The elementary impedance spectra were analysed based on the Randles equivalent circuit. The determined change in resistance as a function of the charge transfer potential is shown in Fig. 5-4A and the change in the Warburg coefficient in Fig. 5-4B.

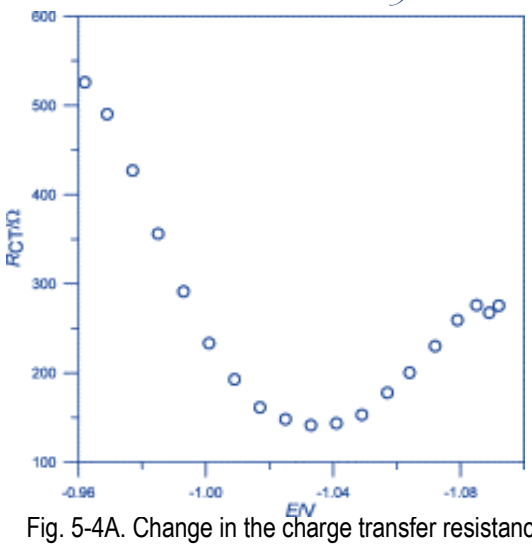

Fig. 5-4A. Change in the charge transfer resistance $\mathrm{R_{CT}}$ as a function of potential

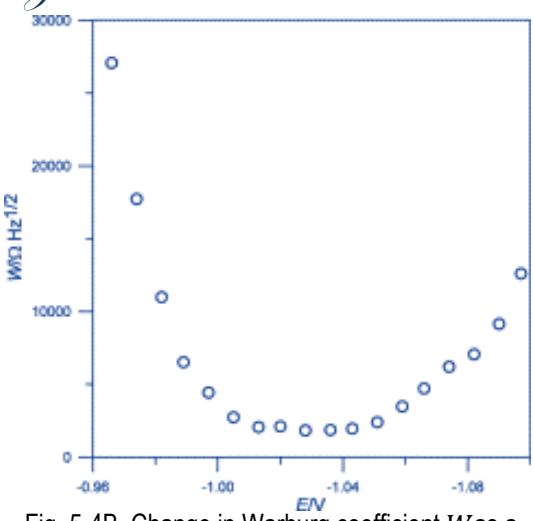

Fig. 5-4B. Change in Warburg coefficient W as a function of potential

The obtained experimental results are in perfect agreement with the mechanism and type of control of the reaction $Cd^{2+} + 2e^- = Hg(Cd)$

The determined rate constant and diffusion coefficient values coincided with literature data.
Impedance investigations of the $Cd^{2+} + 2e^- = Hg(Cd)$ reaction were performed in another measurement variant (*K. Darowicki, P. Slepski, Instantaneous electrochemical impedance spectroscopy of electrode reactions, Electrochimica Acta, Volume 49, Issue 5, 25 February 2004, Pages 763-772)*. Measurements were made for constant potentials under conditions of change in drop surface area.

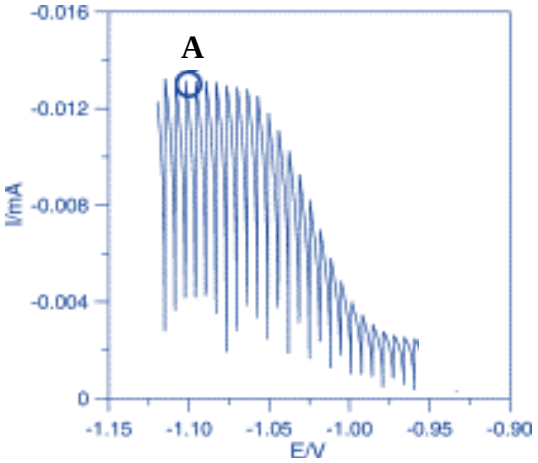

Fig. 5-5A. Polarogram of the reduction reaction of 2 mM $Cd(II)$ in $0.5M$ Na_2SO_4. Sampling frequency$fs = 6144$, length of analysing window $L = 1024$ samples

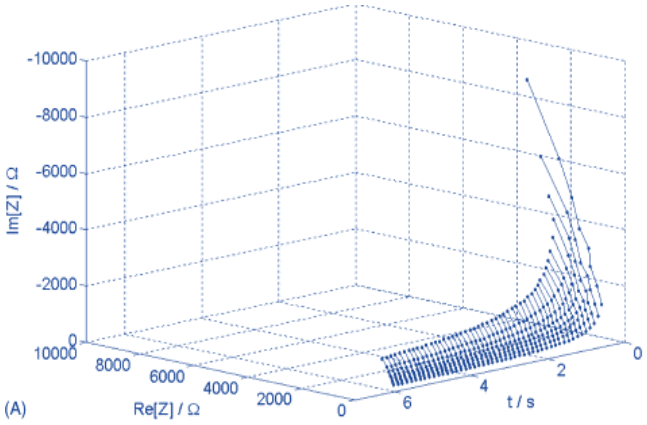

Fig. 5-5B. Chrono-impedance spectrogram of cadmium reduction reaction at potential $E = -1.100\ V$ in 2 mM $Cd(II), 0.5M\ Na_2SO_4$ solution. Sampling frequency $fs = 6144$, length of analysing window $L = 1024$

Despite the steady potential, measurement conditions were not stationary due to the growth dynamics of mercury drop. The determined time changes in the charge transfer resistanceR_{CT}, the Warburg coefficient W and the double electrical layer capacitance C_{DL} were related to the change in the surface of the mercury drop in accordance with the formula:

$$A(t) = A_o \left(\frac{t}{t_0}\right)^{2/3} \tag{5-2}$$

where: t_0 – drop duration time, $A(t)$ – drop surface area, A_o – drop surface area at breakoff.

5.3. Impedance of modified electrodes

The DEIS method was used in adsorption studies on electrodes (*K. Darowicki, A. Karolkowska, Sz. Wysmulek, Surface Charge Density Spectra: Complex Analysis of the Electrical Double Layer Developed from Measurements of Hexanol Adsorption Kinetics, Journal of Physical Chemistry C, Volume 129, Issue 1, Pages 801 - 8119 January 2025)*

Polyaniline (PANI) is considered one of the most promising electrode materials for flexible supercapacitors. As such, it has been the subject of a variety of studies based on different measurement techniques. The synthesis and properties of PANI have been extensively studied due to the growing interest in their polymerization mechanisms and redox transformations between the conductive and passive states. This electropolymerized polymer from an aqueous solution is stable in water and air. We performed the aniline polymerization studies using DEIS (*K. Darowicki, J. Kawula, Impedance characterization of the process of polianiline first redox transformation after aniline electropolymerization, Electrochimica Acta, Volume 49, Issue 27, 30 October 2004, Pages 901-914)*
The obtained chronovoltamperogram is shown in Fig. 5.6.

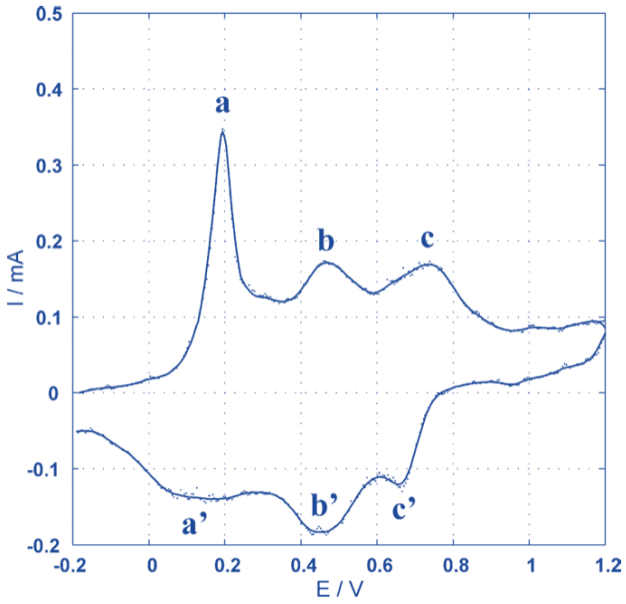

Fig. 5-6. Chronvoltamperogram of aniline electropolymerization. Potential scan rate $3mV/s$

The $a \leftrightarrow a'$ peaks correspond to the first redox process of oxidation-reduction of PANI, leading to the formation of cation radicals. The $b \leftrightarrow b'$ peaks are not clearly identified, but are presumed to be responsible for oxidation-reduction by-products and intermediates. The $c \leftrightarrow c'$ peaks correspond to the second redox process of PANI, leading to the formation of the dication-diradical. We considered the area of occurrence of the first $a \leftrightarrow a'$ peak to be of particular interest and should be studied in detail.

Fig. 5-7 A presents impedance and complex capacitance spectra for the region between 0.1 and 0.4 V for anode sweep and the region between 0.3 V and 0.05 V for cathode sweep.

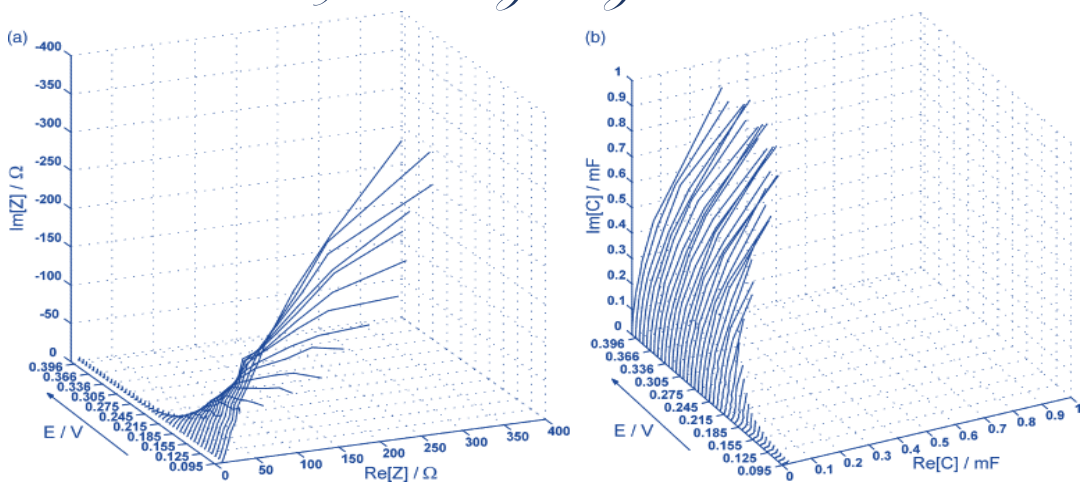

Fig. 5-7A. Potentiodynamic spectrograms determined for anode sweep for anode peak $(-a-)$ in the potential range of 0.100 V to 0.400 V: A) Impedance spectrogram, B) Complex capacitance spectrogram

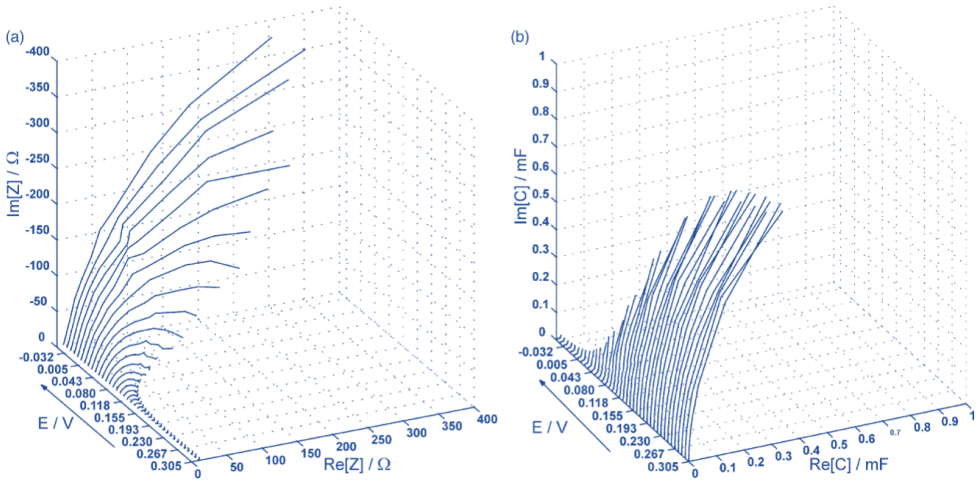

Fig. 5-7A. Potentiodynamic spectrograms determined for cathode sweep for anode peak $(-a'-)$ in the potential range of 0.300 V to -0.050V: A) Impedance spectrogram, B) Complex capacitance spectrogram

The presented procedure for examining redox changes in PANI occurs to be useful. DEIS allows tracking instantaneous changes in the electrochemical properties of PANI film in potentiodynamic conditions. The presented results were further analysed using the proposed electrical equivalent circuit and provided insight into the nature of the process. Changes in electrochemical parameters were consistent with previous publications and expectations. The proposed equivalent circuit turned out to be correct in the redox transformation analysis of the conductive polymer layer.

We investigated the carbon electrodes obtained by PVD employing the same approach as for the electrodes with the polyaniline layer. (*J. Ryl, L. Burczyk, R. Bogdanowicz. M. Sobaszek, K. Darowicki, Study on surface termination of boron-doped diamond electrodes under anodic polarization in H2SO4 by means of dynamic impedance technique, Carbon, Volume 96, January 2016, Pages 1093-1105; J. Ryl, R. Bogdanowicz, P. Slepski, M. Sobaszek, K. Darowicki, Dynamic Electrochemical Impedance Spectroscopy (DEIS) as a Tool for Analyzing Surface Oxidation Processes on Boron-Doped Diamond Electrodes, Journal of the Electrochemical Society, Volume 161, r, H359, April 2014, J. Ryl, A. Zielinski, L. Burczyk, Robert Bogdanowicz, T. Ossowski, K. Darowicki, Chemical -Assisted Mechanical Lapping of Thin Boron-Doped Diamond Films: A Fast Route Toward High Electrochemical Performance for Sensing Devices, Electrochimica Acta, Volume 242, 10 July 2017, Pages 268-27; M. Sobaszek K. Siuzdak, J. Ryl, M. Sawczak, S. Gupta S. B. Carrizosa, M. Ficek, B. Dec, K. Darowicki, R. Bogdanowicz, Diamond Phase (sp^3-C) Rich Boron-Doped Carbon Nanowalls (sp^2-C): Physicochemical and Electrochemical Properties, The Journal of Physical Chemistry C, Volume121/Issue 38, September 2017).*

The processes of inhibiting corrosion reactions were also studied. (*H. Gerengi., K. Darowicki, G. Bereket, P. Slepski, Evaluation of corrosion inhibition of brass-118 in artificial seawater by benzotriazole using Dynamic EIS, Corrosion Science, Volume 51, Issue 11, November 2009, Pages 2573-257).*

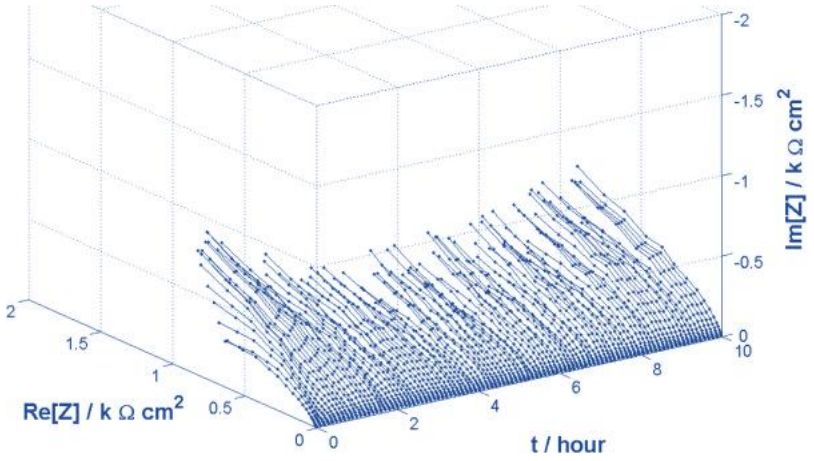

Fig. 5.9A. DEIS impedance spectrogram for brass-118, without inhibitor in artificial seawater

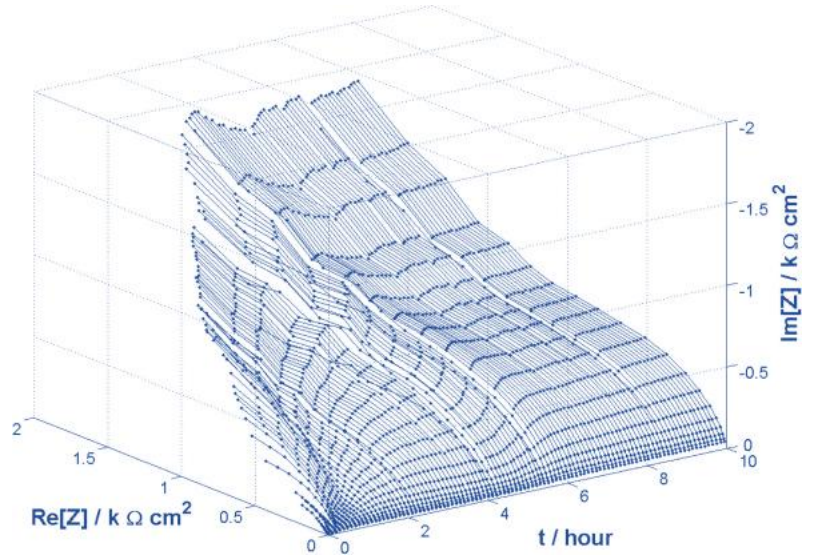

Fig. 5.9B. DEIS impedance spectrogram for brass-118, with the addition of 0.010 M benzotriazole to artificial seawater

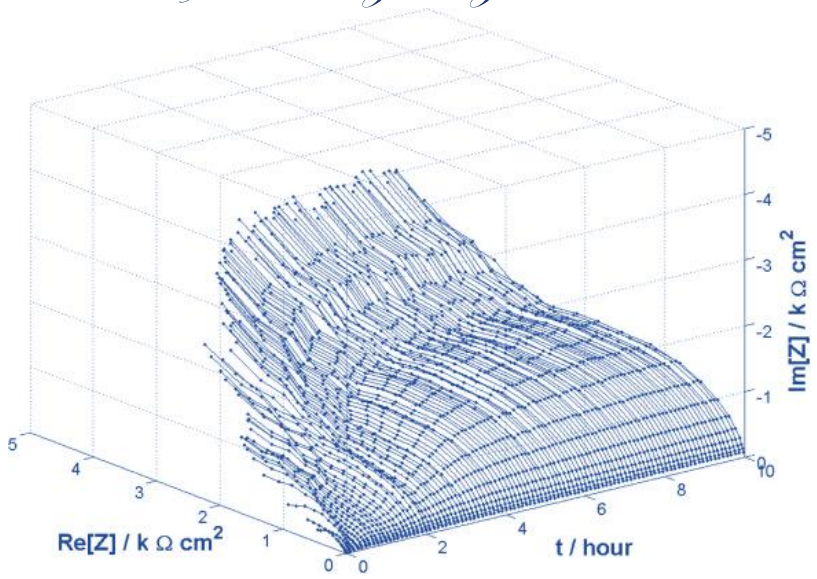

Fig. 5.9B. DEIS impedance spectrogram for brass-118, with the addition of 0.020 M benzotriazole in artificial seawater

The inhibition effect and its changes with time were calculated.

5.4. Impedance of pitting corrosion

Pitting corrosion is a dangerous form of local corrosion that can cause perforations of passivated steels and other materials. It is difficult to observe due to the small diameters of the pits and the fact that they are often covered with corrosion products. Additionally, it is difficult to simulate in laboratory tests due to the long incubation time. Due to its non-stationary nature, it is not investigated with classical impedance spectroscopy. Novel studies of pitting corrosion processes based on the Dynamic Electrochemical Impedance Spectroscopy method were carried out. (*K. Darowicki, S. Krakowiak, P. Slepski, Evaluation of pitting corrosion by means of dynamic electrochemical impedance spectroscopy, Electrochimica Acta 49 (2004) 2909–2918)*
The changes in current and impedance caused by the pitting corrosion are shown in Fig. 5-10A and Fig. 5-10B.

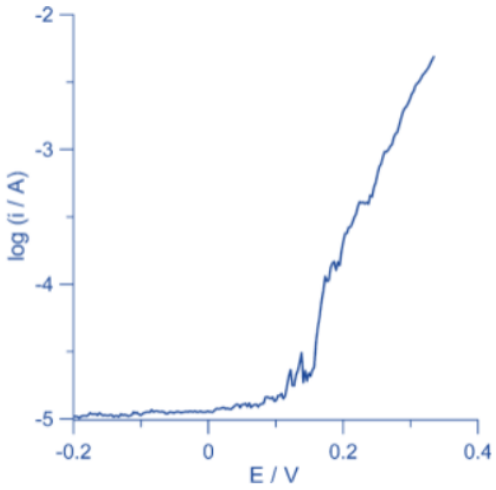

Fig. 5-10A. Potentiodynamic diagram of pitting corrosion of $304L$ steel in $0.5M\ NaCl$. Surface area $A = 0.5\ cm^2$. Potential scan rate $dE/dt = 1mV/s$

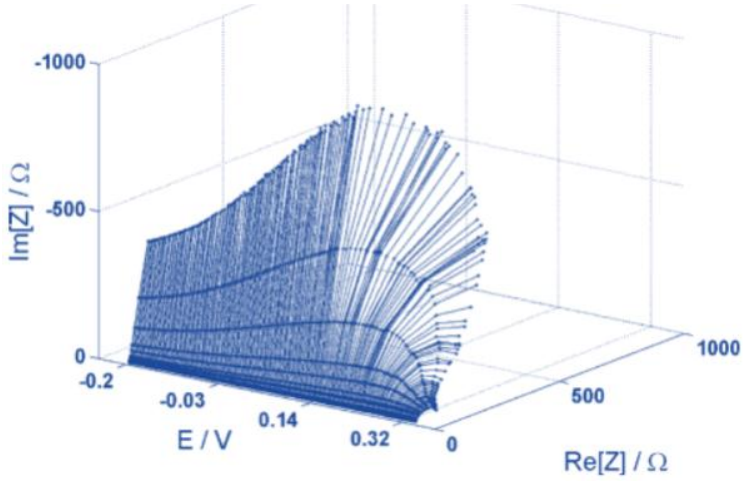

Fig. 5-10B. Impedance spectrogram of pitting corrosion of $304L$ steel in $0.5M\ NaCl$. Surface area $A = 0.5\ cm^2$. Potential scan rate $dE/dt = 1mV/s$

The polarization curve clearly indicates the initiation and subsequent development of pitting corrosion. What is surprising is the successive increase in the impedance of 304 L steel as the potential increases, and the direct current also increases in the same range. After reaching the potential E=0.14 V, the current continues to increase, but the accompanying impedance decreases. It

is an area of metastable development of pitting corrosion. When the potential E=0.32 is reached, there is a sharp increase in pitting corrosion. It is accompanied by a reduction in impedance

A more detailed analysis showed that the passive layer consists of a thin and compact inner part and a thicker, porous outer part. This result is as expected and agrees with previous studies. However, for the first time, reliable results of the capacitance values of both sublayers were obtained in the range of the metastable potential and spontaneous development of pitting, i.e. in previously undefined conditions. In addition to the changes in capacitance of both sublayers, it has been experimentally shown that the transport of ions and vacancies through both sublayers is subject to the laws of diffusion. The corresponding Warburg impedances are measures of diffusion resistance. The charge transfer resistance inside the pit is a potential function. It has been shown that the corrosion process of 304 L steel inside the pits is activation-controlled. The pitting corrosion process of 304 L stainless steel in the potential range of metastable pitting is also activation-controlled. Summarizing, the method of measuring electrode impedance under potentiodynamic conditions is an effective tool in the study of passive layer structures. The method allowed for the study of ion transport through passive layers. This technique provided reliable and comprehensive information regarding the metastable and spontaneous development of pitting and the kinetics of electrode processes inside the pit.

Analysing impedance changes, we indicated that in the first stage the impedance increases with increasing potential (Fig. 5-10B). This area can be called the pre-initiation pitting corrosion area. This aspect is of particular interest because it provides the opportunity to predict pitting corrosion. In the paper (*S. Krakowiak, K. Darowicki, P. Slepski, Impedance investigation of passive 304 stainless steel in the pit pre-initiation state, Electrochimica Acta 50 (2005) 2699–2704)*, we discussed this problem. Figure 5-11 shows changes in the complex capacitance of the 304 steel in the range of potentials preceding pitting corrosion.

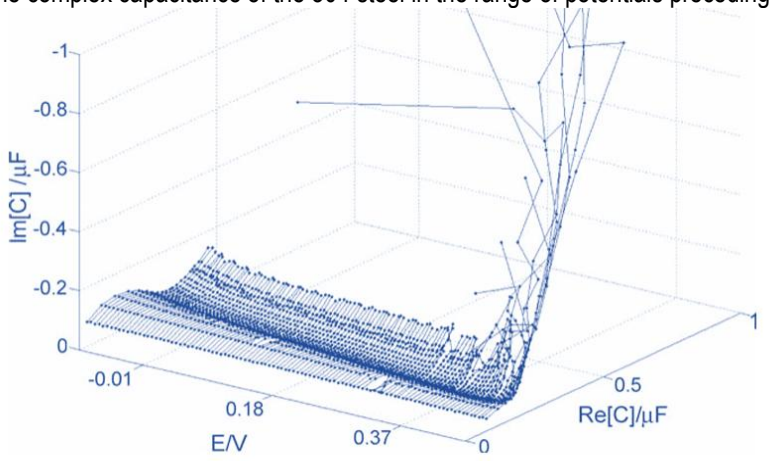

Fig. 5-11. Complex capacitance spectrogram of $304\mathrm{L}$ steel in $0.5\mathrm{M\ NaCl}$. Surface area $\mathrm{A} = 0.02\ \mathrm{cm}^2$. Potential scan rate $\mathrm{dE/dt} = 5\mathrm{mV/s}$

Single spectra of complex capacitance are in the shape of semicircles depressed by an angle of $\pi/4$. This form of complex capacitance spectra indicates rapid relaxation of the groups we have not identified. These may be hydrated $\mathrm{Cr_2O_3}$ molecules. As the potential increases, the complex capacitance decreases. The capacitance responsible for relaxation, which is determined by the diameter of the semicircle, also decreases. The initiation of the pit results in an increase in the imaginary part of the complex capacitance. This effect is related to electrochemical processes inside the pit.

The development of corrosion pitting on stainless steel in chloride solution proceeds in three distinct steps: nucleation, metastable growth, and stable growth. Due to its transient nature, the process of metastable pitting corrosion has not yet been impedance tested. The development of the DEIS measurement methodology has created new research perspectives, including the possibility of testing pitting corrosion in a metastable state *(S. Krakowiak, K. Darowicki, P. Ślepski, Impedance of metastable pitting Corrosion, Journal of Electroanalytical Chemistry, Volume 575, Issue 1, 15 January 2005, Pages 33-38).*

In the metastable state, the initiation and development of the corrosion pit occur, which is repassivated under the influence of the environment. Changes in pitting corrosion current under metastable conditions are shown in Fig. 5-12.

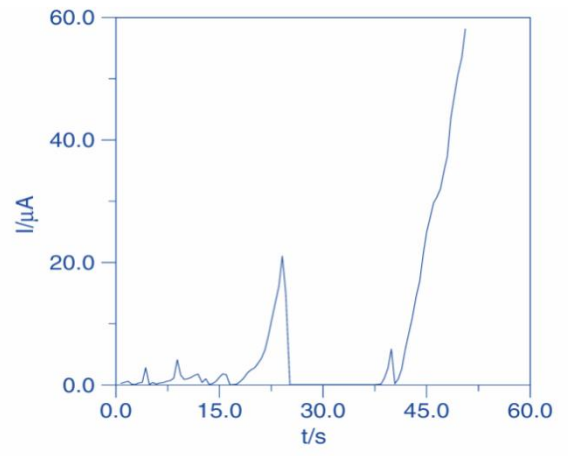

Fig. 5-12A. Changes of the current over time for 304 steel under metastable conditions in $0.5\,M\,NaCl,\ E = 0.650V$ versus $Ag/AgCl$

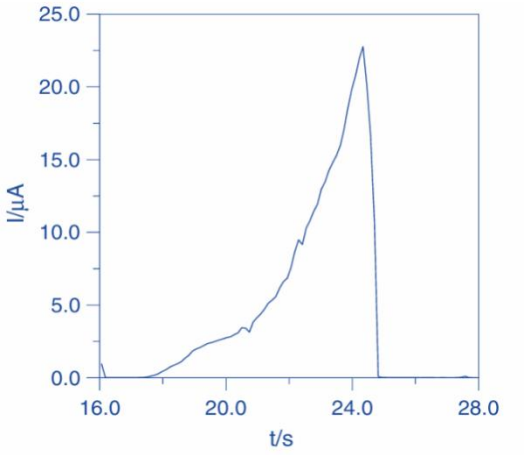

Fig. 5-12B. Selected metastable over time current peak of 304 steel in $0.5\,M\,NaCl,\ E = 0.650V$ versus $Ag/AgCl$

Under metastable conditions, the current-time register consists of a series of peaks of identical shape, differing in scale. We selected the best developed peak for analysis. The current of the metastable peak increases exponentially and then decreases rapidly due to repassivation. Such short-lived processes of pitting development and subsequent repassivation have never been impedance analysed. Our results are the first in the world.

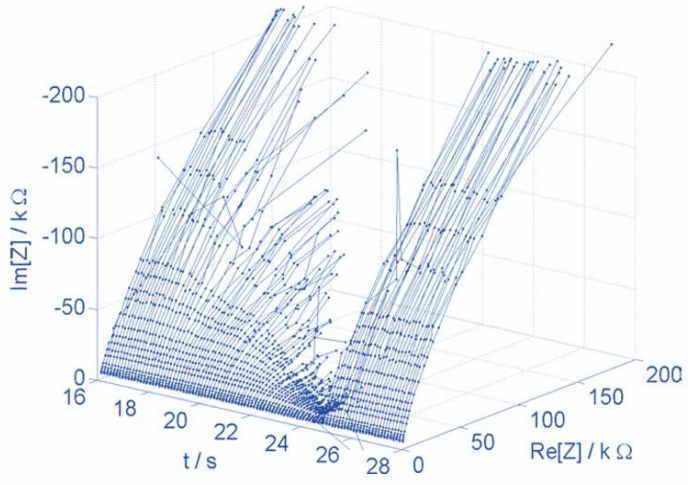

Fig. 5-13. Chrono-impedance spectrogram of the pit formation and repassivation process, Fig. 5-12B

At the beginning, the impedance spectra of 304 L steel have a characteristic form corresponding to the passive steel. The formation of a metastable peak is accompanied by a decrease in impedance. Impedance spectra representing the lowest impedance are in the form of semicircles. This is a situation in which a pit has been formed and activation-controlled corrosion processes develop inside it. So far, it was believed that the development of metastable pitting is diffusion-controlled. Our research clearly denies this. Impedance measurements of pitting corrosion in potentiodynamic conditions are one of the measurement variants. Another variant is impedance measurements under controlled current conditions *(J. Orlikowski, A. Jazdzewska, R. Mazur, K. Darowicki, Determination of pitting corrosion stage of stainless steel by galvanodynamic impedance spectroscopy, Electrochimica Acta, Volume 253, 1 November 2017, Pages 403-412).*

A new galvanostatic (G-DEIS) approach in the study of dynamic pitting corrosion processes allowed the following conclusions to be drawn: G-DEIS can be used to build corrosion monitoring systems. The free measurement corresponds to a zero direct current.

DEIS measurements are the first valuable impedance characteristics of initiation, metastable growth, and permanent growth of pits.

DEIS is a powerful tool in pitting corrosion research. The impedance of metastable pitting was evaluated for the first time. The electrochemical reactions inside active pits are controlled by the charge transfer process. The ability to assess the charge transfer resistance makes it possible to determine the corrosion dynamics inside pits. The electrolyte resistance inside the active pits also depends on time. Changes in the double electrical layer capacitance inside the active pit as a function of time are a very good measure of the growth dynamics of pitting.

5.5. Corrosion under mechanical stress conditions

Corrosion resistance and susceptibility to stress corrosion, especially of welds, depend on many variables, such as the physicochemical parameters of the corrosive environment, material composition and microstructure, mechanical properties and mechanical stresses. In the presence of chloride ions, welds are susceptible to various types of local corrosion, including pitting corrosion, crevice corrosion, and stress corrosion cracking. Mechanical stresses can accelerate corrosion processes. The lifetime of metastable pitting and the peak currents depend on the stresses. Stresses influence the intergranular, pitting and crevice corrosion processes. For this reason, we addressed the topic of monitoring corrosion changes as a function of stress. A system for testing the influence of stresses on corrosion processes is presented in Fig. 5-14.

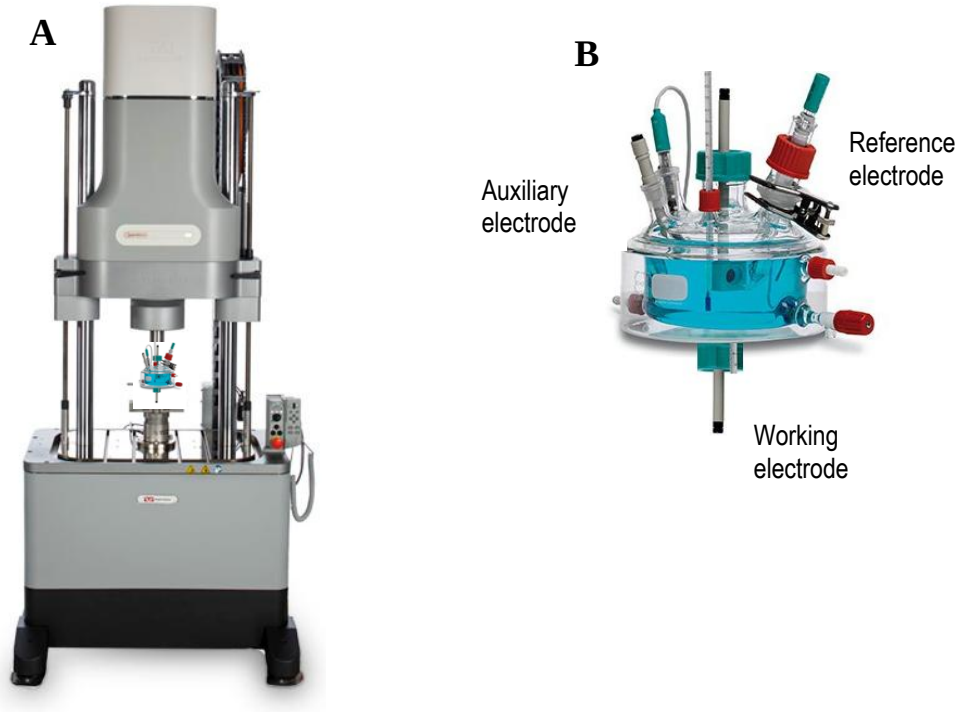

Fig. 5-14. System for corrosion tests under tensile stress conditions, (A) Tensile testing machine, (B) Three-electrode measurement cell.

The rod samples were subjected to mechanical interactions in the tensile testing machine, and at the same time they were embedded in an electrochemical cell. In this way, corrosion tests were carried out under controlled conditions of constant and/or variable stresses. Such a measurement system, employing a potentiostat/galvanostat, enabled dynamic impedance DEIS tests. *(K. Darowicki, J. Orlikowski, A. Arutunow, Investigations of the passive layer cracking by means of Dynamic Electrochemical Impedance Spectroscopy, Electrochimica Acta, Volume 48, Issue 28, 15 December 2003, Pages 4189-4196).*

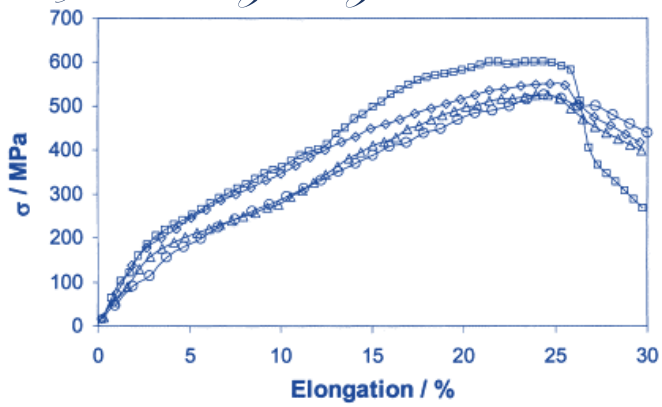

Fig. 5-15. Stress-strain characteristics of 304 steel, determined for various electrochemical states: (▵) $E = -0.300$ V, (○) $E = -0.200$ V, (◊) $E = -0.150$ V, (□) $E = -0.000$ V.

Elastic deformation is observed for an elongation of <3%, while plastic deformation is obtained in the range of 3 to 25%; this fact does not depend on the polarization.

Impedance spectra collected during electrode elongation are illustrated in Fig. 5-16.

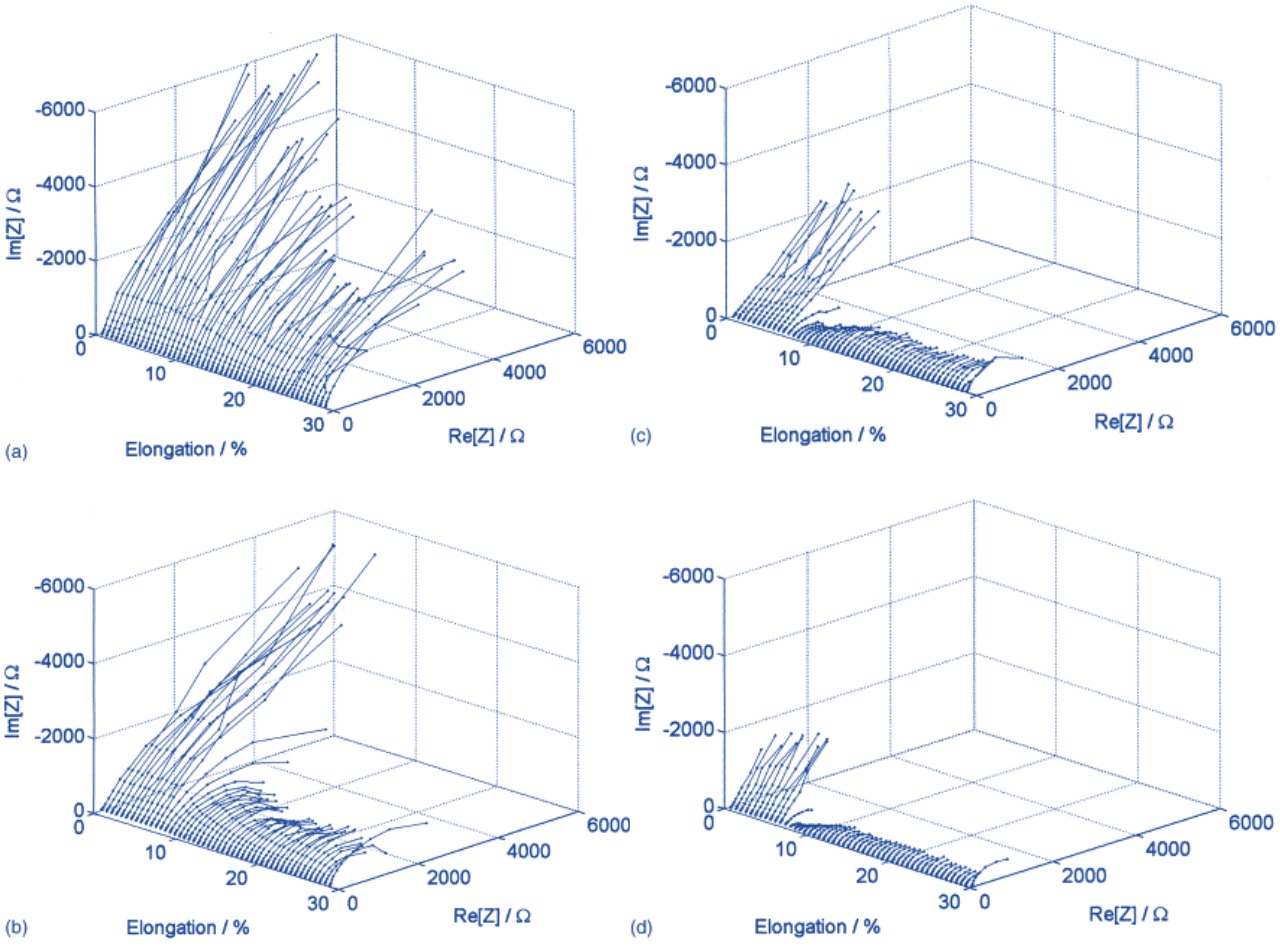

Fig. 5-16. Impedance diagrams determined as a function of the elongation of 304 steel electrodes, and the fixed potentials: (a) $E = -0.300$ V, (b) $E = -0.200$ V, (c) $E = -0.150$ V, (d) $E = 0.000$ V.

The phenomenon of the passive layer cracking under tensile stress can be assessed using dynamic electrochemical impedance spectroscopy. Classical impedance techniques would not produce precise results regarding this dynamics, as such

electrochemical processes occur too quickly. Impedance spectrograms obtained from measurements as a function of elongation (Fig. 5-16) reveal two regions. The spectra in the first region refer to the passive state and are diffusive in character (straight lines), while the others reflect the active state (semicircles) of the stainless steel being tested. In addition, these two regions of impedance spectra are well correlated with tensile stresses (see Fig. 5-14). These spectra reflect the transition from a passive to an active region for the samples tested.

Detailed analysis of the processes occurring inside the passive layer is possible utilizing an appropriate analysing window and an appropriate measurement frequency range. The moment of the passive layer cracking can be observed clearly. The change in charge transfer resistance of the passive layer unequivocally defines the cracking dynamics of the passive layer.

The stress experiment was performed in a different configuration. A constant stress value of 380 MPa was applied and passive layer changes were observed for the different electrode potentials imposed. After filtering the DC current out, the changes in impedance versus time are shown in Fig. 5-17.

We are pioneers in impedance testing of fast, non-stationary corrosion processes, including the processes forced by mechanical interactions.

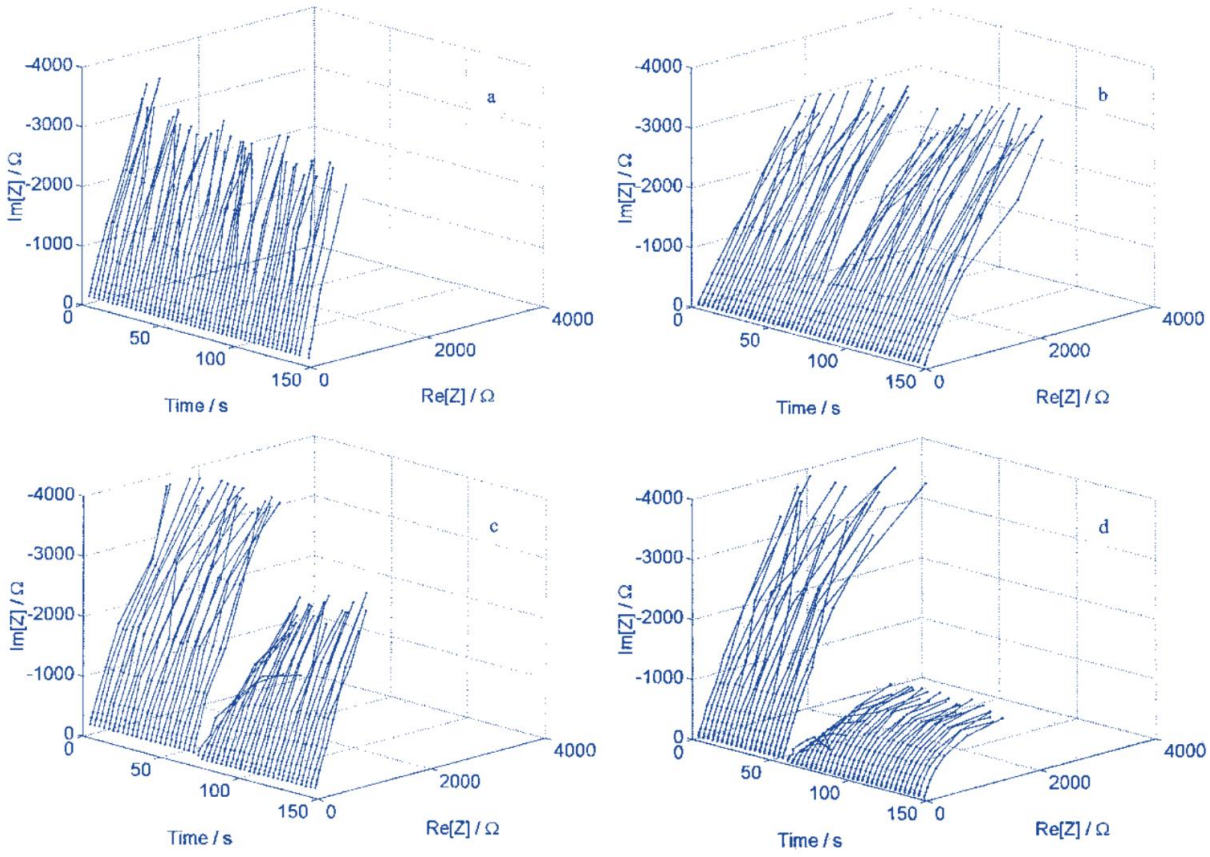

Fig. 5-17. Changes in impedance as a function of time for stressed samples made of 304 steel: A) $E = -0.300$ V; b) $E = -0.200$ V, C) $E = -0.150\ V$, D) $E = -0.000\ V$

The dependence of the time-to-rupture of the passive layer on the applied potential is clearly visible. The issue of cracking of passive layers was discussed in detail in the following papers. (*K. Darowicki, J. Orlikowski, A. Arutunow, Detection of stress corrosion cracking dynamics by dynamic electrochemical impedance Spectroscopy, Corrosion Engineering, Science and Technology, The International Journal of Corrosion Processes and Corrosion Control, Volume 39, Pages 255-260 November 2013; K. Darowicki, A. Arutunow, J. Orlikowski, Dynamic electrochemical impedance spectroscopy measurements of passive layer cracking under static tensile stresses, Journal of Solid State Electrochemistry, Volume 8, Issue 6, Pages 352 - 359May*

2004; K. Darowicki, A. Arutunow, J. Orlikowski, Analysis of electrochemical parameters in time domain during the passive layer cracking occurring on the 304L stainless steel in chlorides solution under tensile stresses, Electrochimica Acta, Volume 49, Issue 28, Pages 5069 - 50781 November 2004.

The time ranges and the ranges of relative elongation for the transition from passive to active state during the cracking process have been effectively established. Impedance changes in these ranges were determined. Changes in the charge transfer resistance and the electrical double layer capacitance were measured. A significant influence of tensile stresses and potential on changes in the impedance and electrochemical parameters of the system in the time domain was demonstrated.

The Portevin-Le Chatelier (PLC) effect is revealed on stress-strain characteristics as serration caused by load or as sudden elongation during plastic deformation of many alloys. This effect is influenced by temperature, strain rate and pre-treatment. This is the most obvious example of plastic instability in alloys. The theoretical foundations of the PLC effect were developed by Cottrel. This phenomenon has been and is being studied extensively. Our aim was to investigate this phenomenon under electrochemical conditions. In other words, we wanted to detect the surface Portevin-Le Chatelier effect. Our research, like the previous ones, was original and never analysed before. In Fig. 5-18 we show the serration effect determined for the A9 5251 aluminium alloy. The electrode subjected to mechanical interactions was simultaneously impedance analysed. (*K. Darowicki, J. Orlikowski, Impedance analysis of Portevin-Le Chatelier effect on aluminium alloy, Electrochimica Acta, Volume 52, Issue 12, 10 March 2007, Pages 4043-4052).*

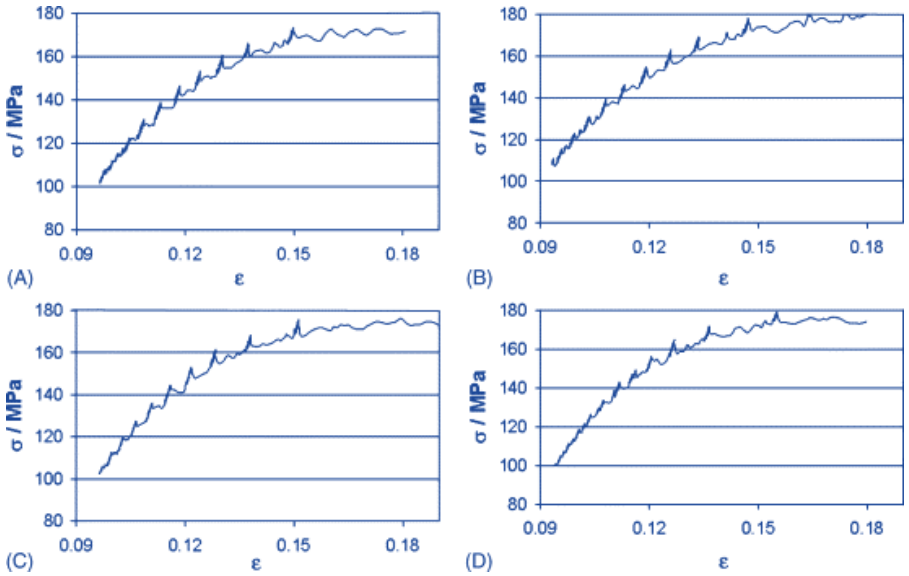

Fig. 5-18. ε = ε(σ) dependence determined for A9 5251 alloy in borate buffer with the addition of 2 mM NaCl for different electrode potentials: A) $E = -0.725\,V$, B) $E = -0.700\,V$, C) $E = -0.660\,V$ and D) $E = -0.590\,V$. Sampling frequency $fs = 50\,kHz$, strain rate $d\varepsilon/dt = 5 \times 10^{-3}\,s^{1}$.

The PLC effect is a non-stationary, oscillatory process, so a dynamic version of electrochemical impedance spectroscopy was used. Fig. 5-19 shows electrode impedance variations as a function of strain for different electrode potentials.

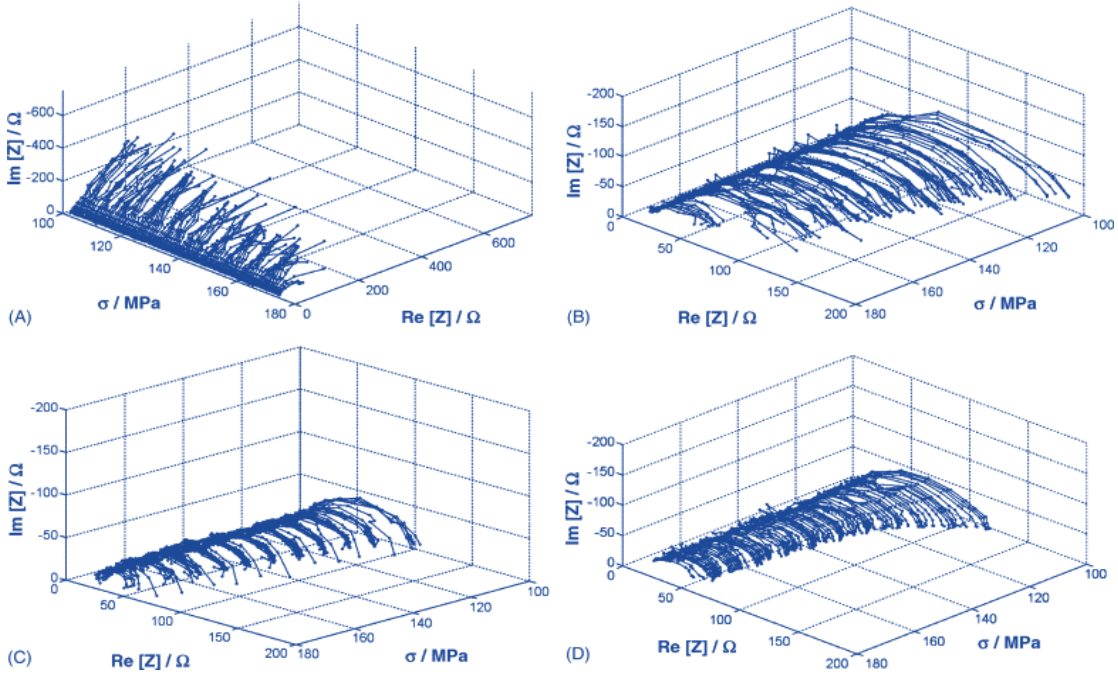

Fig. 5-19. Impedance spectra determined for A9 5251 alloy in borate buffer with the addition of 2 mM NaCl for different electrode potentials: (A) $E = -0.725\,V$, (B) $E = -0.700\,V$, (C) $E = -0.660\,V$ and (D) $E = -0.590\,V$. Sampling frequency $fs = 50\,kHz$, strain rate $d\varepsilon/dt = 5 \times 10^{-3}\,s^{-1}$.

Analysis of DC current variations, obtained by filtration from DEIS registers for different levels of anodic polarization, showed that oscillations of both current and strain occurred at identical stress values. It can therefore be concluded that the harmonic component compositions of the PLC effect for the different potentials are identical. This means that the mechanical effect of PLC is not related to the electrochemical conditions occurring on the surface of the samples. Studies have shown that the electrochemical, surface PLC effect is related to both mechanical conditions and the level of anodic polarization. This process is multi-stage, its course and form are the functions of stress. The factor determining the occurrence of the electrochemical, surface PLC effect is the dynamics of the transition from the passive state to the active state and vice versa.

Our achievement is the impedance reflection of the Portevin-Le Chatelier effect.

In addition to stress corrosion and pitting corrosion, the DEIS technique was effectively used in intergranular corrosion studies. (*A. Arutunow, K. Darowicki, DEIS evaluation of the relative effective surface area of AISI 304 stainless steel dissolution process in conditions of intergranular corrosion, Electrochimica Acta, Volume 54, Issue 3, Pages 1034 - 10411 January 2009, A. Arutunow, K. Darowicki, Impact of sensitization on dissolution process of AISI 304 stainless steel during intergranular corrosion evaluated using DEIS technique, Journal of Solid State Electrochemistry, Volume 13, Issue 11, Pages 1687 - 1694November 2009).*

We investigated cavitation phenomena. (*J. Ryl, P. Slepski, K. Darowicki, Evaluation of cavitation erosion-corrosion degradation of mild steel by means of dynamic impedance spectroscopy in galvanostatic mode, Corrosion Science, Volume 53, Issue 5, Pages 1873 - 1879May 2011; J. Ryl, K. Darowicki, Impedance monitoring of carbon steel cavitation erosion under the influence of corrosive factors, Journal of the Electrochemical Society, Volume 155, Issue 4, Pages P44-P492008.*

Not only pitting and stress corrosion cracking of stainless steels, but also pitting and stress corrosion of aluminium and magnesium alloys were studied with the DEIS technique. (*K. Darowicki, J. Orlikowski, A. Zielinski, Investigation of changes in the type B PLC effect of Al-Mg-Cu type alloy for inski strain rates, Materials Science and Engineering: A Volume 496, Issue 1-2, Pages 478 - 48225 November 2008*; *S. Krakowiak, K. Darowicki, Electrochemical and acoustic emission studies of aluminum pitting Corrosion, Journal of Solid State Electrochemistry, Volume 13, Issue 11, Pages 1653 – 1657 November 2009*; *J. Orlikowski, K. Darowicki, Investigations of pitting corrosion of magnesium by means of DEIS and acoustic emission, Electrochimica Acta Volume 56, Issue 23, Pages 7880 - 788430 September 2011*; *J. Orlikowski, J. Ryl, S. Krakowiak, K. Darowicki, Instantaneous impedance monitoring of aluminum alloy 7075 corrosion in borate buffer with admixed chloride ions, Corrosion, Volume 71, Issue 7, Pages 828 - 8381 July 2015).*

5.6. Impedance mapping of surface

Atomic force microscopy (AFM) is a technique employed in surface analysis, not necessarily metallic one. The AFM technique provides qualitative as well as quantitative information on many physical properties, including size, morphology, surface texture and roughness. Scanning is usually carried out over areas up to 100 μm. AFM provides high resolution and 3D visualization. Typically, AFM instruments have a vertical resolution of less than 0.1 nm and an XY resolution of about 1 nm. Photo 5-20A shows the AFM microscope and the scheme of its operation principle, Fig. 5-20B.

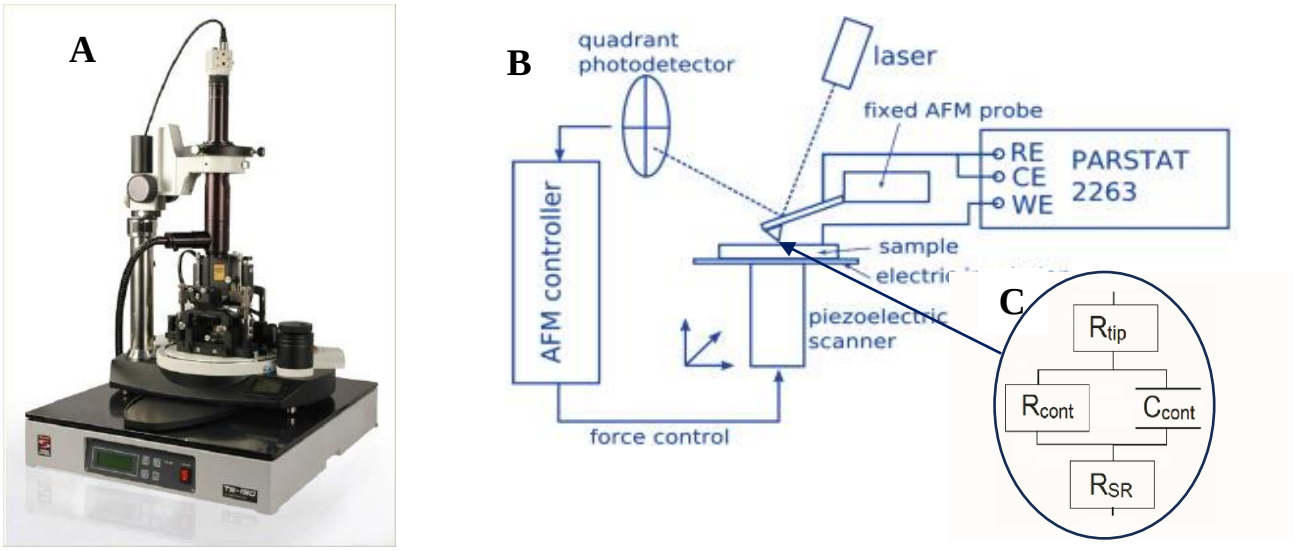

Photo. 5-20. (a) NTEGRA Aura AFM microscope (NT-MDT), (B) AFM Scheme of AFM operation principle, C) Electrical equivalent circuit for tip-surface contact, R_{tip} – tip resistance, R_{cont} – contact resistance, C_{cont} – contact capacitance, R_{SR}- spreading resistance

AFM is a type of profilometer, the scanning probe is a tip made of an appropriate material and appropriately shaped in the form of a needle. The vertical tip movement is reflects the profile of the scanned surface. This mapps its morphology. In our solution, a pack of elementary sinusoidal signals was applied between the moving tip and the analyzed surface. (*K. Darowicki, A. Zieliński, K.J. Kurzydłowski, Application of dynamic impedance spectroscopy to atomic force microscopy, Science and Technology of Advanced Materials, Volume 9, Number 4, November 2008; A Zieliński, K. Darowicki, Implementation and validation of multisinusoidal, fast impedance measurements in atomic force microscope contact mode, Microscopy and Microanalysis, Volume 20, Issue 3, Pages 974 - 981June 2014*; *A. Zielinski, J, Ryl, L. Burczyk.K. Darowicki, Local impedance imaging of boron-doped polycrystalline diamond thin films, Applied Physics Letters, Open AccessVolume 105, Issue 1329 September 2014 Article number 131908).*

The condition for such implementation is the conductivity of the current through the tip material. In this way, changes in impedance were obtained as a function of the tip position. Under scanning conditions, an impedance is determined, the spectrum of which is assigned to each pixel of the scanned surface. Localized impedance measurements provide an overview of the electromechanical surface properties of materials, which is essential in many research areas. We strongly believe that local impedance measurements in AFM contact mode should always be supplemented with DFL impedance/resistance curves. In contact mode, the DFL signal is used as a parameter to characterize the force of interaction between the tip and the surface. There is a linear relationship between DFL value and force. (*M. T. Tobiszewski, A. Arutunow, K. Darowicki, Application of Dynamic Impedance Spectroscopy to Scanning Probe Microscopy, Microscopy & Microanalysis, Volume, 20, Pages 582–585, 2014).*

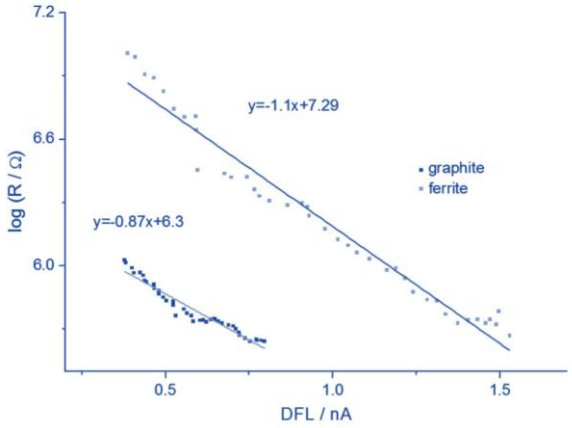

Fig. 5-21. Exemplary relationships between the logarithm of the spreading resistance and the contact force determined for graphite and ferrite.

Extrapolation of the curves to a force of F = 0 (DFL = 0) gives results for the undeformed surface when the tip initially contacts the surface. The above allows for a more accurate and unique comparison of electromechanical properties for each phase. (*M. Tobiszewski, A. Zielinski, K. Darowicki, Dynamic nanoimpedance characterization of the atomic force microscope tip-surface contact, Microscopy and Microanalysis, Open Access, Volume 20, Issue 1, Pages 72 – 77c February 2014).*
Moreover, the methodology presented here provides a good starting point for in-situ local electrochemical impedance measurements in AFM contact mode. For example, the topographic image and the image of changes in contact resistance were compared.

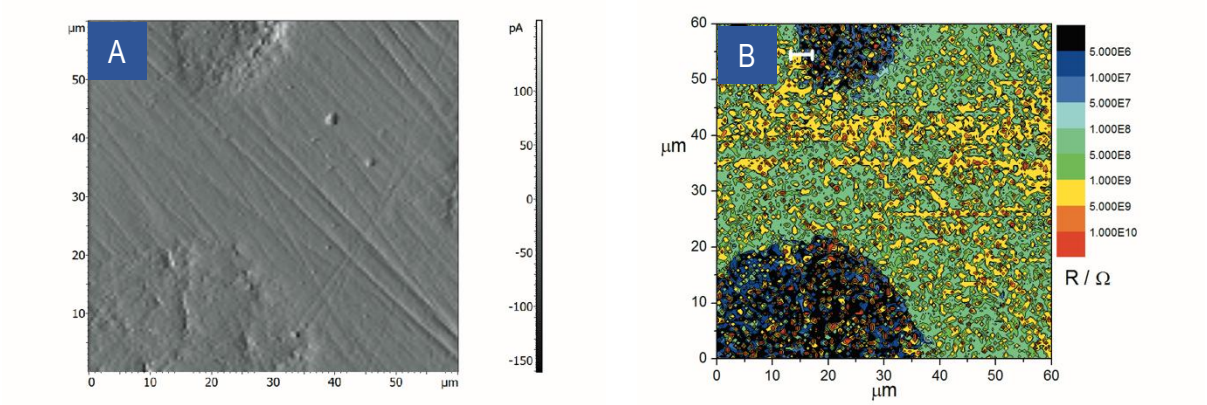

Fig. 5-22. (A) Topographic AFM image of the cast iron sample, (B) image of changes in impedance of the same sample

The impedance measurement procedure described above has been applied to study different regions of a microprocessor system containing a semiconductor structure. (*K. Darowicki, A. Zielinski, Mesoscopic impedance analysis of solid materials' Surface, Electrochimica Acta, Volume 55, Issue 26, 1 November 2010, Pages 7761-7765).*
The topography of the area is shown in Fig. 5-23 (height in the scale bar expressed in µm). The existence of electrical contact was confirmed by spreading resistance measurements. The AC current amplitude image obtained in the previously described mode of the impedance imaging (bias voltage 0 V, AC voltage amplitude 70 mV and set point 2 nA) is shown in Fig. 5-24 (current in the scale bar expressed in nA). Both images confirm a consistent, qualitative, spatial distribution of AC current amplitude correlated with the surface topography.

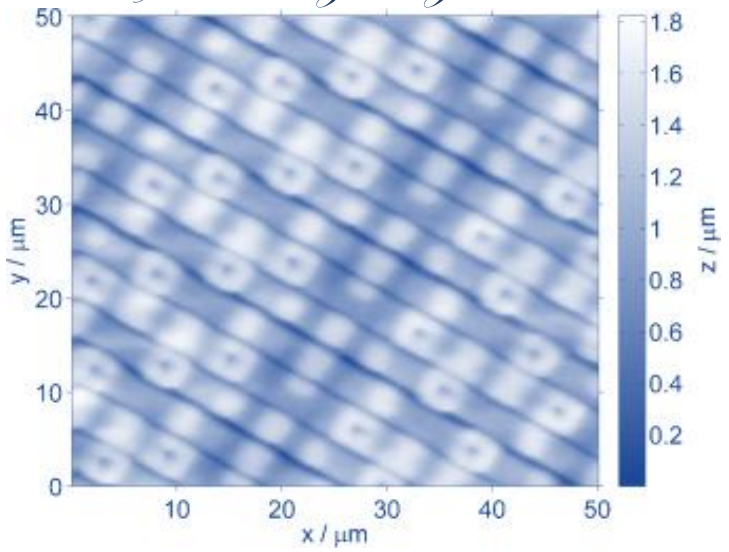

Fig. 5-23A. Topography of the semiconductor region of the test sample (height in the scale bar expressed in µm). Contact mode, set point 2 nA and scan rate1 Hz

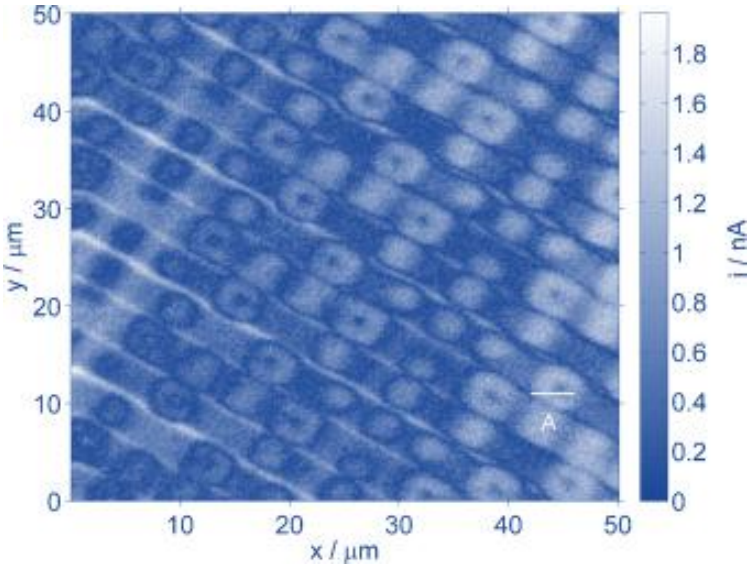

Fig. 5-23B. The AC current amplitude image obtained for the region illustrated in Fig. 5-23A. (bias voltage 0 V, AC voltage amplitude 70 mV, scan rate 1 kHz, set point 2 nA and current in the scale bar expressed in nA)

Impedance surface scanning in AFM mode is our impedance imaging concept

Various AFM measurement modes are implemented in practice. On the other hand, impedance spectroscopy is the fundamental method for determining the electrical properties of materials. This creates the possibility of distinguishing alloy phases. (*A. Arutunow, M. Tomasz Tobiszewski, K. Darowicki, Electrical and mechanical characterization of two-phase alloys by means of scanning probe microscopy in dynamic impedance spectroscopy mode, Journal of Alloys and Compounds, Volume 619, 15 January 2015, Pages 172-176).*

The diagram below shows the impedance changes determined for the ferrite phase and austenitic phase of 2205 duplex steel.

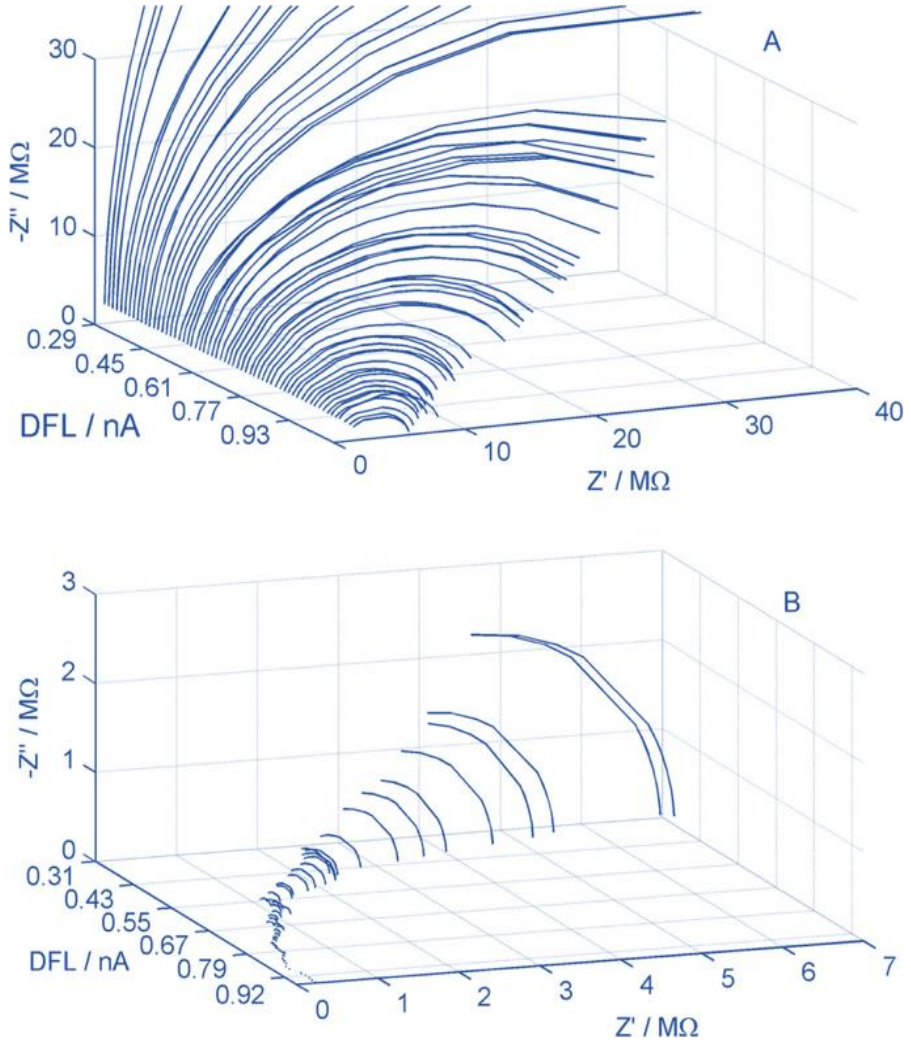

Fig. 5-25. Exemplary local impedance spectra determined for 2205 duplex steel: (A) austenitic phase, (B) ferritic phase

Comparison of impedance diagrams as a function of the tip-surface contact force indicates the possibility of quick differentiation between the austenitic phase and the ferritic phase. (*K. Darowicki, A. Zieliński, Application of multisine nanoscale impedance microscopy to heterogeneous alloy surface investigations, Surface and Interface Analysis, Volume 47, Issue 12, Pages 1109 – 1113 December 2015).*

As we have already demonstrated, contact impedance measurements performed using AFM and submicron-scale positioning are a promising diagnostic methodology in modern material technology. (*A. Zielinski, M. Cieslik, M. Sobaszek, R. Bogdanowicz, K. Darowicki, J. Ryl, Multifrequency nanoscale impedance microscopy (m-NIM): A novel approach towards detection of selective and subtle modifications on the surface of polycrystalline boron-doped diamond electrodes, Ultramicroscopy, Volume 199 Pages 34-45, February 2019).*

The impedance scanning method is useful in testing carbon layers and their modification. In addition to the resistance changes imaging, it is possible to map contact capacitance.

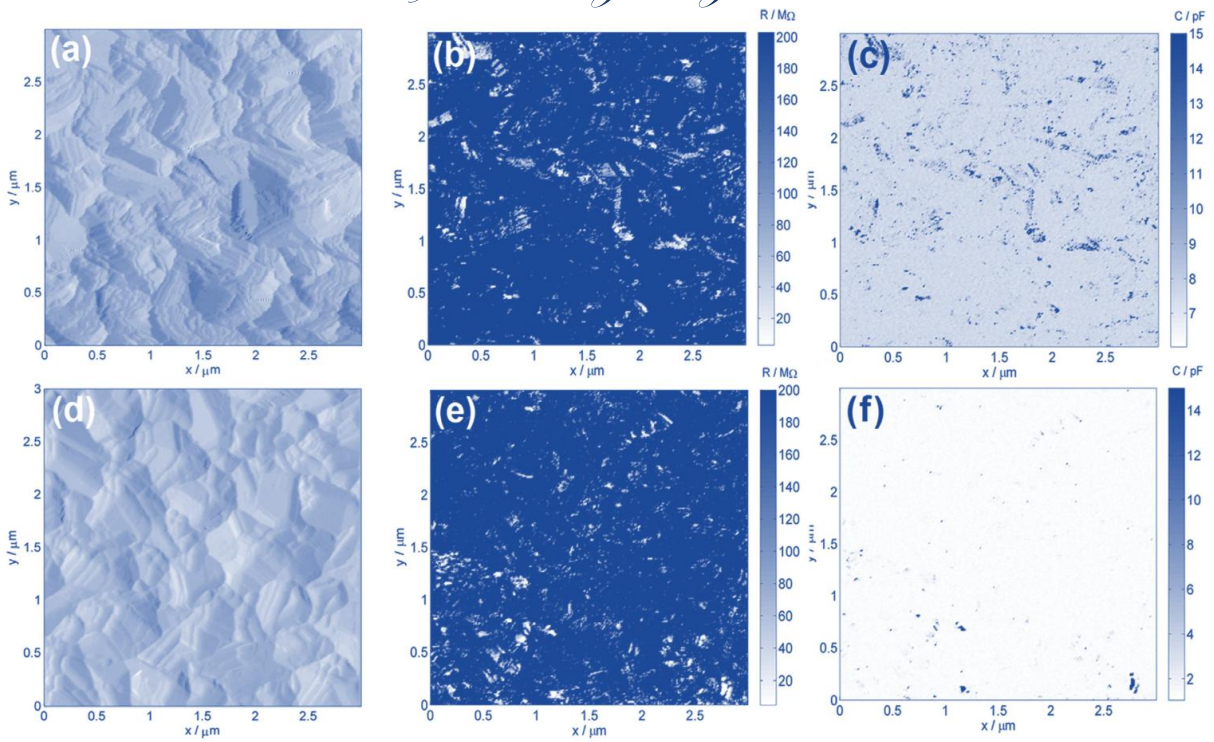

Fig. 5-26. Images of OT-BDT layers after electrochemical oxidation obtained at two different scan rates, (a-c) 0.1Hz, (d-f) 1 Hz. Images (a,d) are AFM contour micrographs. Images (b,e) are resistance distributions. Images (c,f) are electrical capacitance distributions.

Nanoimpedance measurements in AFM mode allow for precise analysis of subtle changes in local electrical properties on a submicroscopic scale. The main advantage of our approach is the ability to obtain extended information about the electrical nature of the surface. Nanoimpedance scans obtained in AFM mode very often reveal undesirable effects such as 'rostering'. Removing this effect required the development of an effective algorithm for identifying and limiting the interaction of several harmonics. (*M. Kiwliszo, J. Smulko, K. Darowicki, A. Zielinski, Improving AFM Images with Harmonic Interference by Spectral Analysis, Microscopy & Microanalysis, Volume 18, Pages 186–195, 2012).*

The most effective algorithm was the one involving the use of Fourier transformation to remove boundary distortions in subsequent columns and rows of the saved image. Other algorithms have proven less successful. Fig. 5-27 shows the effect of our modification.

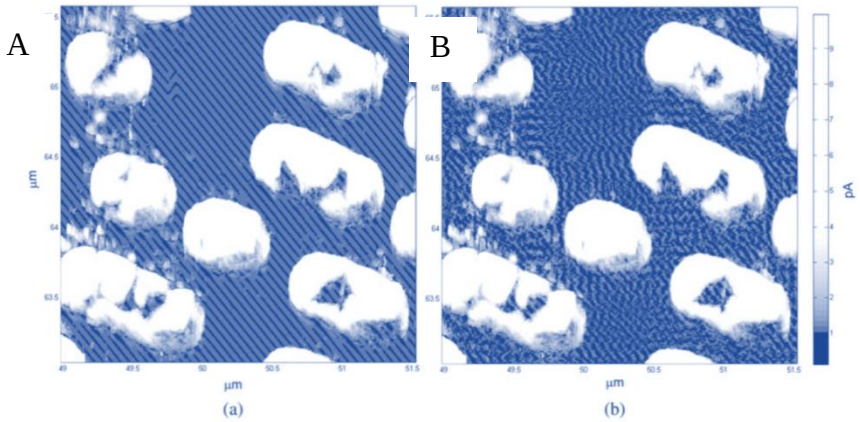

Fig. 5-27. (a) Nano-impedance image obtained in AFM mode, (B) Nano-impedance image after application of the developed algorithm

In Fig. 5-27A, a mesh suggesting the regular structure of the analysed material is clearly visible. The application of the correction algorithm (Fig. 5-27B) reveals that this is the result of digital image processing.

5.7. Impedance analysis of fuel and electrochemical cells

Fuel cells are used in many sectors, including: transportation, construction, energy storage, power plants, vehicles, etc. Compared to conventional combustion-based technologies, fuel cells have several advantages. They can operate at higher efficiency than internal combustion engines and can convert chemical energy in the fuel directly into electricity with efficiencies exceeding 60%. Fuel cells have lower or zero emissions compared to internal combustion engines. Hydrogen cells only emit water, solving critical climate problems because they do not emit carbon dioxide. There are also no air pollutants that create smog and cause health problems. Fuel cells are quiet during operation because they have few moving parts. Hydrogen resources are also a significant issue, which means that fuel cells will become one of the primary sources of energy in the near future.

Investigation of fuel cells and monitoring their operation has become one of the challenges. The implementation of DEIS to assess the state and efficiency of fuel cell operation gave excellent results. *(K. Darowicki, E. Janicka, M. Mieliniczek, L. Gawel, J. Mitzel, J. Hunger, The influence of dynamic load changes on temporary impedance in hydrogen fuel cells, selection and validation of the electrical equivalent circuit, Applied Energy, Volume 251, 1 October 2019, 113396).*

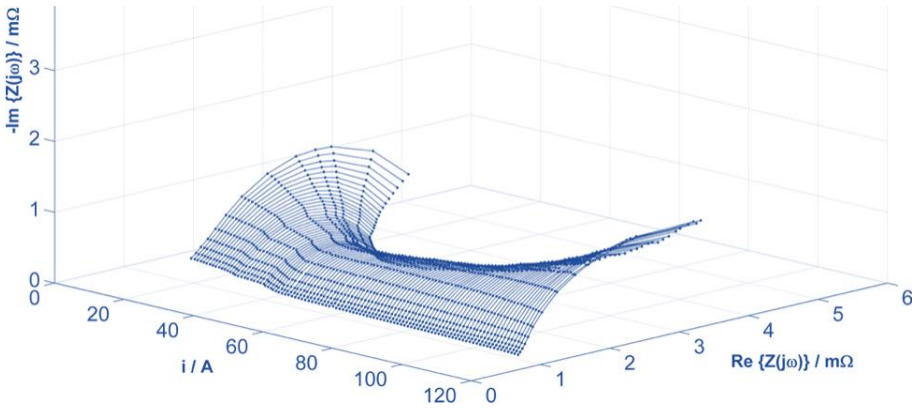

Fig. 5-28A. PEM fuel cell impedance spectrogram obtained in galvanodynamic mode. Geometric surface S = 96 cm^2, current load change rate di/dt=50mAs^{-1}, measurement frequency range from 5Hz to 1123Hz.

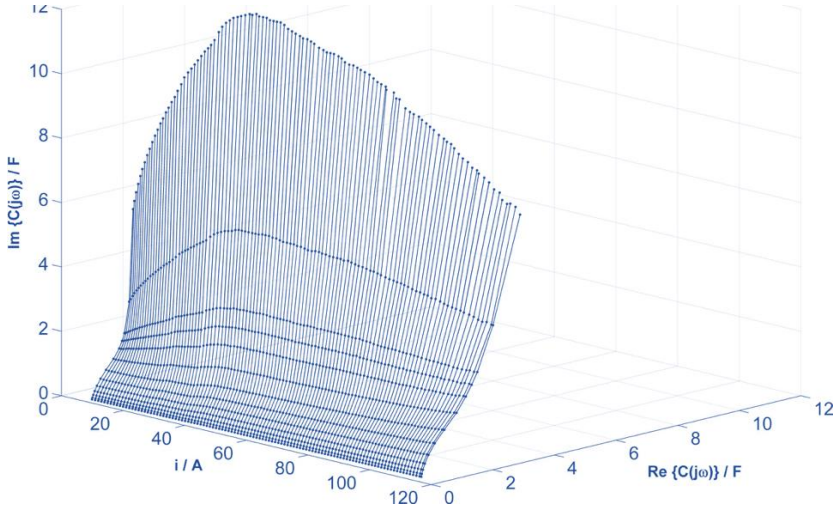

Fig. 5-28B. Complex capacitance diagram for PEM fuel cell obtained in galvanodynamic mode. Geometric surface S = 96 cm^2, current load change rate di/dt=50mAs^{-1}, measurement frequency range from 5Hz to 1123Hz.

DEIS measurements made it possible to determine the range of currents corresponding to the minimum impedance and the maximum complex capacitance. Detailed analysis of the obtained impedance spectrogram allowed establishing an electrical equivalent circuit representing the anode of the fuel cell, Fig. 5-29B.

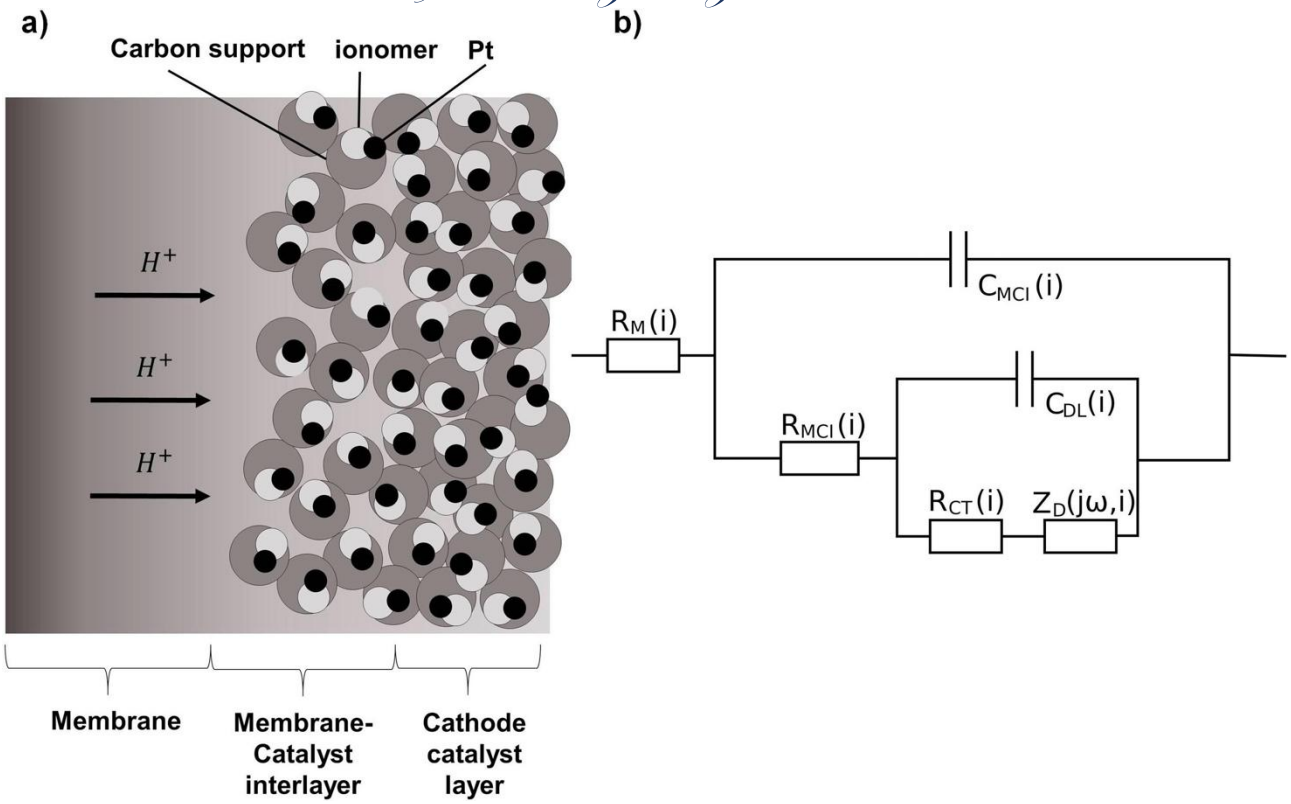

Fig. 5-29. A) Cross-sectional scheme of the cathodic part of MEA, B) Electrical equivalent circuit employed for the analysis of instantaneous impedance spectra, $R_M(i)$ – membrane resistance, $R_{MCI}(i)$ - interlayer resistance, $R_{CT}(i)$ - charge transfer resistance, $Z_D(j\omega,i)$ - impedance of the element describing diffusion in the finite thickness layer, $C_{MCI}(i)$ - catalyst layer capacitance, $C_{DL}(i)$ - electrical double layer capacitance

Complex capacitance spectra reveal the existence of two capacities. In the low limit frequency range, complex capacitance spectra tend to infinity. DC current load has a strong influence on the shape of complex capacitance spectra. The spectra take relatively high values for the optimal DC current range.

The combination of DC and AC measurements not only provides verification of the completeness and accuracy of the impedance results, but more importantly, produces instantaneous impedance spectra as a function of current. This allowed us to describe the impact of processes occurring in a fuel cell on its operation and with changing current loads. The presented relationships between the parameters of the equivalent circuit in relation to the current gave a comprehensive characterization of the impedance of the operation of a fuel cell with a proton exchange membrane. The current range is optimal when the charge transfer resistance and diffusion resistance reach a minimum. This is due to the fact that these electrochemical processes occur with the least obstacles. A local maximum of capacitance is also observed for the same current range. In addition, we presented the possibility of assessing changes in the thickness of the diffusion layer depending on the amount of energy generated. It is not possible to quickly determine optimal current conditions using classic impedance measurements. The presented dynamic electrochemical impedance spectroscopy methodology allows for obtaining reliable results in dynamic operating conditions. Thus, this method can be used as an online tool for monitoring and diagnostics of the fuel cell during operation. Dynamic impedance measurement can also be successfully used as a helpful tool in the fuel cell design process.

The efficiency of the entire fuel cell stack depends on the efficiency of individual elementary cells. Thus, it is extremely important to be able to characterize all the cells in the stack simultaneously. (*K. Darowicki, E. Janicka, M. Mielniczek, A. Zielinski, L. Gawel, J. Mitzel, J. Hunger, Implementation of DEIS for reliable fault monitoring and detection in PEMFC single cells and stacks, Electrochimica Acta, Volume 292, 1 December 2018, Pages 383-389).*

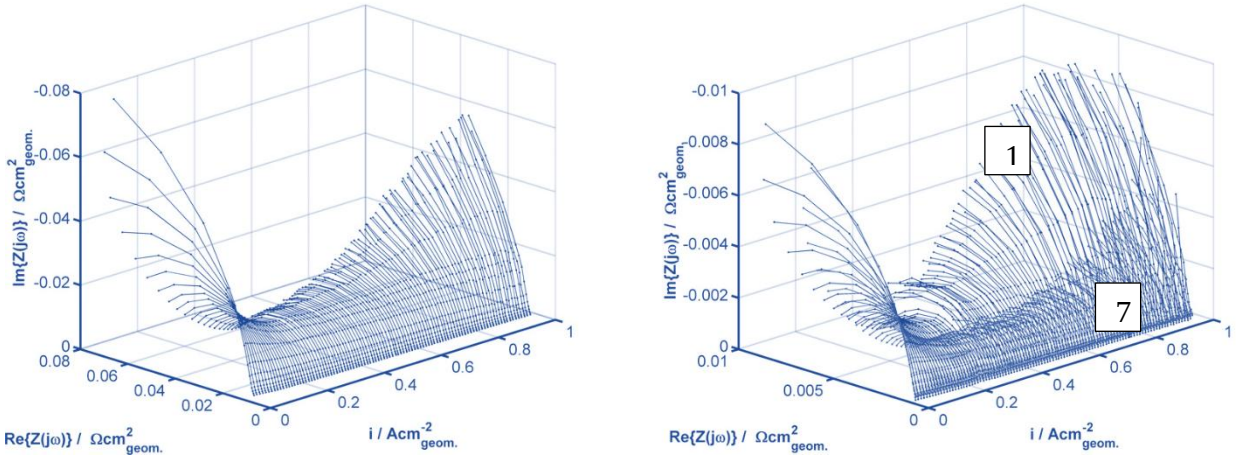

Fig. 5-30. A) Impedance spectrogram determined for the stack of 10 cells, B) Comparison of impedance spectrograms of cell no. 1 (defected) and cell no. 7 (correct operation). Current scan rate $di/dt = 20\ mAs^{-1}$.

he DEIS method was successfully applied to diagnose the cell responsible for the reduced efficiency of the entire stack. The proposed diagnostic method makes it possible to simultaneously obtain the impedance of single cells and the entire stack as a function of variable operating parameters in a dynamic system, such as a stack upon the electrical load changes. The use of the proposed statistically preferred equivalent circuit allows obtaining a data library of parameter values under variable stack operating conditions. This enables not only the diagnostics of faulty cells, but also the identification of the causes of failure. The implementation of the proposed method provides information on whether the failure is reversible or involves poor optimization of operating conditions.

For a fuel cell to function properly, the ion exchange membrane must be hydrated. If it is not fully humidified, conduction decreases, and therefore more energy is consumed during the proton transport phenomenon. However, if it is not sufficiently moisturized, it essentially stops acting as a proton transporter. Because a hydrogen fuel cell consumes hydrogen and oxygen to produce electricity and water, a relatively large amount of water is produced. This creates the problem of potential flooding of the catalyst layer. For these reasons, humidity evaluation is one of the most important tasks, implying the correct operation of the cell. (*E. Janicka, M. Mielniczek, L. Gawel, K. Darowicki, P. Landowska. The impact of air humidity on the operation of proton exchange membrane fuel cells determined using dynamic electrochemical impedance spectroscopy, Electrochimica Acta, Volume 341, 1 May 2020, 136036).*

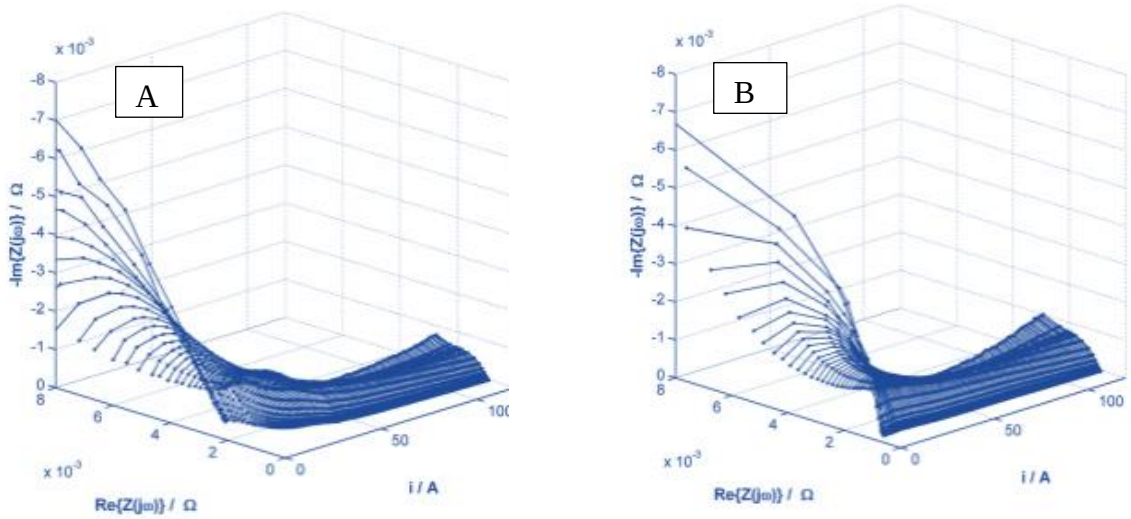

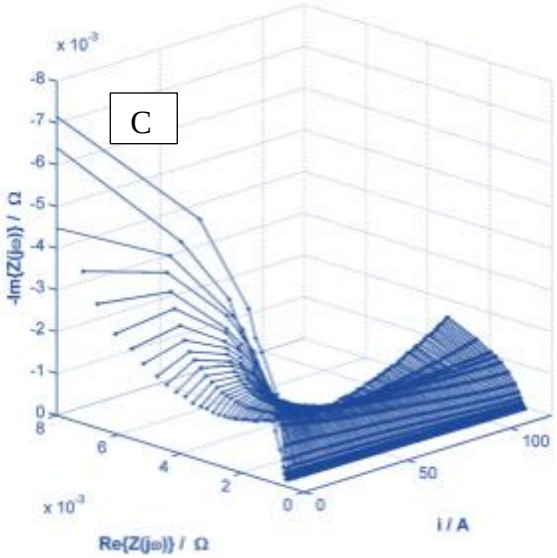

Fig. 5-31. Fuel cell impedance spectrograms determined for different relative humidities: A) 10%, B) 30%, C) 90%. Geometric surface of the membrane S = 96 cm^2, current load change rate $di/dt=50mAs^{-1}$

Dynamic impedance diagnostics of fuel cells is our original proposal.

Analysis of impedance spectrograms as a function of current load for various fixed levels of relative humidity ensures that optimal operating conditions are met. A monotonic decrease in charge transfer resistance was observed with increasing current and humidity. Changes in the Warburg coefficient are more multifaceted. The dependence of the Warburg coefficient on the current is in the form of a saddle curve. For extremely low currents and low humidity, the transport rate is reduced, as is the case with high humidity and high currents. The presented procedure allows for a clear selection of the optimal intake air humidity depending on the amount of energy generated by the cell. It has been demonstrated through a comprehensive analysis that to achieve the best performance of the cell during its dynamic operation, it is necessary to automatically adjust humidity changes. Changes in humidity and current should be correlated to achieve minimum impedance.

- To ensure the best efficiency, the RH value of the supplied air should vary depending on the current fuel cell load.
- For low current values (below 30 A), RH has the greatest impact on membrane resistance and interlayer resistance, with optimal performance obtained at RH above 35%.
- For higher current values (above 50 A), air humidity has the greatest influence on diffusion processes, with best results obtained at low RH below 20%.

Another, perhaps the most important parameter determining the efficiency of fuel cell operation is hydrogen purity. Cleanliness specifications are crucial to ensuring optimal equipment performance. Advanced purification systems are typically used to guarantee cleanliness in accordance with industry standards, including SAE J2719 and ISO 14687:2019 for hydrogen fuel quality. Pollutants in hydrogen fuel, such as CO, H_2S, NH_3, organic sulphur and carbon compounds, and carbon and hydrogen compounds, as well as in air pollutants, such as NOx, SOx and small organic compounds, are transferred with fuel and air streams to the anodes and cathodes of the cell. They cause performance deterioration and sometimes permanent damage to membrane electrode assemblies. It is therefore important to develop a methodology for diagnosing the cathode state.

For this purpose, we used the DEIS methodology developed by us. (*K. Darowicki, L. Gawel, M. Mielniczek, A. Zielinski, E. Janicka, J. Hunger, L. Jorissen, The impedance of hydrogen oxidation reaction in a proton exchange membrane fuel cell in the presence of carbon monoxide in hydrogen stream, 2020, Applied Energy, p. 115868)*

Fig. 5-32A shows a time impedance spectrogram of a fuel cell, the hydrogen fuel of which meets the standard requirements.

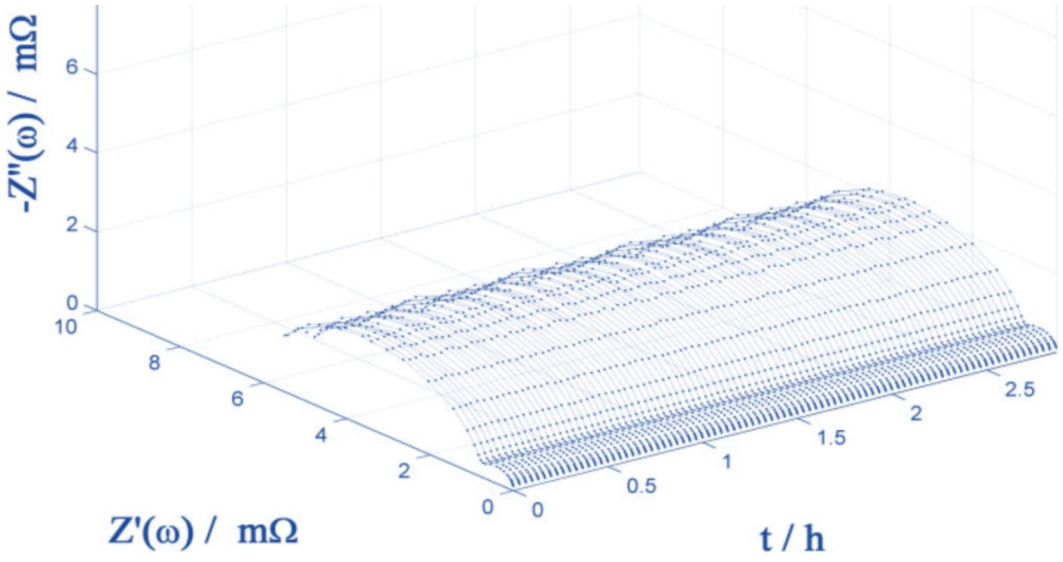

Fig. 5-32A. Chrono-impedance spectrogram of a hydrogen fuel cell determined for constant current density $j = 2\ Acm^2$ in the absence of carbon monoxide CO

The high-frequency region includes the anode impedance. Low-frequency semicircles are the characteristics of the cathode. Impedance spectra do not change as a function of time, and stable operation of the hydrogen fuel cell is observed.

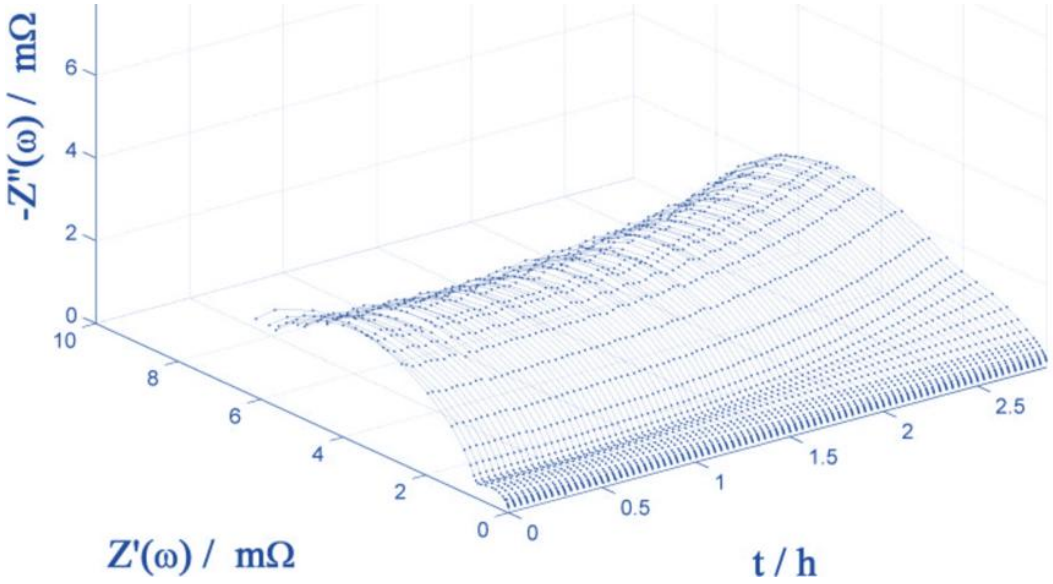

Fig. 5-32B. Chrono-impedance spectrogram of a hydrogen fuel cell determined for constant current density $j = 2\ Acm^2$ in the presence of 125 ppb of carbon monoxide CO

The introduction of 125 ppb of CO into hydrogen fuel resulted in changes of the spectra. After one and a half hours, the cathode impedance increased in the high-frequency region. This effect is fully revealed for the higher carbon monoxide CO content in hydrogen.

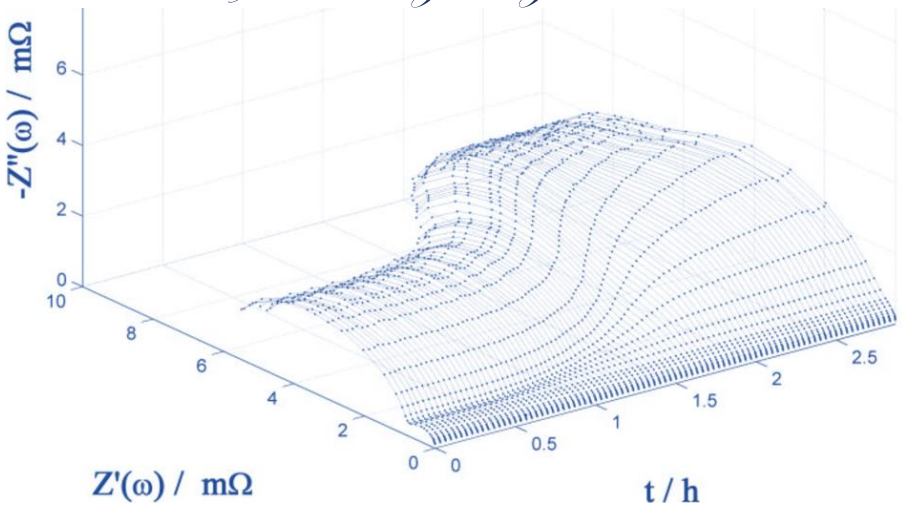

Fig. 5-32C. Chrono-impedance spectrogram of a hydrogen fuel cell determined for constant current density $j = 2\ Acm^2$ in the presence of 250 ppb of carbon monoxide CO

The obtained results indicate a significant influence of carbon monoxide in the hydrogen stream on the anode impedance during cell operation. Carbon monoxide with a concentration of 125 ppb has a marginal impact on the anode efficiency. Contamination of the hydrogen supply with carbon monoxide at a concentration of 250 ppb or higher has a significant influence on the anode impedance and voltage drop at the cell terminals. Changes in the impedance of the entire cell are directly caused by changes occurring at the anode during the supply of fuel with different carbon monoxide concentrations. This level of testing has never been performed dynamically before. *(K. Darowicki, E. Janicka, M. Mielniczek, L. Gawel, An integral-differential method for impedance determination of the hydrogen oxidation process in the presence of carbon monoxide in the proton exchange membrane fuel cel, International Journal of Hydrogen Energy, Volume 45, Issue 51, Pages 27551 - 2756216 October 2020).*

Therefore, the tests utilizing electrochemical impedance spectroscopy did not allow for an unequivocal identification of the anode impedance or validation of the conclusions regarding the obtained trend of changes in the anode parameters of the equivalent circuit during exposure to carbon monoxide, and it was not possible to determine the rate of changes over time. That is why the dynamic electrochemical impedance spectroscopy technique is an ideal tool for diagnosing and monitoring the condition of fuel cells under real, dynamic operating conditions, even when the level of hydrogen pollution with carbon monoxide is extremely low.

In addition to fuel cell research, we used impedance spectroscopy to evaluate electrochemical cells. (*K. Darowicki, K. Andrearczyk, Determination of occurrence of anodic excursion peaks by dynamic electrochemical impedance spectroscopy, atomic force microscopy and cyclic voltammetry, Journal of Power Sources, Volume 189, Issue 2, Pages 988 - 99315 April 2009; P. Slepski, K. Darowicki, A. Kopczyk, K. Andrearczyk, Electrochemical impedance studies of AB_5-type hydrogen storage alloy, Journal of Power Sources, Volume 195, Issue 9, Pages 2457 - 24621 May 2010*; *K. Darowicki, K. Andrearczyk, Determination of occurrence of anodic excursion peaks by dynamic electrochemical impedance spectroscopy, atomic force microscopy and cyclic voltammetry, Journal of Power Sources, Volume 189, Issue 2, Pages 988 - 99315 April 2009).*

5.8. Polynomial analysis, differential and relative spectra

As a result of EIS measurements, we obtain an impedance spectrum, which is a local characteristic of the investigated process obtained under steady, time-invariant conditions. A single impedance spectrum provides us with limited information. Analysis of a single spectrum comes down to correlating experimental results with adopted electrical equivalent circuits. The circuit with the smallest fitting error to the experimental results is chosen as a representative one. In practice, there is significant freedom in the selection of electrical equivalent circuits, and the conditions for selecting the correct circuit are not unequivocal either. Nevertheless, the non-linear least squares technique is a very valuable tool for analysing complex frequency dispersions.

In the DEIS method, a set of impedance spectra is obtained that are a function of an independent variable. Each of the individual spectra can be analysed separately by a non-linear least squares method and a selection of representative electrical equivalent circuit. In this way, the dependencies between individual parameters of the circuit and the independent variable are obtained. We have developed a different, original polynomial way of recording and analysing spectrograms

(K. Darowicki, A. Zielinski, M. Mielniczek, E. Janicka, L. Gawel, Polynomial description of dynamic impedance spectrogram — Introduction to a new impedance analysis method, Electrochemistry Communications, Volume 129, August 2021, 107078).

As usual, in such situations, we performed an impedance analysis of a model electrical circuit.

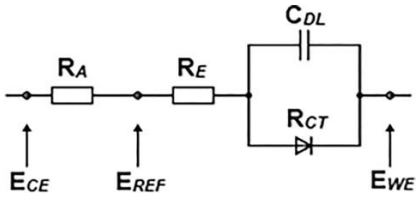

Fig. 5-33. Investigated model electrical circuit

The model electrical circuit employed in dynamic impedance measurements consisted of charge transfer resistance, electrical double layer capacitance, and electrolyte resistance. The points marked in the scheme indicate the electrode connection points: counter electrode, reference electrode, and working electrode. A resistor connected in series was used as a fuse.

The impedance spectrogram of this electrical circuit is illustrated in Fig. 5-34.

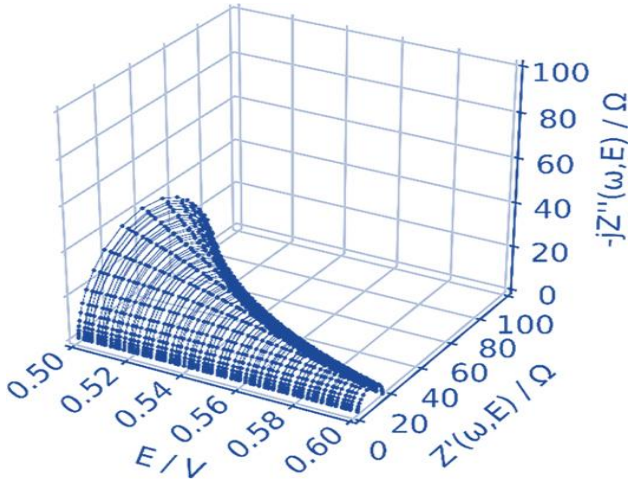

Fig. 5-34. Impedance spectrogram obtained by DEIS for the model circuit during voltage changes from 0.50 to 0.60 V.

On impedance spectra, points of the same frequency are arranged in a monotonic way and can be formally described using polynomials. As a result, a formula for obtaining more complex spectrograms was created. *(K. Darowicki, Sz. Wysmułek, A. Karólkowska, Polynomial analysis as a new way of describing dynamic impedance spectra – Differential and relative impedance spectra, Electrochemistry Communications, Open Access, Volume 150May 2023 Article number 107476).*

For each i-th frequency, we get two polynomials:

$$f_i \rightarrow \begin{Bmatrix} Z'(f_i,x) \approx a'_1 + a'_2 x + a'_3 x^2 + \cdots + a'_n x^n \\ Z''(f_i,x) \approx b''_1 + b''_2 x + b''_3 x^2 + \cdots + b''_n x^n \end{Bmatrix} \quad (5\text{-}3)$$

Polynomial notation is the starting point for performing a number of simple mathematical operations on impedance spectrograms. Polynomial notation of spectrograms allows addition, subtraction, multiplication, division, convolutional multiplication, integration, and differentiation. These arithmetic operations on polynomials are an alternative to digital integration and differentiation and create new possibilities for automation, diagnostics, and monitoring of electrochemical energy sources. These operations can be used for more advanced analytical purposes, such as:

differentiation $$f_i \rightarrow \begin{Bmatrix} \frac{dZ'(f_i,x)}{dx} \approx a'_2 + 2a'_3 x + \cdots + na'_n x^{n-1} \\ \frac{dZ''(f_i,x)}{dx} \approx b''_2 + 2b''_3 x + \cdots + nb''_n x^{n-1} \end{Bmatrix} \quad (5\text{-}4A)$$

or integration: $$f_i \rightarrow \begin{Bmatrix} \int Z'(f_i,x)\,dx \approx a'_0 + a'_1 x + a'_2 \frac{x^2}{2} + a'_3 \frac{x^3}{3} + \cdots + a'_n \frac{x^{n+1}}{n+1} \\ \int Z''(f_i,x)\,dx \approx b'_0 + b'_1 x + b'_2 \frac{x^2}{2} + b'_3 \frac{x^3}{3} + \cdots + b'_n \frac{x^{n+1}}{n+1} \end{Bmatrix} \quad (5\text{-}4B)$$

Differentiation of polynomials leads directly to the differential spectrogram.

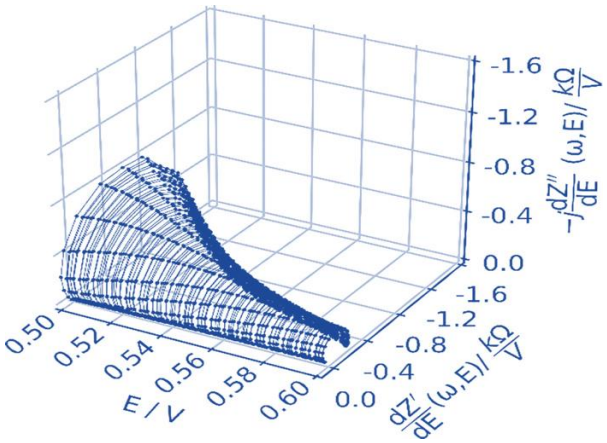

Fig. 5-35. Differential impedance spectrogram obtained via polynomial differentiation.

The combination of basic polynomials (5-3) and differential polynomials (5-4) for each i-th frequency is the way to obtain a relative impedance spectrogram.

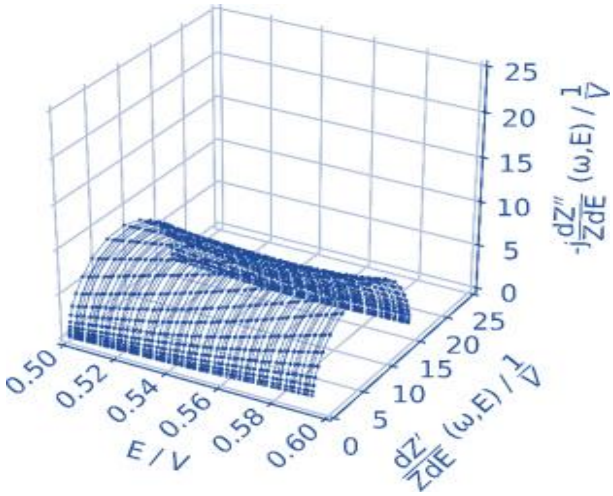

Fig. 5-37. Relative impedance spectrogram obtained via polynomial approach.

The differential impedance spectrogram as well as the relative or integral spectrogram are our new concepts in impedance analysis

The combination of dynamic electrochemical impedance spectroscopy with polynomial analysis offers many new possibilities. The main advantage of the discussed approach is the relativity of the obtained data, which allows making the examined processes independent of the influence of the surface. Furthermore, using the polynomial analysis procedure, differential impedance spectrograms can be obtained. Their differential characteristics make it possible to determine the rate of change of impedance as a function of a specific variable, which allows for a deeper understanding of the kinetics of a given process. Using relative impedance spectra, it is possible to directly and quickly compare electrochemical systems such as fuel cells and supercapacitors, as well as previously studied and widely discussed systems such as protective coatings and specific corrosion processes.

Each procedure requires determining the level of credibility of the operations carried out. This procedure is also necessary for spectrograms. It is reasonable to ask how the elementary impedance spectrum is related to the previous spectrum and the following spectrum. In other words, what is the level of correlation.

For single impedance spectra, validation of impedance data is essential to verify their reliability. The Kramers-Kronig transformation is used to verify data obtained from classical electrochemical impedance measurements (EIS). The data obtained from dynamic electrochemical impedance spectroscopy (DEIS) can be verified in the same way, but in this case, there is no information about the internal consistency between each individual spectrum in the entire spectrogram. To meet these challenges, we proposed an approach using the ACF autocorrelation function to verify DEIS time series. *(K. Darowicki, Sz. Wysmułek, A. Karólkowska, L. Gaweł, Validation of dynamic electrochemical impedance spectrograms using autocorrelation function, Journal of Electroanalytical Chemistry, Volume 9621 June 2024 Article number 118255).*

Autocorrelation functions are described by the following equations:

$$ACF\{Z'(f_i,t)\} = \frac{1}{T}\int_0^T Z'[f_i,t] * Z'[f_i,(t+\tau)] \tag{5-5A}$$

$$ACF\{Z''(f_i,t)\} = \frac{1}{T}\int_0^T Z''[f_i,t] * Z''[f_i,(t+\tau)] \tag{5-5B}$$

where: $ACF\{Z'(f_i,t)\}$ - autocorrelation function of the real part of impedance for the i-th frequency, $ACF\{Z''(f_i,t)\}$ – autocorrelation function of the imaginary part of impedance for the i-th frequency, f_i – i-th frequency, τ – time shift, T – duration of the entire register, t – time

Impedance measurements of the dissolution of carbon steel in an acidic environment were carried out in two variants. The first variant is impedance measurements using the spectrum-by-spectrum method (EIS method). The second variant is measurements of the same process using the DEIS method.

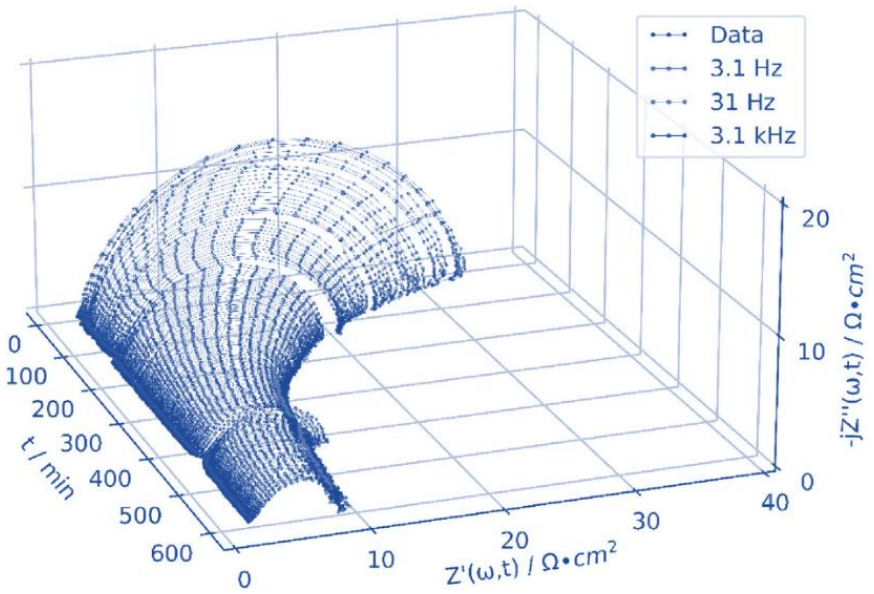

Fig. 5-38A. Impedance spectrogram obtained from sequential EIS measurements of a carbon steel electrode in a 1 M HCl environment, for benzimidazole concentration c = 4 mM.

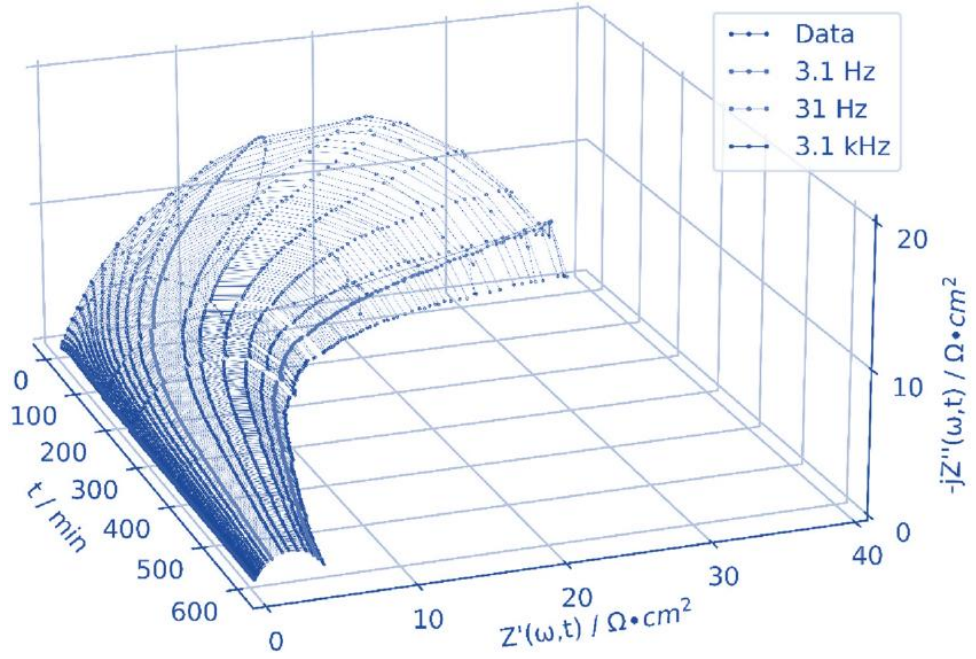

Fig. 5-38B. Impedance spectrogram obtained by DEIS of a carbon steel electrode in a 1 M HCl environment, for a benzimidazole concentration c = 4 mM.

To compare these two variants of determining impedance spectrograms, we performed a correlation analysis. Fig. 5-39A shows changes in the autocorrelation function in the frequency range applied and in the examined time range for the spectrum-by-spectrum sequential method. On the other hand, Fig. 5-39B illustrates the corresponding autocorrelation functions determined for DEIS measurements.

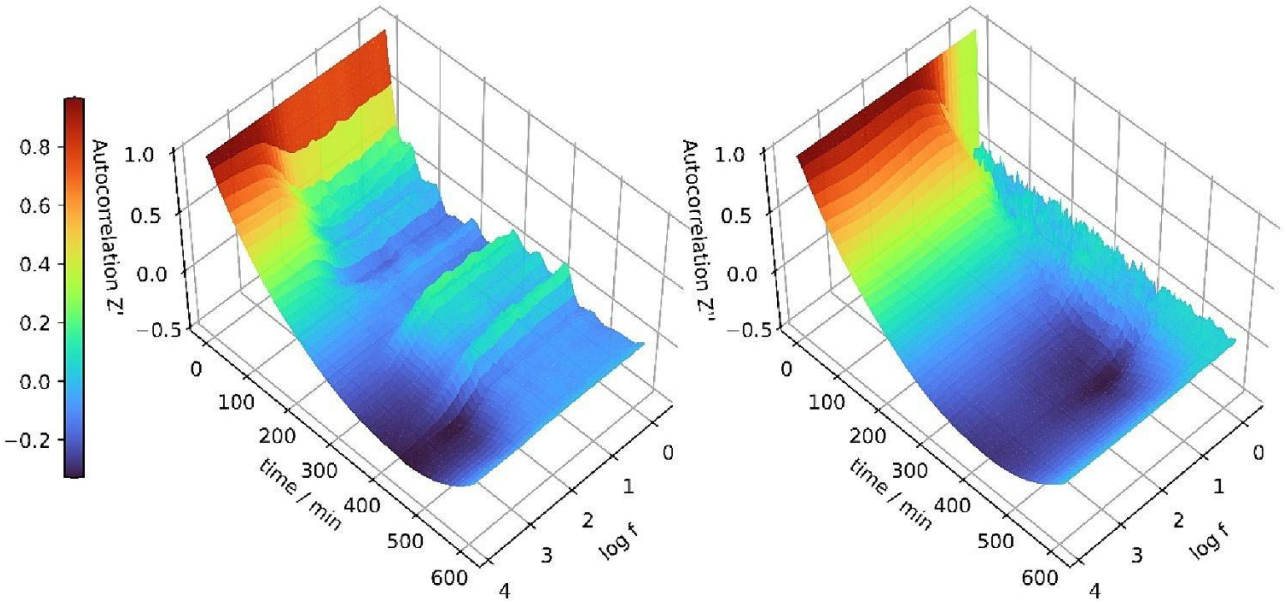

Fig. 5-39A. Autocorrelation functions of real and imaginary parts of impedance measured by static EIS method in sequential mode as a function of measurement time

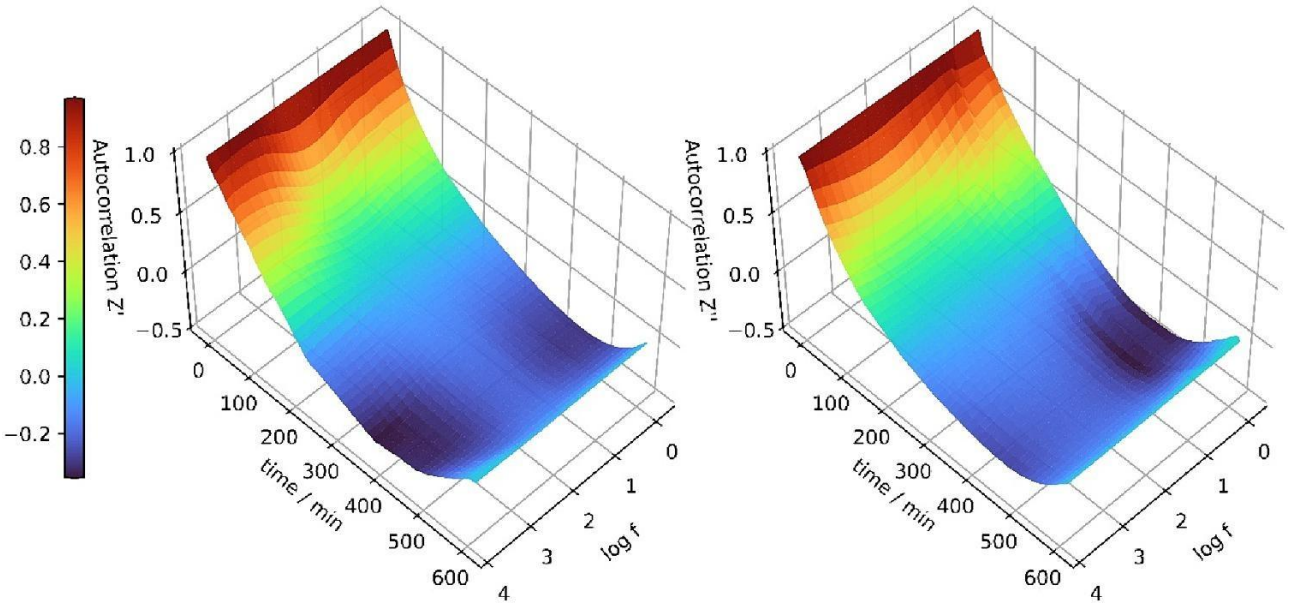

Fig. 5-39B. Autocorrelation functions of real and imaginary parts of impedance measured by the dynamic DEIS method as a function of measurement time

The combination of impedance spectra as a function of an independent variable increases the reliability and the analytical value of impedance measurements. The resulting spectrograms are a more complete characterization of the electrochemical process under study than single impedance spectra. Nevertheless, the analytical value of the determined spectrograms may vary. This depends mainly on the measurement methodology and the consistency of the determined impedance values for individual frequencies. Comparing the autocorrelation results obtained from static EIS and dynamic DEIS measurements, it is clear that EIS data for low frequencies are not consistent. Determining impedance spectrograms using the EIS method, i.e., spectrum by spectrum, raises measurement concerns. The impedance spectrogram determined in this way is not internally consistent. The autocorrelation functions for the results obtained using the DEIS technique are completely different. In this situation, a complete correlation of individual spectra can be found. The full correlation concerns changes in the real part of the impedance as a function of time and the imaginary part of the impedance as a function of time over the entire applied frequency range. When analysing the variability of impedance as a function of a selected independent variable, in particular analysing changes in impedance as a function of time, it is necessary to determine the coherence of the obtained results. This issue concerns changes in the real part and the imaginary part of impedance. The ACF autocorrelation function is a suitable tool for validating spectrograms. By using ACF, it is possible to check the consistency of the impedance spectrogram over the entire range of the time domain, as well as over the frequency range. The proposed three-dimensional autocorrelation graphs show the internal time correlation of each point of the real part and the imaginary part of the impedance in the frequency range applied.

6. PHOTOGRAPHIC DOCUMENTATION OF SCIENTIFIC AWARDS AND MEDALS CEREMONIES

Presidential Palace in Warsaw, Warsaw – 7th July 2000, President of the Republic of Poland Aleksander KWAŚNIEWSKI, presentation of the professorial nomination

Main Town Hall in Gdańsk, Gdańsk – 28th January 2017, Mayor of Gdańsk Paweł ADAMOWICZ, presentation of the Jan Heweliusz Scientific Award of the Mayor of Gdańsk

Amber Expo Exhibition and Congress Centre, Gdańsk – 7th March 2019, Speaker of the Senate of the Republic of Poland Bogdan BORUSEWICZ, presentation of the Pomeranian Employers Award 'Primum Cooperatio' named after prof. B. Mazurkiewicz

Voivodeship Office in Gdańsk, Gdańsk – 30th June 2020, Minister Andrzej DERA, presentation of the Knight's Cross of the Order of Polonia Restituta

Auditorium of the Gdańsk University of Technology, Gdańsk – 1st October 2021, Rector of GUT prof. Krzysztof WILDE, presentation of dignity: 'Personality of the Gdańsk University of Technology'

Artus Court in Gdańsk, Gdańsk – 5th December 2024, Mayor of Gdańsk Aleksandra DULKIEWICZ, Chairman of the City Council Agnieszka OWCZARCZAK, Gdańsk City Council, presentation of the St. Wojciech Medal

7. ORIGIN AND SUMMARY OF BASIC RESEARCH ACHIEVEMENTS

My basic research activity is not dispersed, it is strictly defined and focuses on time-frequency investigation of electrochemical and corrosion processes. I was inspired with this topic by the supervisor of my B. Sc. thesis, Ph.D. D. Sc. Tadeusz Szauer. Within my B. Sc. thesis, I assessed corrosion inhibitors for oil and lubricant anticorrosion additives using impedance technique. To achieve this goal, we built an analogue system for impedance measurements based on the Polish UNIPAN 272 transmittance analyser.

During this time, I gained thorough knowledge of linear circuit theory. I owe my electrochemical orientation in research activity to the internship I completed in the laboratories of prof. Zbigniew Galus at the Faculty of Chemistry of the University of Warsaw. As part of the internship, I learned about electrochemical methods and electroanalysis. I familiarized with the research methodology on mercury electrodes.

Having solidly established electrochemical knowledge, I began investigations on the kinetics and reaction mechanism of cadmium ion reduction on mercury electrodes in the presence of n-pentanol. I also studied the adsorption kinetics of n-pentanol on a hanging mercury electrode. I conducted these tests based on impedance measurements. The results of the research became the basis for my Ph. D. thesis, supervised by prof. Józef Kubicki from the Wrocław University of Science and Technology.

The basic limitations in the applicability of classical Electrochemical Impedance Spectroscopy (EIS) are the non-linearity and non-stationarity of the investigated electrochemical processes. Overcoming these limitations of EIS has become the goal of my further research work. I performed mathematical analyses of the influence of the amplitude of the sinusoidal voltage perturbation signal on the impedance of the first-order electrode reaction and the two-step reaction accompanied by adsorption of the intermediate product. I compared the theoretically determined impedances with the experimental results of actual reactions. When examining processes in non-linear conditions, I limited myself to the impedance of the first harmonic. Determining changes in charge transfer resistance versus perturbation amplitude enabled the formulation of a corrected Stern-Geary relationship. This relationship became the basis for determining the corrosion rate without any preliminary assumptions regarding the value of Tafel coefficients.

At the same time, I started to deepen my knowledge of signal analysis. The acquisition of LabView 'National Instruments' software has become a turning point towards digital systems and sophisticated mathematical methods of analysis. At my request, employees of the Institute of Mathematics, GUT delivered a 30-hour series of lectures on distribution methods of time-frequency analysis and wavelet transformation. Based on distribution methods, in particular the Wigner-Ville distribution, we conducted time-frequency analyses of the Belousov-Zhabotinsky reaction. These were one of the first studies of chemical and later electrochemical oscillations in the joint time-frequency domain. A disadvantage of the Wigner-Ville distribution is the generation of oscillatory interterms that obscure the form of spectrograms. We attenuated these undesirable artifacts by using modified distributions such as Choi-Williams distribution and cone-shaped distribution. This type of analysis clearly showed the time evolution of frequency changes and changes in oscillation energy.

Having specialized digital measurement cards at our disposal, we started recording and analysing electrochemical noise. The wavelet transformation proved particularly useful. Based on the filter bank method, we decomposed the time registers of electrochemical noise into details. It turned out that the rate of corrosion processes is better correlated with the characteristics of the filtered frequency band and not with the global characteristics of the entire register. For the study of electrochemical noise, we employed one of the higher order spectral methods, the bispectral method, which proved to be effective in evaluation of the intensity of pitting corrosion processes.

The Short Time Fourier Transformation (STFT) has proven to be a very useful mathematical tool in non-linear and non-stationary studies of electrode processes. The use of STFT transformation has highlighted the harmonic structure of signals. The most important issue was to obtain true time changes in the amplitudes of individual harmonic components and the Faradaic rectification current. The theoretical harmonic relationships developed were verified by experimental results obtained from the analysis of a non-linear electrical system under variable potential conditions. Conducting the STFT transformation allowed the variable current signal to be decomposed into harmonic components, the analysis of which allowed to reproduce very precisely the electrical parameters of the examined non-linear electrical system.

This success became the starting point for the development of Dynamic Electrochemical Impedance Spectroscopy (DEIS). This time, instead of a single sinusoidal voltage, a pack of sinusoids with fixed amplitudes and selected frequencies was used. Synchronously performing the STFT transformation of the current response pack and the voltage perturbation pack ensured the determination of impedance for selected frequencies as a function of time or other independent variable. DEIS tests of the model non-linear electrical circuit confirmed the correctness of the measurement solutions adopted. An additional confirmation was the Kronig-Kramers transformation of elementary impedance spectra. DEIS has also been verified in studies of well-defined actual electrode reactions.

The development and introduction of the DEIS technique into measurement practice has created new measurement possibilities. Our achievement is demonstration of the usefulness of DEIS in investigations of electropolymerization processes, assessing inhibition processes and evaluation of electrochemical changes occurring on the carbon layers. We were the first to perform impedance measurements reproducing the initiation of pits, the development and repassivation of metastable pits, and the proper development of pitting of 304 steel and aluminium alloys. The DEIS method has proven to be an effective tool in the study of intergranular corrosion and corrosion-erosion. We were the first to assess the condition of passive layers under variable mechanical stresses. Under electrochemical conditions, the Portevin Le-Chatelier effect was revealed. Our original solution was the impedance assessment of the condition of electrochemical cells and fuel cells under variable, non-stationary operating conditions. The DEIS technique coupled with AFM microscopy was used for impedance mapping of the alloy surfaces and assessing the condition of polymer coatings.

The outcome of DEIS investigation are sets of impedance spectra that form spectrograms. The polynomial description of spectrograms we introduced opened up new analytical spaces. We have shown that this method of describing spectrograms leads directly to differential, integral and relative spectrograms. This is a new quality in measurement and impedance analysis.

The presented theoretical studies and measurement results on non-stationary processes are my own concepts and achievements, which have been noticed and honoured with a number of scientific distinctions and awards. For developing the DEIS method, the Main Board of the Polish Chemical Society honoured me with the Jan Zawidzki Medal, and Mayor of Gdańsk Paweł Adamowicz awarded me the Jan Heweliusz Scientific Award of the City of Gdańsk. For all my basic and applied scientific research, I received the St. Wojciech Medal, which after the honorary citizenship of the city, is the highest distinction in Gdańsk.

End of part two